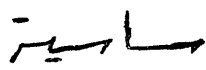


TO MY MOTHER ... 

ProQuest Number: 11016673

All rights reserved

INFORMATION TO ALL USERS

The quality of this reproduction is dependent upon the quality of the copy submitted.

In the unlikely event that the author did not send a complete manuscript and there are missing pages, these will be noted. Also, if material had to be removed, a note will indicate the deletion.



ProQuest 11016673

Published by ProQuest LLC (2019). Copyright of the Dissertation is held by the Author.

All rights reserved.

This work is protected against unauthorized copying under Title 17, United States Code
Microform Edition © ProQuest LLC.

ProQuest LLC.
789 East Eisenhower Parkway
P.O. Box 1346
Ann Arbor, MI 48106 – 1346

THE EFFECT OF SYMMETRIC AND
ASYMMETRIC FRACTURES ON TRANSIENT
PRESSURE BEHAVIOR OF GAS WELLS

by

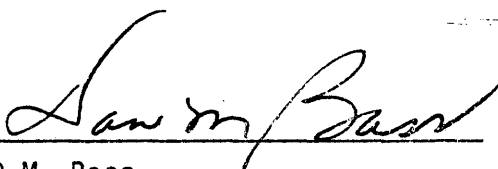
Mahmoud A. Shagroni

A dissertation submitted to the Faculty and the Board of Trustees
of the Colorado School of Mines in partial fulfillment of the requirement
for the degree of Doctor of Philosophy (Petroleum Engineering).

Signed: 
M.A. Shagroni

Golden, Colorado

Date: Dec 14, 1979

Approved: 
D.M. Bass
Thesis Advisor and
Head of Department

Golden, Colorado

Date: Dec 14, 1979

ABSTRACT

A study was made of the mathematical theory of gas well drawdown and buildup testing for the purpose of evaluating the effect of symmetric, asymmetric fracture and real gas properties on gas well testing.

The Iterative Alternating Direction Implicit Procedure (ADIP) was used to solve the finite-difference equations for a two-dimensional model.

Analysis of numerical results from the computer model showed the invalidity of buildup type curve analysis in evaluating gas reservoirs because of the variation of real gas properties with time and the failure of superposition because of the multi-flow regimes.

It has been shown that the position with respect to the wellbore of an infinite conductivity fracture has no effect on the flow solution during the linear flow regime when μc is evaluated at the time of the pressure observation.

It has been shown that the formation flow capacity and the fracture length can not be calculated from the "linear" flow period curve, but must use data obtained from the "radial" flow period. This method of calculating formation flow capacity and fracture length is more accurate than other methods which use gas properties at initial pressure. After the end of the linear flow period the effect of fracture position starts to affect the solution at different flow times which depend on the fracture length.

The superposition principle was checked by buildup tests during different stages of depletion and was found to be invalid for evaluating

fractured gas wells. This could be explained by the non-linearity of flow equations written in terms of $m(p)$ and that the flow regime is time dependent.

CONTENTS

	Page
ABSTRACT	iv
LIST OF TABLES AND FIGURES	ix
ACKNOWLEDGEMENTS	xiii
INTRODUCTION	1
REVIEW OF LITERATURE	2
<u>MATHEMATICAL DEVELOPMENT</u>	6
Continuity Equation	6
Darcy's Law	7
Equation of State	8
Real-Gas Pseudo-Pressure	8
Diffusivity Equation	9
Finite Differences	10
Finite Difference Equation in its Application Form	12
<u>COMPUTER MODEL</u>	17
Assumptions	17
Grid System	18
Method of Solution	18
Validity of the Model	20
<u>RESULTS</u>	26
<u>DISCUSSION OF RESULTS</u>	33
A. Real-gas pseudo-pressure function	33
B. Theory of dimensionless variables	33

TABLE OF CONTENTS (con't)

	Page
C. Type curve analysis for pressure buildup data	42
D. Superposition and pressure buildup.	50
E. Short time solution	74
F. Basic drawdown solution	79
G. Calculation of fracture length	92
<u>CONCLUSIONS.</u>	94
<u>RECOMMENDATION FOR FURTHER RESEARCH</u>	96
<u>NOMENCLATURE</u>	97
<u>APPENDICES</u>	101
A. <u>Mathematical Development</u>	101
Continuity Equation	101
Darcy's Law	102
Equation of State	104
Real Gas Potential	105
Finite Differences	106
B. <u>Handling of Pressure and Temperature</u>	
<u>Dependent Variables</u>	112
Pseudo-Critical Pressure and Temperature	112
Gas Deviation Factor	112
Gas Compressibility	113
Gas Viscosity	115
Numerical Integration of Real-Gas	
Pseudo-Pressure	115
Interpolation Technique	116

TABLE OF CONTENTS (con't)

	Page
C. <u>Flow Diagram of Numerical Model</u>	122
BIBLIOGRAPHY	126
VITA	132

LIST OF TABLES AND FIGURES

Page

TABLE

1. Comparison between computer solution and solution obtained from Equation 31	22
2. Input data which were held constant	26
3. Data sets used by numerical model	27
4. Sample of computer solution - Constant mass rate at the sand face	29
5. Sample of computer solution - Constant flow rate at the sand face	31
6. Fracture length calculation	93

FIGURE

1. Schematic sketch of vertical fracture flow model.	23
2. Grid pattern for modeling a vertically fractured gas reservoir	24
3. Comparison between published solution and model solution for liquid case	25
4. Effect of holding the quantity (μc) in the time coefficient Constant at the initial pressure on the drawdown solution . .	37
5. Effect of formation permeability on the calculated $m(p)$ behavior at the wellbore	38
6. Effect of production rate on the calculated $m(p)$ behavior at the wellbore	39
7. Plot of Figures 5 and 6 data using new definition of dimensionless time	40
8. Example of drawdown and buildup pressures measured in the borehole for the theoretical development of type curve analysis.	41
9. Actual pressure buildup data compared to converted drawdown data normally used for type curve analysis	44

LIST OF TABLES AND FIGURES (con't)

	Page
10. Actual pressure buildup data compared to converted drawdown data normally used for type curve analysis	45
11. Actual pressure buildup data compared to converted drawdown data normally used for type curve analysis	46
12. Actual pressure buildup data compared to converted drawdown data normally used for type curve analysis	47
13. Actual pressure buildup data compared to converted drawdown data normally used for type curve analysis	48
14. Actual pressure buildup data compared to converted drawdown data normally used for type curve analysis	49
15. Superposition and actual buildup solutions - Constant mass rate at the sand face.	53
16. Superposition and actual buildup solutions - Constant mass rate at the sand face.	54
17. Superposition and actual buildup solutions - Constant mass rate at the sand face.	55
18. Superposition and actual buildup solutions - Constant mass rate at the sand face.	56
19. Superposition and actual buildup solutions - Constant mass rate at the sand face.	57
20. Superposition and actual buildup solutions - Constant mass rate at the sand face.	58
21. Superposition and actual buildup solutions - Constant flow rate at the sand face.	59
22. Superposition and actual buildup solutions - Constant flow rate at the sand face.	60
23. Superposition and actual buildup solutions - Constant flow rate at the sand face.	61
24. Horner plot - Constant mass rate at the sand face	62
25. Horner plot - Constant mass rate at the sand face	63
26. Horner plot - Constant mass rate at the sand face	64

LIST OF TABLES AND FIGURES (con't)

	Page
27. Horner plot - Constant mass rate at the sand face	65
28. Horner plot - Constant flow rate at the sand face	66
29. Horner plot - Constant mass rate at the sand face	67
30. Horner plot - Constant mass rate at the sand face	68
31. Horner plot - Constant mass rate at the sand face	69
32. Horner plot - Constant mass rate at the sand face	70
33. Horner plot - Constant flow rate at the sand face	71
34. Horner plot - Constant flow rate at the sand face	72
35. Horner plot - Constant flow rate at the sand face	73
36. Effect of fracture position during the linear flow period.	76
37. Effect of fracture position during the linear flow period.	77
38. Effect of fracture position during the linear flow period.	78
39. Semilog plot of (P_{wf}) as a function of flow time - Constant mass rate at the sand face	83
40. Semilog plot of (P_{wf}) as a function of flow time - Constant mass rate at the sand face	84
41. Semilog plot of (P_{wf}) as a function of flow time - Constant mass rate at the sand face	85
42. Semilog plot of (P_{wf}) as a function of flow time - Constant mass rate at the sand face	86
43. Semilog plot of (P_{wf}) as a function of flow time - Constant mass rate at the sand face	87
44. Semilog plot of (m_{wf}) as a function of flow time - Constant mass rate at the sand face	88
45. Semilog plot of (P_{wf}) as a function of flow time - Constant flow rate at the sand face	89

LIST OF TABLES AND FIGURES (con't)

	Page
46. Semilog plot of (P_{wf}) as a function of flow time - Constant flow rate at the sand face	90
47. Semilog plot of (P_{wf}) as a function of flow time - Constant flow rate at the sand face	91

FIGURES

A-1 Cubic Elemental Volume of Flow System	109
A-2 Schematic of Reservoir Model.	110
A-3 Space-Time Grid Index System	111
B-1 The Relation of the Deviation Factor Z Function with Pressure for 0.7 Gravity Gas.	117
B-2 The Relation of the Compressibility Function with Pressure for a 0.7 Gravity Gas at Temperature 200°F	118
B-3 The Relation of the Viscosity Function with Pressure for 0.7 Gravity Gas at Temperature of 200°F	119
B-4 The Relation of the $m(p)$ Function with Pressure for a 0.7 Gravity Gas at Temperature of 200°F	120
B-5 The Relation of (μc) Function with $m(p)$ for 0.7 Gravity Gas at a Temperature of 200°F	121
C-1 Flow Chart of Numerical Model	122
C-2 Flow Chart of Numerical Model (con't)	123
C-3 Flow Chart of Numerical Model (con't)	124
C-4 Flow Chart of Numerical Model (con't)	125

ACKNOWLEDGEMENTS

The author's most sincere appreciation is expressed to Dr. Daniel M. Bass, Head of Petroleum Engineering Department, for acting as a thesis advisor and for his continuous attention and encouragement throughout this study. Also, the author would like to thank Dr. C.W. Van Kirk, Dr. D.W. Hilchie, Dr. R.S. Fisk, and Prof. D.I. Dickinson for serving as committee members and for their valuable suggestions.

The author is greatly obliged to the Libyan people for their financial support during the period of his graduate study.

INTRODUCTION

Hydraulic fracturing has become a standard well completion practice in low permeability reservoirs. As a result of a number of studies, an increase in understanding of fractured-well behavior has been obtained.

Transient pressure tests on fractured wells can overcome the objections to stabilize flow tests by indicating when a stable pressure gradient is reached.

The transient pressure test can be used to determine formation flow capacity and effective wellbore radius.

The slope of well pressure-time curve during the linear flow period has been used^{5,6} to determine the fracture length. Also, the slope and position of the transient pressure-log time may be used to determine the flow capacity and wellbore size after a sufficient lapse of time so that the pressure gradient in the vicinity of the fractures becomes constant.

All studies of the flow behavior for a fractured well consider vertical fractures which extend an equal distance on both sides of the wellbore.

The objectives of this study are:

1. Investigate possible effect of the practice of using a constant μc ,
2. Investigate possible effect of the practice of using superposition,
3. Investigate possible effect of fracture not being symmetrical,
4. Effect of constant rate and constant mass boundary conditions.

A numerical simulator of a fully implicit finite difference was derived to investigate this study.

REVIEW OF LITERATURE

It was recognized early that intercepting fractures can strongly affect the transient flow behavior of a well and as a consequence, the application of a classical method to the analysis of transient pressure data under this situation can produce erroneous results. Several methods were proposed in the past to solve this problem.

In 1968, Russel and Truitt⁴ presented a method to correct the results obtained from application of Horner's method¹¹ to the analysis of pressure build-up data. Tables of dimensionless wellbore pressure versus dimensionless time were presented for different values of fracture penetration.

In 1968, Clark⁵⁴ presented a method for analysis for pressure fall-off data in fractured injection wells. His work was based mainly on the work of Russell and Truitt⁴ and consisted of a combination of two graphical techniques: one based on linear flow theory (P_{ws} vs \sqrt{t}), and the other based on radial theory (P_{ws} vs $\log t$).

Also, in 1968, Millheim and Cichowicz⁵⁵ published a paper concerning the analysis of pressure transient data for a fractured gas well produced from a low permeability formation. They indicated that a well test duration of at least 24 hours might be required in order to establish transient radial flow conditions.

The effect of non-darcy flow on the behavior of fractured wells was studied by Wattenbarger and Ramey⁸. It was assumed that the non-darcy flow occurred in the formation, and it was found that the turbulence effect did not stabilize during the linear flow period. These authors showed that

the formation flow conductivity (Kh) may be underestimated if pressure data are affected by non-Darcy flow.

Raghaven, Cady, and Ramey⁵⁶ presented a detailed study of the method proposed by Russell and Truitt⁴. Furthermore, the applications of Miller, Dyes, and Hutchinson¹², Muskat⁹, and type-curve matching methods to the analysis of pressure data for fractured wells were examined thoroughly.

Gringarten, Ramey, and Raghaven^{5,30} published new information concerning the application of well test analysis to fractured wells. Three basic solutions were presented: namely, the infinite conductivity for vertical fractures and the uniform flux solution for vertical and horizontal fractures. These authors concluded that the use of the type-curve matching technique with classical methods allows a high confidence level in the interpretation of pressure data.

All of this previous work has increased significantly our understanding of transient fluid flow in hydraulically fractured wells. The Russell-Truitt⁴ studies showed that conventional pressure build-up analysis of data from these wells would yield, under certain circumstances, fairly good estimates of reservoir permeability-thickness and average pressure. They pointed out that the effect of a vertical fracture (in absence of other effects such as formation damage by fracturing fluids) is to cause calculation of a negative pseudo-skin factor from pressure build-up analysis. They also provide a means of estimating fracture half-length. Millheim and Cichowicz⁵⁵ demonstrated that reservoir effective permeability, turbulence coefficient, effective fracture flow area, and fracture efficiency could be obtained from constant rate drawdown testing of vertically fractured low-permeability gas wells. The recent work of Gringarten et al.^{5,30} has provided a sound basis for short-term analysis. Using type-curve

procedures, it is possible to determine the end of the linear flow period and start of the proper semilog straight line on a Horner¹¹ plot.

Principle of Superposition

When fluid flow is described by a linear differential equation and boundary conditions, the principle of superposition and dimensionless variables can be used to reduce the number of solutions required for different magnitudes of the absolute physical parameters. Basically the principle of superposition states that:

If F is the desired solution to a homogeneous,
linear, partial differential equation and $c_1 f_1$,
 $c_2 f_2 \dots c_n f_n$ are known particular solutions
then

$$F = c_1 f_1 + c_2 f_2 + \dots + c_n f_n$$

where c_1, c_2, \dots, c_n are constants required to satisfy the boundary conditions.

When the boundary conditions are time independent, constant production rate case, the principle of superposition shows that the presence of one boundary condition does not affect the response as long as the initial conditions and other boundary conditions are of the same type.

Therefore, there are no interactions among the various responses. The total effect and the solution for the new boundary condition is the sum of the individual effects.

When the boundary conditions are time dependent, variable production rate, an extension of the principle of superposition, known as Duhamel's

theorem can be used.

MATHEMATICAL DEVELOPMENT

The mathematical representation of the fundamental flow equations which describe the flow of fluids through porous media is based upon three basic laws. These three fundamental relationships are the law of conservation of matter, the law of motion as stated by Darcy's Law, and the equation of state which defines the thermodynamic behavior of the system. The forthcoming development of the equations describing the flow in a natural gas reservoir is based upon the following assumptions:

- (1) Real gas of constant composition;
- (2) Reservoir thickness is constant;
- (3) Flow is single-phase, two-dimensional, and isothermal;
- (4) Reservoir rock properties are independent of time, pressure, and spatial location.

Appendix A contains a complete derivation of the governing flow equation.

Continuity Equation

Mathematical equations describing the single-phase flow of gas must be based on the principle of the conservation of matter, that is, mass can neither be created nor destroyed. Matter can be conserved or accounted for by the relationship (Figure A-1 of Appendix A)

$$\text{mass in} - \text{mass out} = \text{mass change} \quad \dots (1)$$

The mathematical expression for this statement of the conservation of

matter is the familiar continuity equation

$$\nabla (\rho V) = - \frac{\partial(\rho\phi)}{\partial t} , \quad . . (2)$$

Where

ρ = fluid density,

V = flow velocity,

ϕ = porosity,

t = time, and

∇ = divergence operator.

Darcy's Law

For the conditions of laminar flow the velocity term in Equation (2) is defined by Darcy's law as (for negligible inertia forces)

$$V = - \frac{K}{\mu} \nabla P, \quad . . (3)$$

Where

K = reservoir permeability,

μ = fluid viscosity, a function of pressure only for isothermal flow, and

P = pressure.

Permeability is considered independent of gas pressure.

Making use of Darcy's law in rewriting the continuity equation and assuming porosity to be independent of pressure, that is, neglecting rock compressibility, gives

$$\nabla \left(\frac{\rho K \nabla P}{\mu} \right) = \phi \frac{\partial \rho}{\partial t} . \quad . . (4)$$

Equation of State

For ease in handling Equation (4), it is necessary to express density, ρ , in terms of pressure. The relationship between density and pressure can be derived from the gas law for real gas, which is

$$PV = ZnRT, \quad \dots (5)$$

Where

V = volume of gas,

Z = gas compressibility factor,

n = moles of gas,

R = universal gas constant, and

T = absolute temperature.

If the gas density is expressed in terms of the equation of state, as shown in Appendix A, Equation (4) can be rewritten as

$$\nabla \left(\frac{KP \nabla P}{\mu Z} \right) = \phi \frac{\partial(P/Z)}{\partial t} \quad \dots (6)$$

Real-Gas Pseudo-Pressure

For the development of a rigorous diffusivity equation which is not based on the assumptions of small pressure gradients or small changes in gas viscosity and deviation factor, an Equation presented by Al-Hussainy et al⁵⁹ converts pressure to the real-gas pseudo-pressure by defining (excluding their factor of two)

$$m = \int_{P_1}^{P_2} \frac{P'}{\mu Z} dP', \quad \dots (7)$$

Where

m = real-gas pseudo-pressure,

P_1 = the lower pressure at which m is evaluated, and

P_2 = the upper pressure at which m is evaluated.

From the definition given in Equation (7) it follows that

$$\frac{\partial(P/Z)}{\partial t} = \mu c \frac{\partial m}{\partial t}, \quad \dots (8)$$

Where

$$c = \frac{1}{P} - \frac{1}{Z} \frac{dZ}{dP} = \text{gas compressibility}$$

Also,

$$\nabla m = \frac{P \nabla P}{\mu Z} \quad \dots (9)$$

Diffusivity Equation

Rewriting Equation (6) in terms of equations (8) and (9) results in

$$\nabla (\nabla m) = \frac{\phi \mu c}{K} \frac{\partial m}{\partial t} \quad \dots (10)$$

It is important to note that the development of Equation (10), the diffusivity equation in terms of the real-gas pseudo-pressure, involved no simplified assumptions of small pressure gradients or small changes in gas viscosity and deviation factor.

Equation (10) is a second-order non-linear partial differential equation; non-linear because the coefficients μ and c are functions of the real-gas pseudo-pressure m . Analytic solution of this equation is impossible with existing methods, therefore, an approximation to the solution is made using numerical finite-difference techniques.

Finite Difference

Figure (A-2) in Appendix A shows a schematic of the flow system divided into rectangular blocks. When Equation (10) is discretized in time and space and written in finite-difference form for any block (i,j) (for the two dimensional case on the assumption that no source or sink exists), it appears as Equation (11).

$$\begin{aligned}
 & \frac{\frac{m_{i+1,j}^{n*} - m_{i,j}^{n*}}{X_{i+1} - X_i} - \frac{m_{i,j}^{n*} - m_{i-1,j}^{n*}}{X_i - X_{i-1}}}{X_{i+\frac{1}{2}} - X_{i-\frac{1}{2}}} \\
 & + \frac{\frac{m_{i,j+1}^{n*} - m_{i,j}^{n*}}{Y_{j+1} - Y_j} - \frac{m_{i,j}^{n*} - m_{i,j-1}^{n*}}{Y_j - Y_{j-1}}}{Y_{j+\frac{1}{2}} - Y_{j-\frac{1}{2}}} \\
 & = \frac{\phi(\mu c)}{K} i,j^{n*} \frac{m_{i,j}^{n+1} - m_{i,j}^n}{\Delta t} \quad \dots (11)
 \end{aligned}$$

The time level n^* at which to evaluate the m 's in the left-hand side and the ' μc ' product on the right-hand side of Equation (11) must be specified. The simplest choice is to set $n^* = n$ in both sides of Equation (11). The equation would then be explicit and easily evaluated, but it would be restricted by the time-step size limitation required for solution. This time-step size limitation required for stability can be removed if the m 's on the left-hand side of Equation (11) are evaluated at $n+1$. If the time level for the coefficient ' μc ' is also set at $n+1$, then Equation (11) would be fully implicit, which is desirable for several reasons. The primary one is to obtain unconditional stability.

With the time level $n+1$ for evaluating both the m 's on the left-hand side and the coefficient ' μc ' on the right-hand side, Equation (11) can be rewritten as

$$\begin{aligned}
 & \left[\frac{\frac{m_{i+1,j}^{n+1} - m_{i,j}^{n+1}}{X_{i+1} - X_i} - \frac{m_{i,j}^{n+1} - m_{i-1,j}^{n+1}}{X_i - X_{i-1}}}{X_{i+\frac{1}{2}} - X_{i-\frac{1}{2}}} \right. \\
 & \left. + \frac{\frac{m_{i,j+1}^{n+1} - m_{i,j}^{n+1}}{Y_{j+1} - Y_j} - \frac{m_{i,j}^{n+1} - m_{i,j-1}^{n+1}}{Y_j - Y_{j-1}}}{Y_{j+\frac{1}{2}} - Y_{j-\frac{1}{2}}} \right] K \\
 & = \phi (\mu c)_{i,j}^{n+1} \frac{m_{i,j}^{n+1} - m_{i,j}^n}{\Delta t} \quad \dots (12)
 \end{aligned}$$

Equation (12) is the finite-difference equation used in this study to describe the flow of a real gas, subject to the conditions stated throughout the preceding development.

Where

i = spatial index in X - direction,

j = spatial index in Y - direction,

$i+\frac{1}{2}, j$ = the representative value between blocks (i, j) and $(i+1, j)$,

$i, j+\frac{1}{2}$ = the representative value between blocks (i, j) and $(i, j+1)$,

$$X_{i+\frac{1}{2}} = X_i + \frac{X_{i+1} - X_i}{2} ,$$

$$X_{i-\frac{1}{2}} = X_i - \frac{X_i - X_{i-1}}{2},$$

$$Y_{j+\frac{1}{2}} = Y_j + \frac{Y_{j+1} - Y_j}{2},$$

$$Y_{j-\frac{1}{2}} = Y_j - \frac{Y_j - Y_{j-1}}{2},$$

n = time level at beginning of time step,

$n+1$ = time level at end of time step,

n^* = time level where $n^* = n$ or

$$n^* = n + \frac{1}{a} \text{ for } a \geq 1, \text{ and}$$

Δt = size of time step, $t^{n+1} - t^n$.

Appendix A presents the steps between Equations (10) and (11).

Finite-Difference Equation in its Application Form

Equation (12) must be worked into a more usable form to facilitate its handling and solution within the computer. The approach taken here is to represent both sides of the equation in units of million standard cubic feet per day, MMSCF/D**.

The pore volume of any block (i,j) is

$$V_{p_{i,j}} = \Delta X_i \Delta Y_j h \phi \quad \dots (13)$$

Since ϕ already appears on the right-hand side of Equation (12), then multiplying both sides by $\Delta X_i \Delta Y_j h$ gives

$$\Delta X_i \Delta Y_j K h (\text{LHS})^{n+1} = V_{p_{i,j}} (\mu c)_{i,j}^{n+1} \left[\frac{(m_{i,j}^{n+1} - m_{i,j}^n)}{\Delta t} \right] \dots (14)$$

** Standard conditions are 60°F and 14.7 Psia.

The right-hand side of Equation (14) can be converted to units of MMSCF/D by multiplying through by the factor

$$FA = \frac{T_{sc}}{10^6 TP_{sc}}, \quad \dots (15)$$

Where

T_{sc} = absolute temperature at standard conditions, $^{\circ}R$,

T = absolute temperature at reservoir conditions, $^{\circ}R$,
and

P_{sc} = pressure at standard conditions, psia.

The left-hand side of Equation (14) can be expressed in units of MMSCF/D if an additional factor of 0.006328 is applied to the permeability terms. Equation (14) can now be written in units of MMSCF/D as

$$\begin{aligned} (FA) (0.006328) (\Delta X_i \Delta Y_j h) K & \left[\frac{\frac{m_{i+1,j}^{n+1} - m_{i,j}^{n+1}}{X_{i+1} - X_i} - \frac{m_{i,j}^{n+1} - m_{i-1,j}^{n+1}}{X_i - X_{i-1}}}{X_{i+\frac{1}{2}} - X_{i-\frac{1}{2}}} + \right. \\ & \left. \frac{\frac{m_{i,j+1}^{n+1} - m_{i,j}^{n+1}}{Y_{j+1} - Y_j} - \frac{m_{i,j}^{n+1} - m_{i,j-1}^{n+1}}{Y_j - Y_{j-1}}}{Y_{j+\frac{1}{2}} - Y_{j-\frac{1}{2}}} \right] \\ & = (FA) V_{p_{i,j}} (\mu c)_{i,j}^{n+1} \left[\frac{m_{i,j}^{n+1} - m_{i,j}^n}{\Delta t} \right], \quad \dots (16) \end{aligned}$$

Where

K = permeability, md,

V_p = pore volume, cu. ft.,

μ = gas viscosity, cp ,

c = gas compressibility, 1/psia ,

Δt = time-step size, days ,

m = real-gas pseudo-pressure, psia²/cp,

FA = constant, 1/psia ,

h = reservoir thickness, ft.,

$$\Delta X_i = X_{i+1/2} - X_{i-1/2} = \frac{X_{i+1} - X_{i-1}}{2}, \text{ and} \quad \dots (17)$$

$$\Delta Y_j = Y_{j+1/2} - Y_{j-1/2} = \frac{Y_{j+1} - Y_{j-1}}{2} \quad \dots (18)$$

For simplification in writing these Equations, let

$$A_{i,j} = \frac{\Delta Y_j}{X_{i+1} - X_i}, \quad \dots (19)$$

$$B_{i,j} = \frac{\Delta Y_j}{X_i - X_{i-1}}, \quad \dots (20)$$

$$C_{i,j} = \frac{\Delta X_i}{Y_{j+1} - Y_j}, \quad \dots (21)$$

$$D_{i,j} = \frac{\Delta X_i}{Y_j - Y_{j-1}}, \text{ and} \quad \dots (22)$$

$$G_{i,j} = \frac{\phi \Delta X_i \Delta Y_j h}{0.006328 K} \quad \dots (23)$$

Substitution of Equations (17), (18), (19), (20), (21), (22), and (23) into (16) and rearrangement gives

$$A_{i,j} (m_{i+1,j}^{n+1} - m_{i,j}^{n+1}) - B_{i,j} (m_{i,j}^{n+1} - m_{i-1,j}^{n+1})$$

$$\begin{aligned}
& + C_{i,j} (m_{i,j+1}^{n+1} - m_{i,j}^{n+1}) - D_{i,j} (m_{i,j}^{n+1} - m_{i,j-1}^{n+1}) \\
& = G_{i,j} \frac{\mu c}{\Delta t} (m_{i,j}^{n+1} - m_{i,j}^n) \quad . \quad . \quad (24)
\end{aligned}$$

Equation (24) is the finite-difference equation in the two dimensional form with unequally spaced intervals describing the flow among blocks in MMSCF/D.

Equation (24) can be written as

$$\begin{aligned}
& A_{i,j} m_{i+1,j}^{n+1} - (A_{i,j} + B_{i,j}) m_{i,j}^{n+1} + B_{i,j} m_{i-1,j}^{n+1} \\
& + C_{i,j} m_{i,j+1}^{n+1} - (C_{i,j} + D_{i,j}) m_{i,j}^{n+1} + D_{i,j} m_{i,j-1}^{n+1} \\
& = G_{i,j} \frac{(\mu c)_{i,j}^{n+1}}{\Delta t} (m_{i,j}^{n+1} - m_{i,j}^n) \quad . \quad . \quad (25)
\end{aligned}$$

Boundary Conditions

In addition to the non-linear partial differential equation for flow of real gas through porous media, boundary conditions have to be considered in order to complete the mathematical formulation.

1. Boundary condition at the wellbore

A constant mass rate was established by specifying an initial rate in MMSCF at time zero and holding it unchanged throughout the flowing period of the well. This results in a constant mass flow rate at the inner boundary of the reservoir and a constant flow rate at surface conditions. This can be expressed mathematically as:

$$q_{sc} = \frac{2KhT_{sc}}{P_{sc}T} \int_0^{L_f} \left(\frac{\partial m}{\partial y} \right)_{y=0} dx \quad . \quad . \quad (26-a)$$

The constant flow rate at the sand face can be expressed mathematically as:

$$q = 2Kh \int_0^{L_f} \left(\frac{Z}{P} \cdot \frac{\partial m}{\partial y} \right)_{y=0} dx \quad . \quad . \quad (26-b)$$

2. Boundary condition at the reservoir outer boundary:

The condition of no flow across the outer boundary was considered, which can be expressed as:

$$\left(\frac{\partial m}{\partial x} \right)_{x_e} = 0, \text{ and} \quad . \quad . \quad (27)$$

$$\left(\frac{\partial m}{\partial y} \right)_{y_e} = 0. \quad . \quad . \quad (28)$$

3. Boundary condition at the reservoir fracture:

The condition of no pressure gradient within the fracture was considered, which can be expressed mathematically as:

$$m(x,0,t) = m(t)_{\text{wellbore}} \quad 0 \leq x \leq L_f, \quad t \geq 0.$$

Initial Condition

For all boundary conditions discussed above an initial condition of constant pressure was assumed throughout the reservoir, i.e.

$$m(x,y,0) = m_i, \quad . \quad . \quad (29)$$

Where

m_i = initial real-gas pseudo-pressure, psia^2/cp .

COMPUTER MODEL

A single-phase, two-dimensional reservoir simulator was used in this research. The reservoir was divided into a system of grid blocks and a differential equation for each cell was written which describes the fluid flow in that cell. The equations for each cell form a set of simultaneous partial differential equations which can be solved for based on pressure at the wellbore. These differential equations are approximated by a finite difference technique. To determine the desired element size for the model, solutions were made with decreasing element size until further decreases in size had essentially no affect on the calculated pressure. Increasing the number of elements beyond 36×15 resulted in a maximum change in the calculated pressure values of less than 0.1 percent.

The revised alternating directional implicit method was used without an iteration parameter. The computation time was superior to the Peaceman and Rachford⁴¹ method of using half time steps, and the revised ADIP method was stable.

Flow charts for the two-dimensional computer model are shown in Figures C-1, C-2, C-3, and C-4, (see Appendix C).

Assumptions

For the model under consideration, the following assumptions are made about the rock and fluid properties and the flow:

1. Flow of real gas.
2. Isotropic rock properties.

3. Horizontal flow, no gravity effect.
4. No Klinkenberg⁶⁰ effect.
5. Gas saturation = 100% of pore volume.
6. The effects of pressure drop within the fracture and production into the wellbore other than from the fracture are neglected.
7. The drainage area of the well is assumed to take the form of a square as shown in Figure 1.

Grid System

To achieve results of acceptable precision it is necessary to use small dimensions in the vicinity of any discontinuity such as the edge or end of the fracture. Larger dimensions were acceptable at greater distances from these discontinuities.

The length of each successive element was increased exponentially in the direction of the reservoir boundary. The pattern of the grid in Figure (2) illustrates the configuration used in this study.

Method of Solution

Because of poor stability, explicit difference methods are rarely used to solve initial boundary value problems in two or more space dimensions. The use of implicit difference equations is motivated by several desires. The primary one is to obtain unconditional stability with less computer time. However, as a practical matter, it is highly desirable that the resulting simultaneous equations for a single space variable satisfy these wishes reasonably well, the implicit equations so far considered for two or more space variables yield systems of equations

that are quite difficult to solve.

Some iterative methods, particularly the alternating-direction implicit methods, are restricted primarily to parabolic-type problems having constant grid cell dimensions and flow coefficients. For problems of variable element dimensions and flow coefficients the alternating-direction explicit method becomes unstable. Several techniques were tried for solving the matrix equation. The revised alternating-direction implicit procedure (ADIP) method was found to be stable and effective.

This method has been used extensively for flow in rectangles, such as in the x, y plane. The method consists of solving the matrix by first solving implicitly in the x-direction and then re-solving implicitly in the y-direction. That is, it is first assumed that the second derivative in the y-direction is known (from the previous iteration) and the resulting tri-diagonal matrix is solved by the Thomas algorithm. Then it is assumed that the second derivative in the x-direction is known. The matrix is re-arranged and the resulting tri-diagonal matrix is solved by the Thomas algorithm. This procedure can be written for Equation (25) as follows:

$$\begin{aligned} & \left[A_{i,j} m_{i+1,j}^{n+1} - (A_{i,j} + B_{i,j}) m_{i,j}^{n+1} + B_{i,j} m_{i-1,j}^{n+1} \right]^{(K+\frac{1}{2})} + \\ & \left[C_{i,j} m_{i,j+1}^{n+1} - (C_{i,j} + D_{i,j}) m_{i,j}^{n+1} + D_{i,j} m_{i,j-1}^{n+1} \right]^{(K)} = \\ & G_{i,j} (\mu c)_{i,j}^{n+1} \frac{1}{\Delta t} \left(m_{i,j}^{(K+\frac{1}{2})} - m_{i,j}^n \right), \quad \dots (30-a) \end{aligned}$$

$$\begin{aligned}
& \left[A_{i,j} m_{i+1,j}^{n+1} - (A_{i,j} + B_{i,j}) m_{i,j}^{n+1} + B_{i,j} m_{i-1,j}^{n+1} \right]^{(K+1)} + \\
& \left[C_{i,j} m_{i,j+1}^{n+1} - (C_{i,j} + D_{i,j}) m_{i,j}^{n+1} + B_{i,j} m_{i,j-1}^{n+1} \right]^{(K+\frac{1}{2})} = \\
& G_{i,j}(\mu)_{i,j}^{n+1} \frac{1}{\Delta t} \left(m_{i,j}^{(K+1)} - m_{i,j}^{(K)} \right), \quad \dots (30-b)
\end{aligned}$$

Where K and K+1 refer to successive iterations.

The $K+\frac{1}{2}$ is an intermediate solution. Equations (30-a) and (30-b) are solved alternately until a successive solution of Equation (30-b) varies less than 0.001% at every mesh point.

The ADIP method of Equations (30) is similar to that presented by Douglas, Peaceman and Rachford³⁴ in 1959. This is a revision of the original Peaceman and Rachford⁴¹ technique.

Validity of the Model

Although no analytical solution exists for the flow of real gas, a solution does exist if the coefficients viscosity (μ) and compressibility (c) are considered to be independent of pressure. Al-Hussainy and Rameev (1966) present an analytical solution for this assumption of constant coefficients.

$$\begin{aligned}
m_{wf} = m_i - \frac{28,960 q_{sc} T_{sc}^{TP}}{Kh T_{sc}} & \left(\log \left(\frac{0.000264 Kt}{\phi \mu_i c_i r_w^2} \right) \right. \\
& \left. + .3513 \right), \quad \dots (31)
\end{aligned}$$

Where

μ_i = viscosity at initial reservoir pressure,

c_i = compressibility at initial reservoir pressure.

With the model treating the coefficients as constants and considering a well that has not been fractured, the wellbore is treated as a fracture extending an equal distance of 0.33 feet on both sides of the well axis. Table 1 shows the close agreement between the computer solution in this study and the solution computed from Equation (31).

When a fracture extends an equal distance on both sides of the well axis, the model solution using μ_i and c_i in the coefficient was compared to numerical solutions published by Russell and Truitt⁴ for the flow of liquid into a vertical fracture. Figure 3 shows the close agreement between the two solutions. These checks give confidence in the computer programs and in the method of solution.

From the numerical model the following observations were made:

1. The fully implicit difference equation is stable in all cases.
When the coefficient (μc) is evaluated at the beginning of each time step so that the equation is not fully implicit the solution is stable only for extremely small time steps, approximately 10^{-8} hours;
2. The fully implicit equation has lower truncation error than the implicit-explicit equation, permitting larger time steps to be taken;
3. The computation time for the fully implicit equation is three to four times that of the mixed equation per time step solution;
4. The fully implicit equation permitted the time step size to be 10^8 greater than the time step size for the explicit equation; and
5. Successively small elements around the fracture and fully implicit difference equation are recommended to simulate fractured gas reservoirs.

TABLE 1

Comparison between Computer Solution
and Solution Obtained from Equation 31

$P_i = 5000$ Psia, $T = 660^\circ\text{R}$, $r_w = 0.33$ ft., $q_{sc} = 0.01$ MMSCF/D/ft.,
 $K = 1.0$ md, $p_{sc} = 14.7$ Psia, $T_{sc} = 520^\circ\text{R}$.

Time Hours	Computer Solution $m(p)$, 10^9 Psia ² /cp	Solution Obtained From Equation 31 $m(p)$, 10^9 Psia ² /cp
1.0	0.63823	0.637122
3.0	0.63565	0.630956
5.0	0.63445	0.630121
9.0	0.63308	0.628791
11.0	0.63760	0.625682
15.0	0.63188	0.623219
25.0	0.63068	0.621284
29.0	0.63033	0.619327
35.0	0.62976	0.617216

$$R_f = \frac{L_{f1}}{L_{f2}}$$

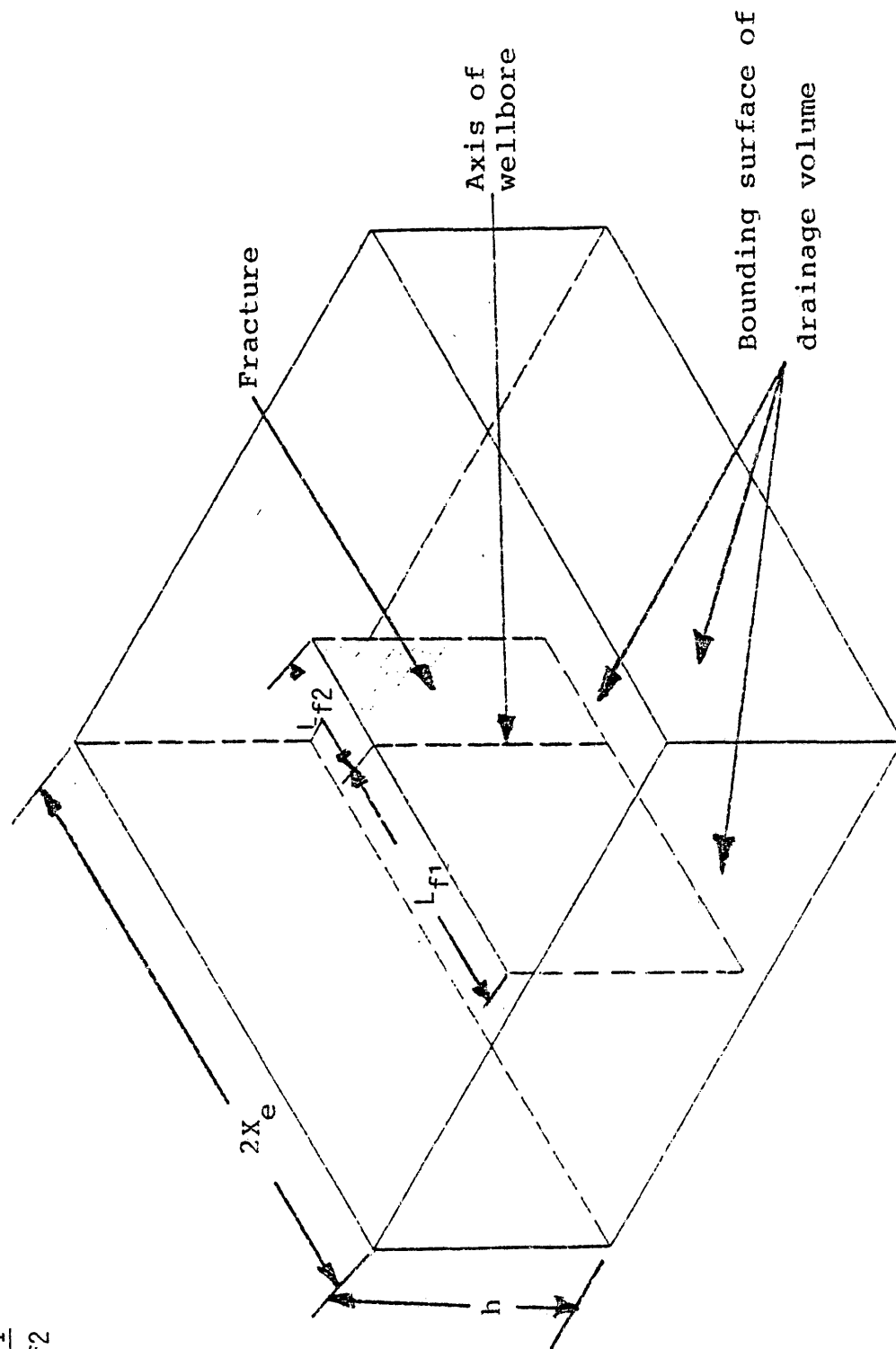


Figure 1. Schematic sketch of vertical fracture flow model.

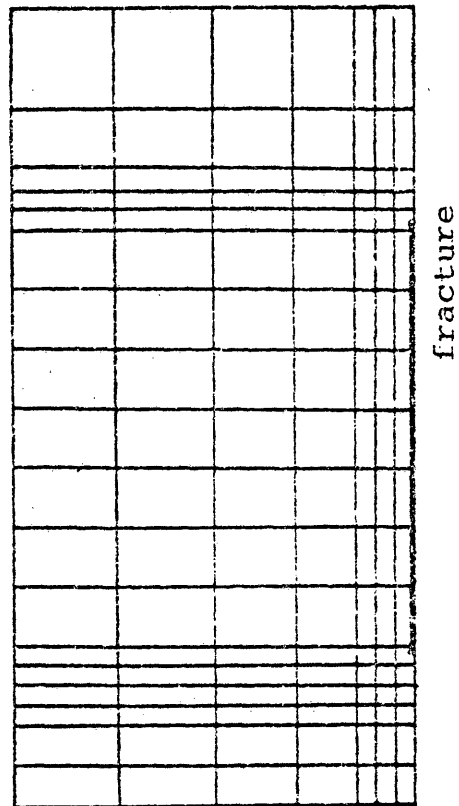
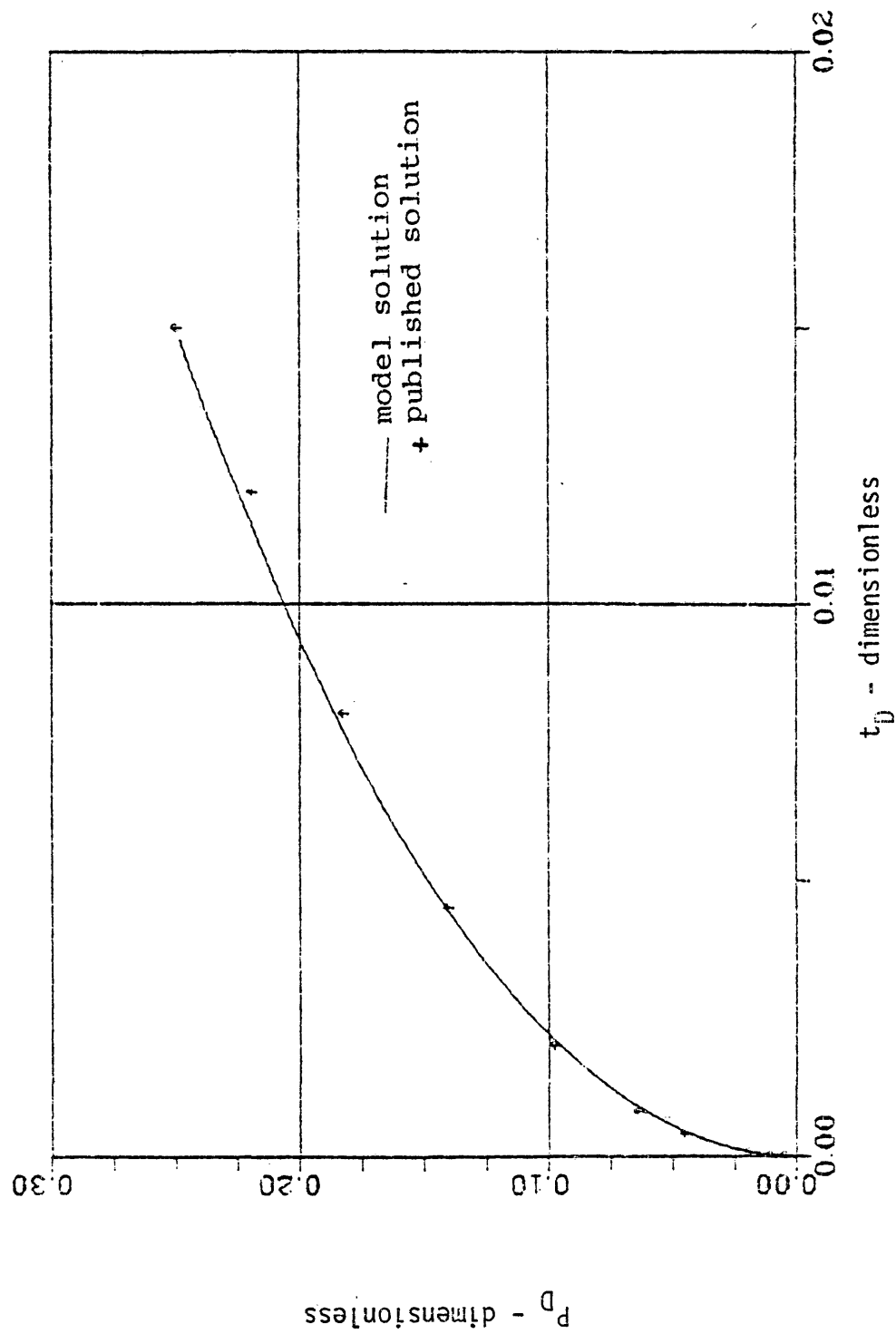


Figure 2. Grid pattern for modeling a vertically fractured gas reservoir.

Figure 3. Comparison between published solution⁴ and model solution for liquid case.



RESULTS

The numerical model was run under two wellbore boundary conditions:

1. Constant mass rate at the sand face,
2. Constant flow rate at the sand face.

Model properties common to all runs are listed in Table 2.

For various cases listed in Table 3 the model was solved with viscosity and compressibility varying as a function of pressure in the $m(p)$ function and held constant at the initial condition in the time coefficient.

Other cases were solved with the viscosity and compressibility varying as a function of pressure in both the time coefficient and the $m(p)$ function.

Tables 4 and 5 represent a model solution for two different cases.

TABLE 2

Input data which were held constant

Well Spacing	160 acres
Gas Gravity	0.7 (air = 1.0)
Original Reservoir	
Pressure	2000 and 5000 psia
Net Porosity	14%
Bottom Hole Temperature	200°F
Total Fracture length, L_f	200, 600, 1200 and 1320 ft.
R_f	0.0, 0.5 and 1.0 (see Figure 1 for definition of R_f)

TABLE 3

Data Sets used by Numerical Model

Data Set	q_{sc} MMSCF/D/ft	K md	P_i psia	L_f ft	R_f
1	0.01	1.0	5000	200	0.0
2	0.01	1.0	5000	200	0.5
3	0.01	1.0	5000	200	1.0
4	0.01	1.0	5000	600	0.0
5	0.01	1.0	5000	600	0.5
6	0.01	1.0	5000	600	1.0
7	0.01	1.0	5000	1200	0.0
8	0.01	1.0	5000	1200	0.5
9	0.01	1.0	5000	1200	1.0
10	0.01	1.0	5000	1320	1.0
11	0.01	10.0	5000	1320	1.0
12	0.01	20.0	5000	1320	1.0
13*	0.01	1.0	5000	1320	1.0
14*	0.01	10.0	5000	1320	1.0
15*	0.01	20.0	5000	1320	1.0
16*	0.01	1.0	5000	1320	1.0
17	0.01	20.0	5000	1320	1.0
18	0.2	20.0	5000	1320	1.0
19*	0.2	1.0	5000	1320	1.0
20	0.01	0.1	5000	200	1.0
21	0.01	1.0	2000	200	1.0
22	0.01	1.0	5000	200	1.0
23**	0.01	1.0	5000	200	1.0
24	0.02	0.1	2000	200	1.0

Table 3 (continued)

Data Set	q_{sc} MMSCF/D/ft	K md	P_i Psia	L_f ft	R_f
25**	0.01	1.0	2000	200	1.0
26	0.05	0.1	2000	200	1.0
27	0.05	1.0	5000	200	1.0
28**	0.02	1.0	5000	200	1.0

* Constant (μc) within the model,

** Constant flow rate at the sand face.

TABLE 4

Sample of Computer Solution
Constant Mass Rate at the Sand Face

$q_{sc} = 0.01$ MMSCF/D/ft., $K = 1.0$ md, $L_f = 200$ ft.,

$R_f = 1.0$, $P_i = 5000$ Psia

Drawdown Solution

<u>Time Hours</u>	<u>m(p) Psia²/cp</u>
2.000000	0.64853E+09
6.600000	0.64725E+09
11.200000	0.64645E+09
15.800000	0.64583E+09
20.400000	0.64539E+09
25.000000	0.64495E+09
29.600000	0.64460E+09
34.200000	0.64424E+09
38.800000	0.64398E+09
43.400000	0.64371E+09
48.000000	0.64349E+09
51.200000	0.64324E+09
104.400000	0.64155E+09
177.500000	0.64084E+09
220.800000	0.64049E+09
264.000000	0.63996E+09
307.200000	0.63950E+09
350.399990	0.63925E+09
393.500000	0.63890E+09
436.800000	0.63872E+09
480.000000	0.63854E+09
539.999990	0.63819E+09
599.999990	0.63783E+09

Buildup Solution $t_f + \Delta t$ Hours $m(p)$ Psia²/cp $t_f = 48$ Hours

49.000000
50.000000
55.000000
60.000000
75.000000
90.000000
105.000000
120.000000

0.64455E+09
0.64508E+09
0.64597E+09
0.64650E+09
0.64738E+09
0.64773E+09
0.64809E+09
0.64826E+09

 $t_f = 2$ Hours

3.000000
4.000000
9.000000
14.000000
29.000000
44.000000
59.000000
74.000000

0.64924E+09
0.64941E+09
0.64959E+09
0.64977E+09
0.64994E+09
0.64996E+09
0.64998E+09
0.65000E+09

 $t_f = 480$ Hours

431.000000
482.000000
467.000000
492.000000
507.000000
522.000000
537.000000
552.000000

0.63960E+09
0.64013E+09
0.64119E+09
0.64190E+09
0.64296E+09
0.64364E+09
0.64437E+09
0.64473E+09

TABLE 5

Sample of Computer Solution
Constant Flow Rate at the Sand Face

$q_{sci} = 0.01$ MMSCF/D/ft., $K = 1.0$ md, $L_f = 200$ ft.,

$R_f = 1.0$, $p_i = 2000$ Psia

Drawdown Solution

<u>Time Hours</u>	<u>m(p) Psia²/cp</u>
2.000000	0.14674E+09
6.500000	0.14576E+09
11.200000	0.14511E+09
15.900000	0.14459E+09
20.400000	0.14420E+09
25.000000	0.14387E+09
29.600000	0.14361E+09
34.200000	0.14335E+09
38.300000	0.14309E+09
43.400000	0.14290E+09
48.000000	0.14270E+09
51.200000	0.14252E+09
134.400000	0.14075E+09
177.600000	0.14010E+09
220.800000	0.13953E+09
264.000000	0.13919E+09
307.200000	0.13893E+09
350.399990	0.13854E+09
393.600000	0.13827E+09
436.300000	0.13801E+09
480.000000	0.13775E+09
539.999990	0.13749E+09
599.999990	0.13723E+09

Buildup Solution

<u>$t_f + \Delta t$ Hours</u>	<u>$m(p)$ Psia²/cp</u>
<u>$t_f = 2$ Hours</u>	
3.000000	0.147265E+09
4.000000	0.14739E+09
9.000000	0.14752E+09
14.000000	0.14765E+09
29.000000	0.14778E+09
44.000000	0.14791E+09
59.000000	0.14805E+09
74.000000	0.14819E+09

$t_f = 48$ Hours

49.000000	0.14348E+09
50.000000	0.14387E+09
55.000000	0.14452E+09
60.000000	0.14505E+09
75.000000	0.14557E+09
90.000000	0.14596E+09
105.000000	0.14622E+09
120.000000	0.14635E+09

$t_f = 480$ Hours

481.000000	0.13854E+09
482.000000	0.13893E+09
487.000000	0.13984E+09
492.000000	0.14049E+09
507.000000	0.14140E+09
522.000000	0.14205E+09
537.000000	0.14257E+09
552.000000	0.14298E+09

DISCUSSION OF RESULTS

A. Real-Gas Pseudo-Pressure Function

The variation of the product (μc) with the $m(p)$ function, Figure (B-5) Appendix B, prevents the $m(p)$ function substitution from linearizing the diffusivity equation. It has been a common practice to treat (μc) as a constant in the time coefficient in order to linearize the equation and permit solution by integration.

Figure 4 illustrates the computed results when the quantity (μc) is held constant in the time coefficient and when it is permitted to vary in the time coefficient with pressure.

The solution when the coefficient (μc) in the time coefficient is constant results in a higher sand face pressure at any time than the solution with a varying time coefficient.

The reason for this divergence is because the quantity ($\mu c/\mu_i c_i$) gets much greater than one as the pressure decreases with time.

B. Theory of Dimensionless Variables

Dimensionless variables have been introduced to the theory of differential equations in order to make the solution independent of the actual values of the various parameters of which constitute a real system.

To achieve this for the flow of real gas in porous media, a suitable definition of three dimensionless variables, m_D , t_D and q_D , has been introduced such that the dimensionless differential equation and the

relevant boundary conditions can be solved once in terms of dimensionless variables for all possible values of the actual parameters. The dimensionless variables defined in the literature⁵ for the flow of real gas in porous media are presented in Equations 32-36.

$$m_D = \frac{T_{sc} Kh(m_i - m)}{P_{sc} T q_{sc}} = \frac{1 - \frac{m}{m_i}}{q_D}, \quad \dots (32)$$

$$q_D = \frac{q_{sc} P_{sc} T}{T_{sc} m_i Kh}, \quad \dots (33)$$

$$t_{Dw} = \frac{Kt}{\phi(\mu c)_i x_w^2}, \quad \dots (34)$$

$$x_D = \frac{x}{x_w}, \quad \dots (35)$$

$$y_D = \frac{y}{y_w}, \quad \dots (36)$$

The general differential equation for the flow of real gas is:

$$\frac{\partial^2 m}{\partial x^2} + \frac{\partial^2 m}{\partial y^2} = \frac{\mu c \phi}{K} \frac{\partial m}{\partial t} \quad \dots (37)$$

Substituting Equations 32, 33, 34, 35 and 36 into Equation 37 results in:

$$\frac{\partial^2 m_D}{\partial x_D^2} + \frac{\partial^2 m_D}{\partial y_D^2} = \frac{\mu c}{(\mu c)_i} \frac{\partial m_D}{\partial t_{Dw}} \quad \dots (38)$$

Because the quantity (μc) varies with m_D , a functional relationship exists between the time coefficient and m_D this leads to a non-linear diffusivity equation in terms of the given dimensionless variables which

means Equation 38 can not be solved independent of the actual parameters in the definition of m_D i.e. q_D .

Based on solutions, when μc in the time coefficient is permitted to vary, the values of wellbore pressure are not independent of the values of the parameters used to define t_D , q_D and m_D .

The deviation because of changes in permeability are illustrated in Figure 5, it is noted that the effect of the variation in (μc) decreases as the permeability increases. At value of permeability of 1 md the permeability calculated based on $(\mu c)/(\mu c)_i = 1$ is 10% lower than the real value. At value of permeability of 10 md the calculated permeability for $(\mu c)/(\mu c)_i = 1$ is 9% lower and for a permeability of 20 md the calculated permeability for $(\mu c)/(\mu c)_i = 1$ is 7% lower than the real value.

The deviation in the calculated model performance because of changes in flow rate are illustrated in Figure 6, it is noted that the effect of not considering the variation in (μc) decreases as the flow rate decreases. At value of flow rate of 0.2 MMSCF/D/ft. the calculated permeability for $(\mu c)/(\mu c)_i = 1$ is 10% lower than the real value. At value of flow rate of 0.01 MMSCF/D/ft. the calculated permeability for $(\mu c)/(\mu c)_i = 1$ is 8% lower than the value of permeability in the model.

The dimensionless time was modified and defined as:

$$\bar{t}_{Dw} = \frac{Kt}{\phi(\mu c)x_w^2} \quad (39)$$

where the quantity (μc) is evaluated at the wellbore pressure at time t rather than at the initial pressure.

Substituting Equations 32, 33, 39, 35 and 36 into Equation 37 results in:

$$\frac{\partial^2 m_D}{\partial x_D^2} + \frac{\partial^2 m_D}{\partial y_D^2} = \left(1 - \frac{t}{\mu c} \frac{\partial}{\partial t} (\mu c)\right) \frac{\partial m_D}{\partial t_{Dw}} \quad (40)$$

It is clear from Equation 40 that the diffusivity equation can not be linearized with the new definition of the dimensionless time variable. However, the data used in Figures 5 and 6 are re-plotted in Figure 7 against the new definition of dimensionless time, \bar{t}_{DL} . It is noted that for all values of permeability and flow rate, the data plots nearly as one line and results in calculated values of permeabilities within an error of only 0.1 percent. It is suspected, as will be shown later, that the use of the new definition of dimensionless time can not be used over the total pressure range to depletion.

Figure 4. Effect of Holding the Quantity (μc) in the Time Coefficient Constant at the Initial Pressure on the Drawdown Solution.

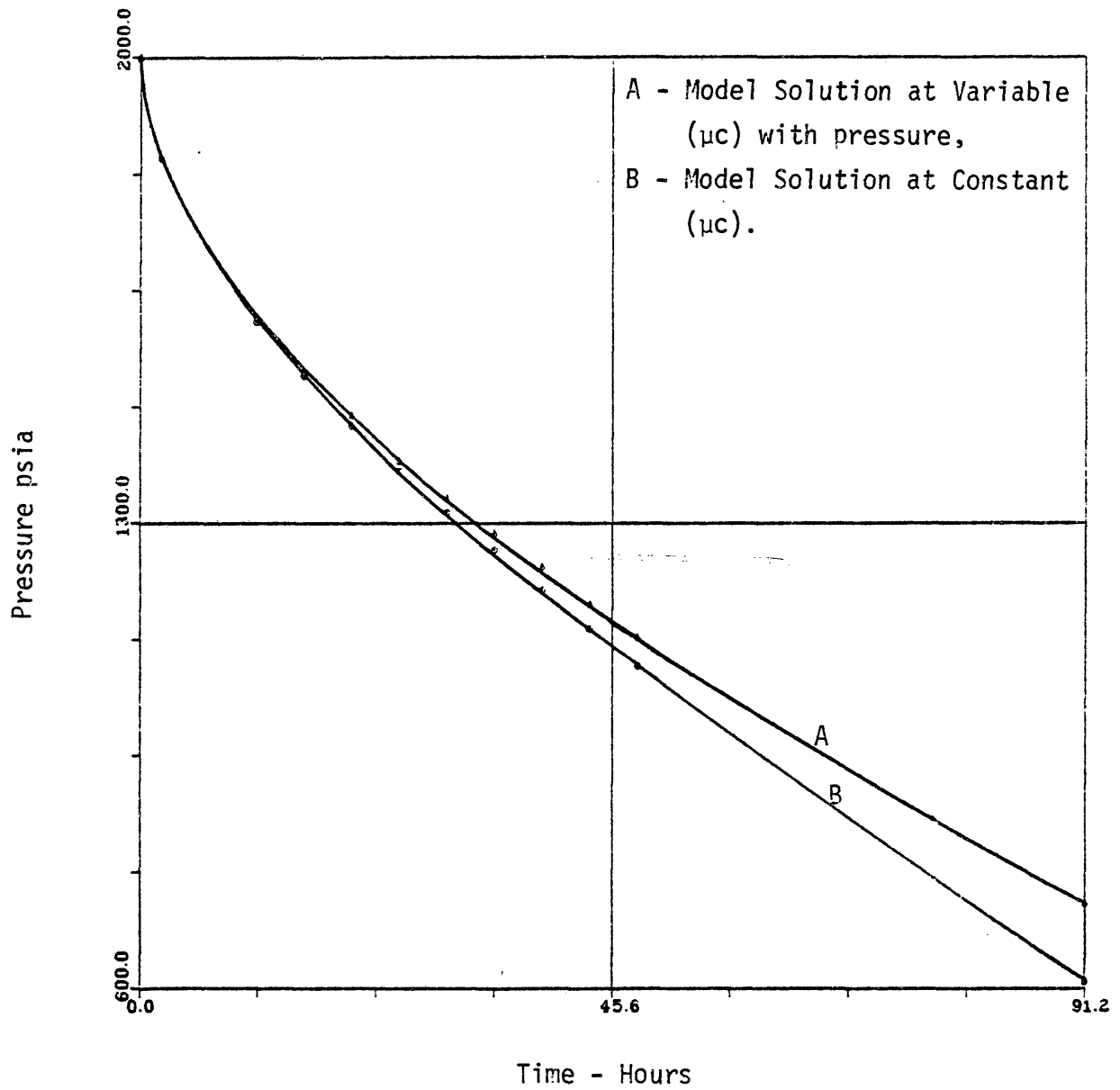


Figure 5. Effect of Formation Permeability on the Calculated $m(p)$ Behavior at the Wellbore.

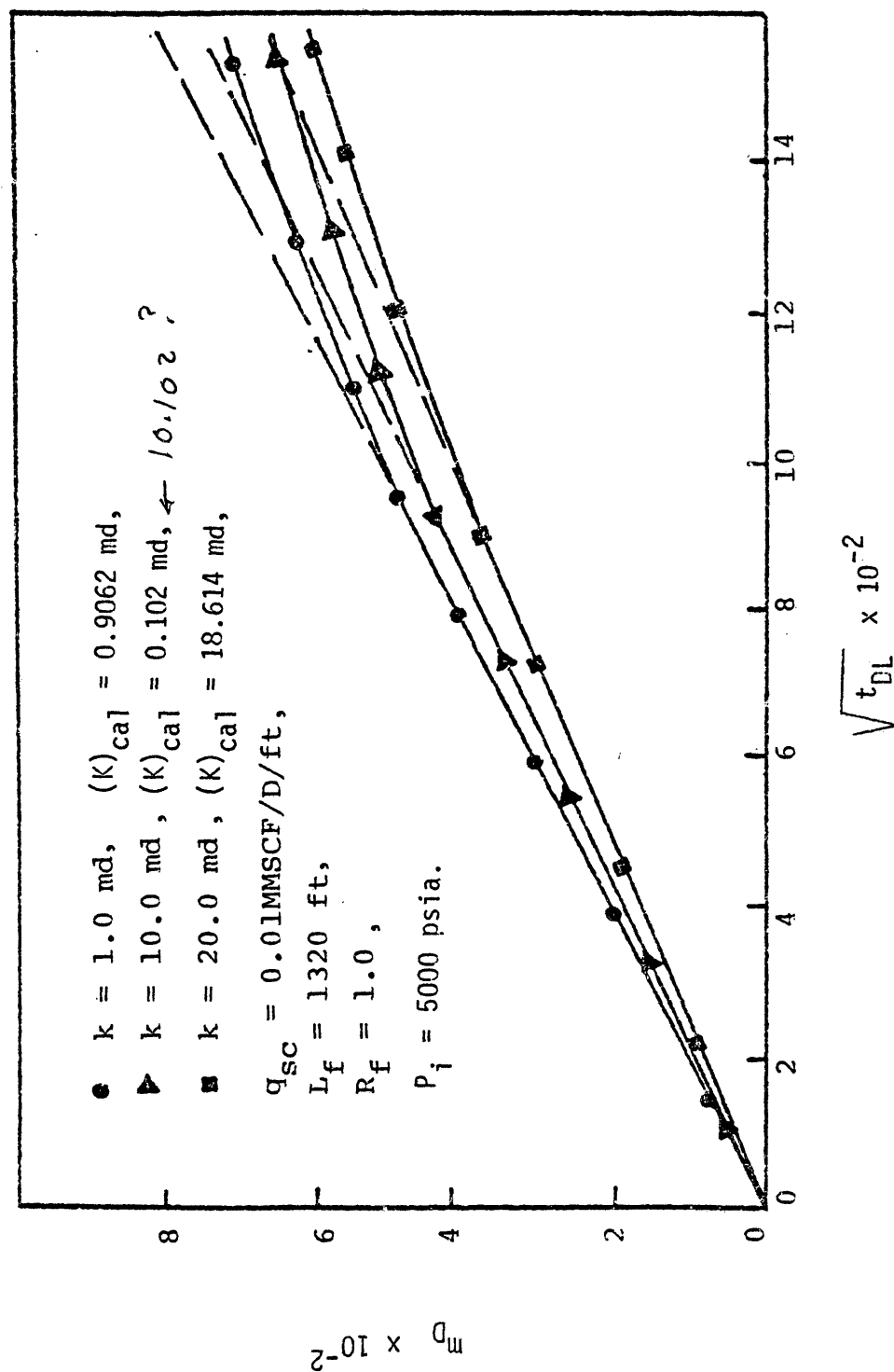


Figure 6. Effect of Production Rate on the Calculated $m(p)$ Behavior at the Wellbore.

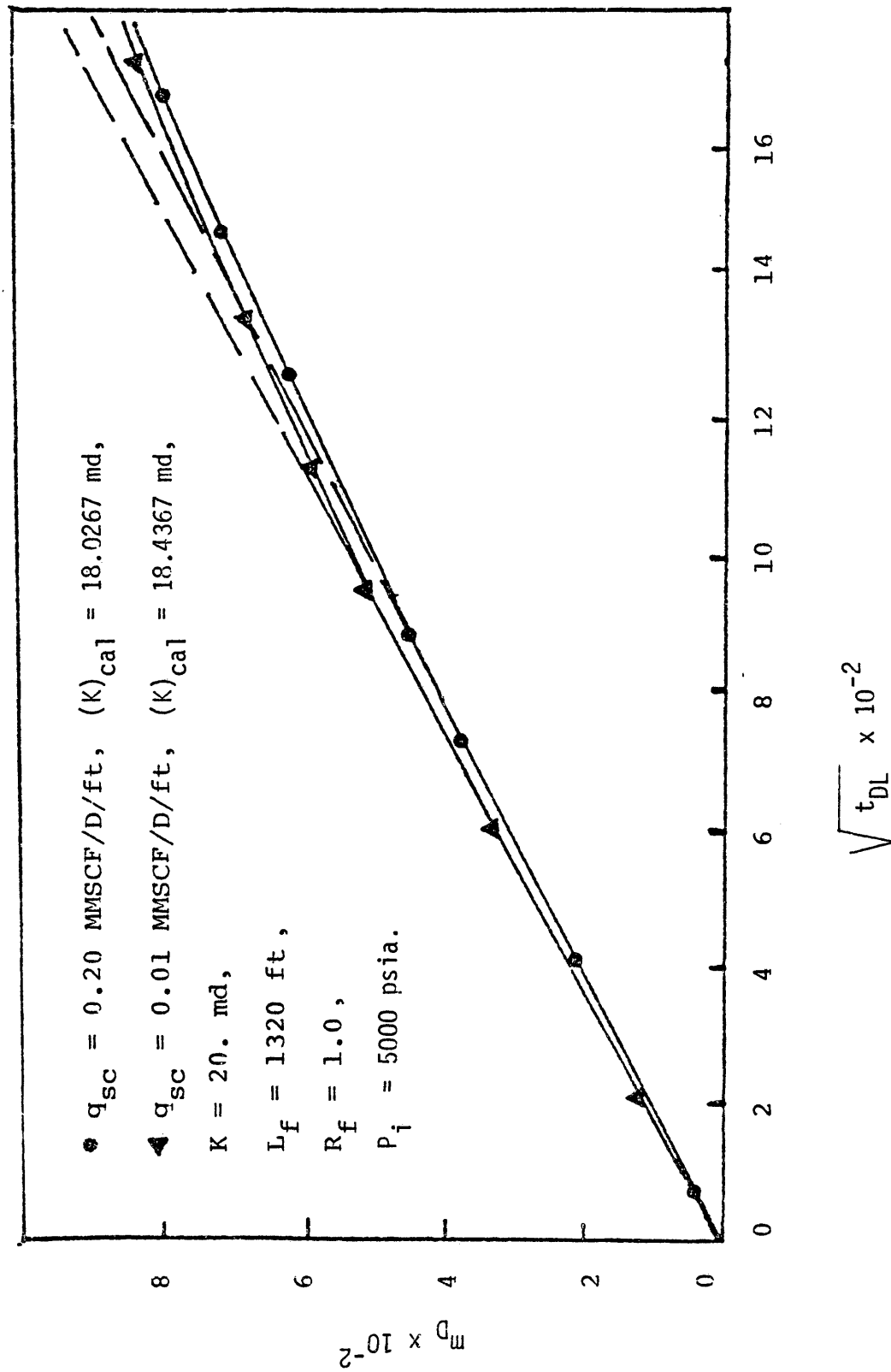


Figure 7. Plot of Figures 5 and 6 Data Using New Definition of Dimensionless Time.

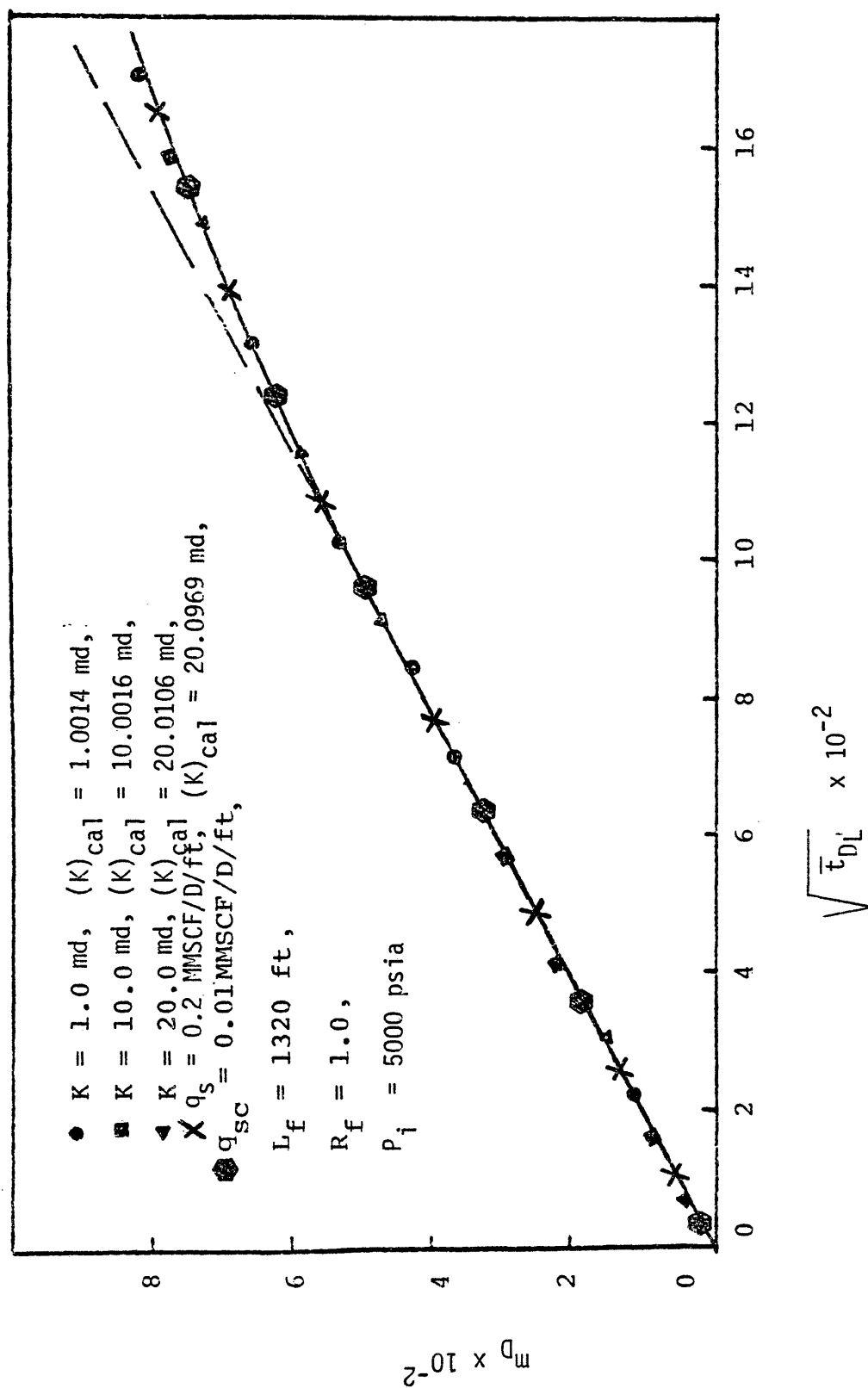
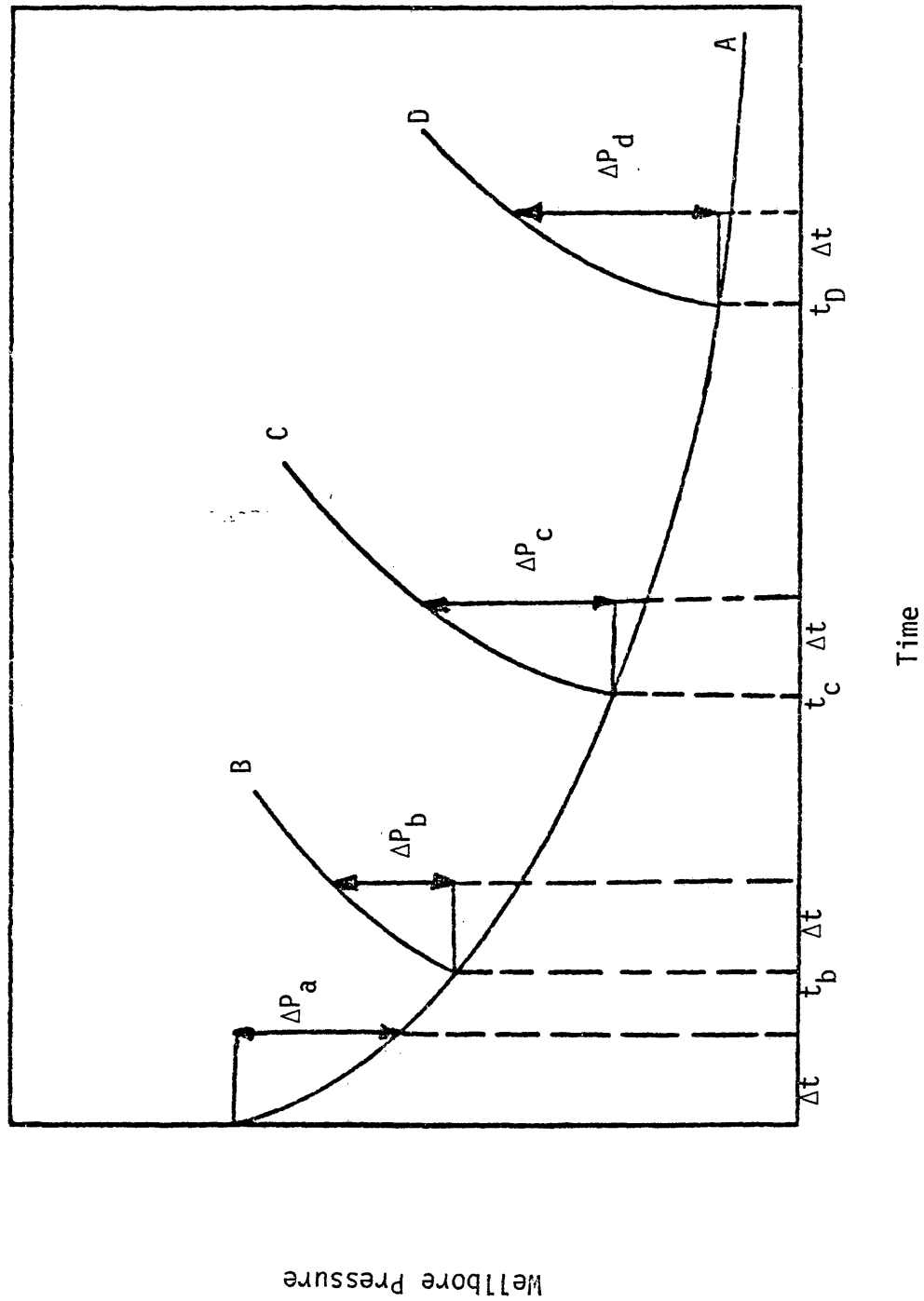


Figure 8. Example of Drawdown and Buildup Pressures Measured in the Borehole for Theoretical Development of Type Curve Analysis.



C. Type Curve Analysis for Pressure Buildup Data

Available type curves give drawdown solutions and are used for the analysis of buildup data. These curves were derived for constant viscosity, compressibility fluid.

Figure 8 is a theoretical plot of a wellbore pressure as a function of time. Type curves claim that a log-log plot of curves B, C, D and A, Figure 8, are identical.

Figures 9 through 14 are log-log plots of dimensionless pressure rise P_{Ds} , which is defined as:

$$P_{Ds} = \frac{1.987 \times 10^{-5} (m(P_{ws}) - m(P_{wf} \text{ at } \Delta t = 0))}{0.5 P_{sc} q_{sc} T}, \quad \dots (41)$$

as a function of the modified dimensionless shut in time \bar{t}_D , which is defined as:

$$\bar{t}_D = \frac{0.000264 K \Delta t}{\phi(\mu c) x_f^2}, \quad \dots (42)$$

For various flow times, t_f , prior to shut in for the pressure build-up period.

The top curve (A) in each figure is the drawdown solution, in this case the dimensionless pressure drop is defined as:

$$P_D = \frac{1.987 \times 10^{-5} T_{sc} Kh [m(P_i) - m(P_{wf})]}{0.5 P_{sc} q_{sc} T} \cdot \dots (43)$$

These figures show that the build-up solution closely coincides with the drawdown solution at the early build-up data when the flow time preceding the build-up is much longer than the build-up times. This early period is primarily controlled by the linear flow characteristics caused by the

hydraulic fracture.

As build-up time increases, the build-up solution diverges farther from the converted drawdown solution and is considerably greater than the divergence at smaller producing times.

The deviation between the converted drawdown solution and the build-up solution because of changes in permeability are illustrated in Figures 13 and 14. It is noted that the separation between the two solutions decrease as the permeability increases, which could be explained as a result of less pressure drop at high permeability.

The separation because of changes in flow rate are illustrated in Figures 10 and 11. It is noted that the separation decreases as the flow rate decreases because of less pressure drop per unit time at low flow rate.

Figures 11 and 12 illustrate the effect of the initial reservoir pressure on the deviation of the build-up data from the converted drawdown solutions. It is noted that the deviation decreases as the initial pressure increases. This could be explained as a result of the high variation of the quantity (μc) with $m(p)$ at low pressure.

If Figures 9 through 14 are plotted in terms of dimensionless time t_D rather than modified dimensionless pressure \bar{t}_D , a greater deviation between the drawdown solution and buildup solutions will be observed because the value of dimensionless time t_D is greater than the value of the modified dimensionless time \bar{t}_D because $(\mu c/\mu c)_i \geq 1$. Figures 9 and 10 show the invalidity of the modified dimensionless time \bar{t}_D at low pressure and large values of time. At low values of pressure the quantity

$\frac{t}{\mu c} \frac{\partial(\mu c)}{\partial t} > 1$, because of the large variation of (μc) with pressure.

Figure 9. Actual Pressure Buildup Data Compared to Converted Drawdown Data Normally used for Type Curve Analysis.

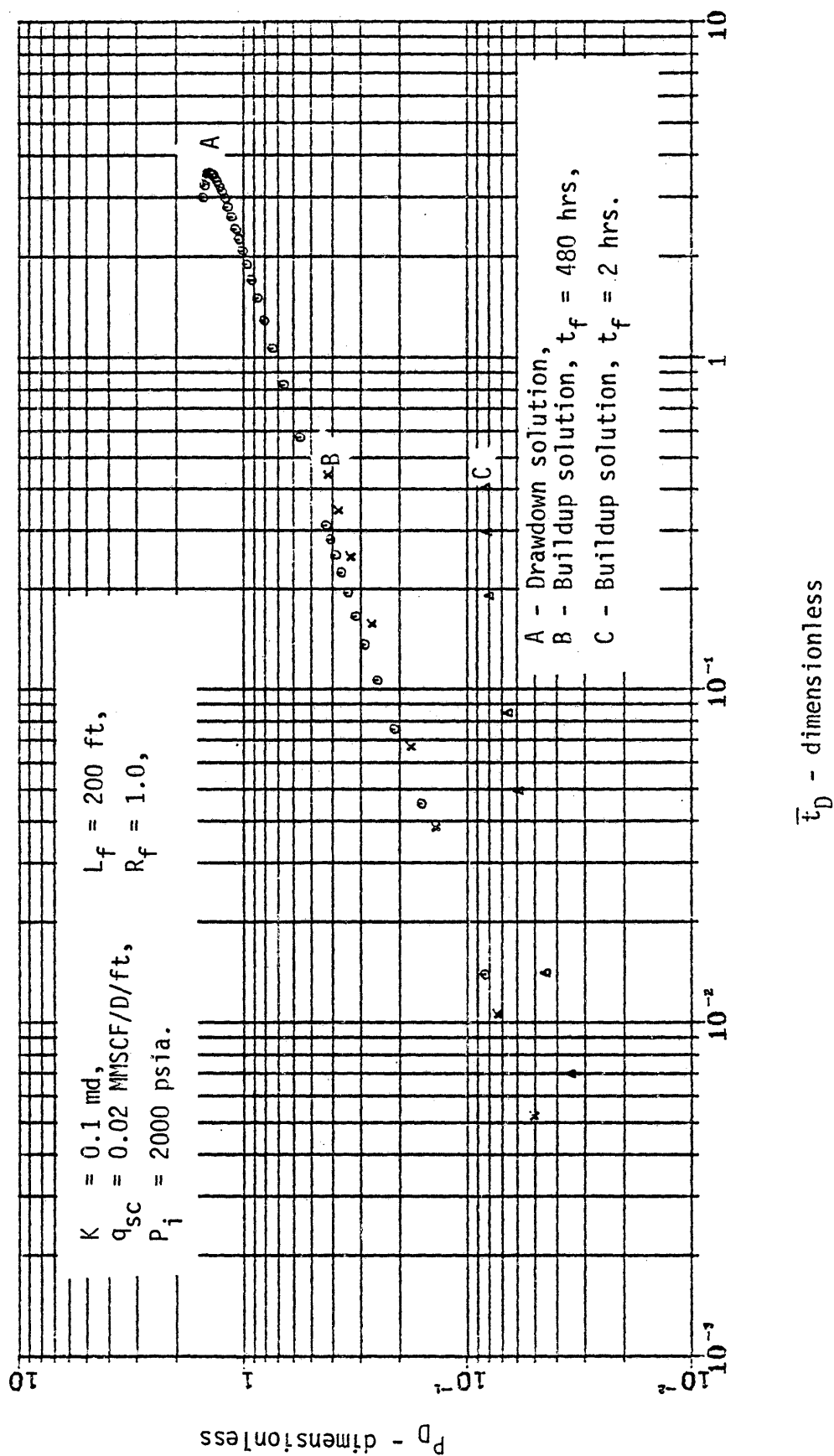


Figure 10. Actual Pressure Buildup Data Compared to Converted Drawdown Data Normally used for Type Curve Analysis.

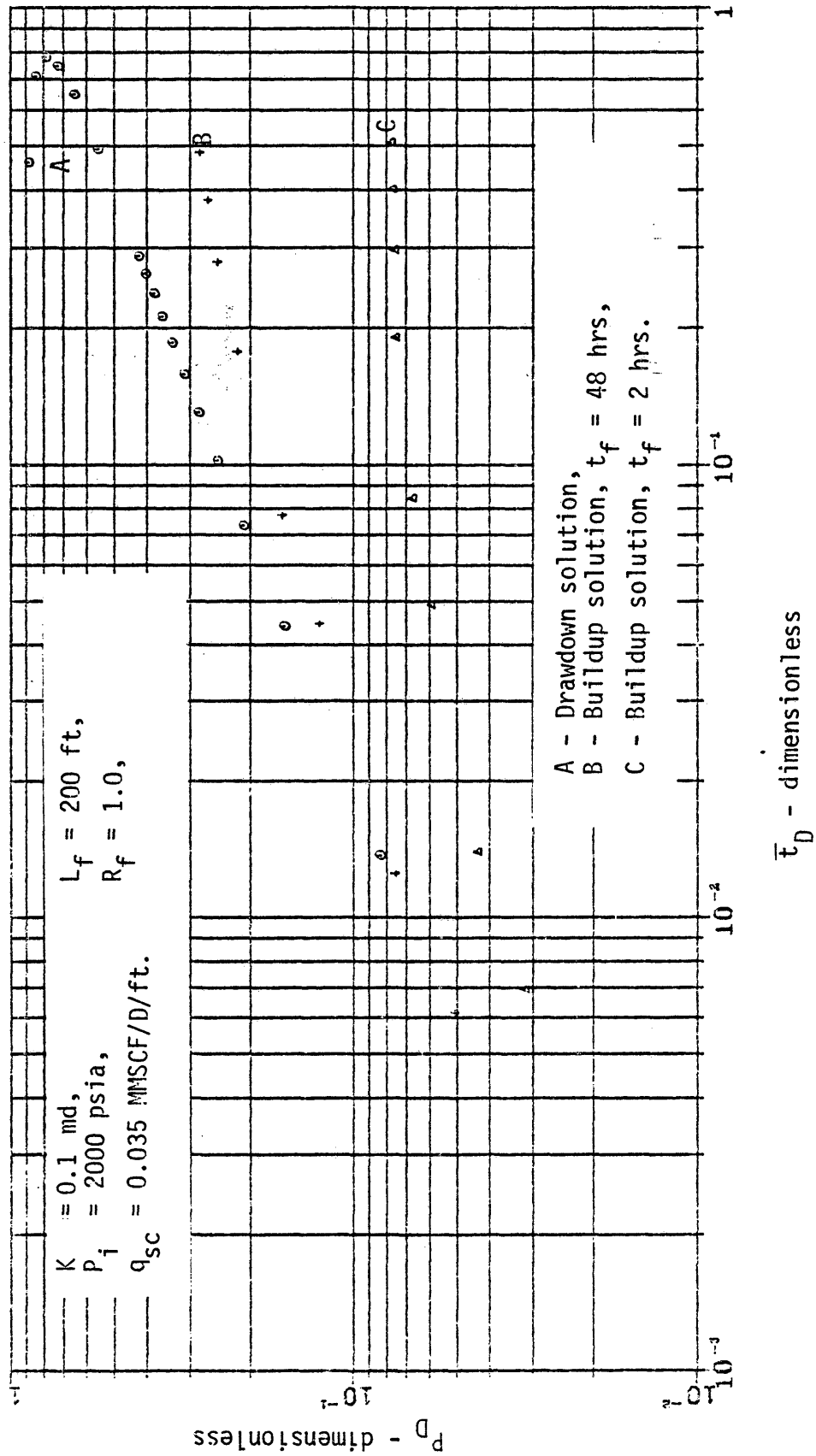


Figure 11. Actual Pressure Buildup Data Compared to Converted Drawdown Data Normally used for Type Curve Analysis.

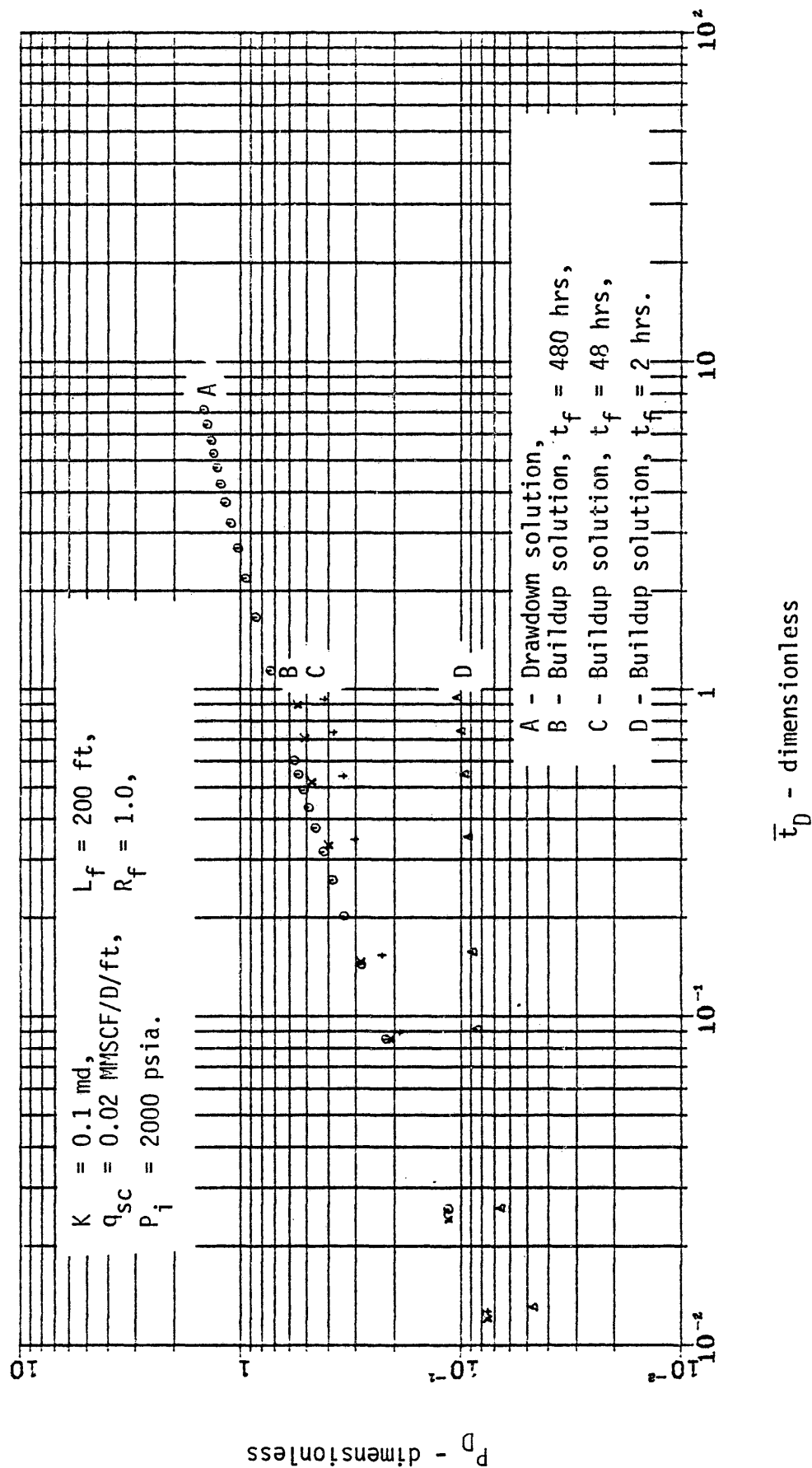
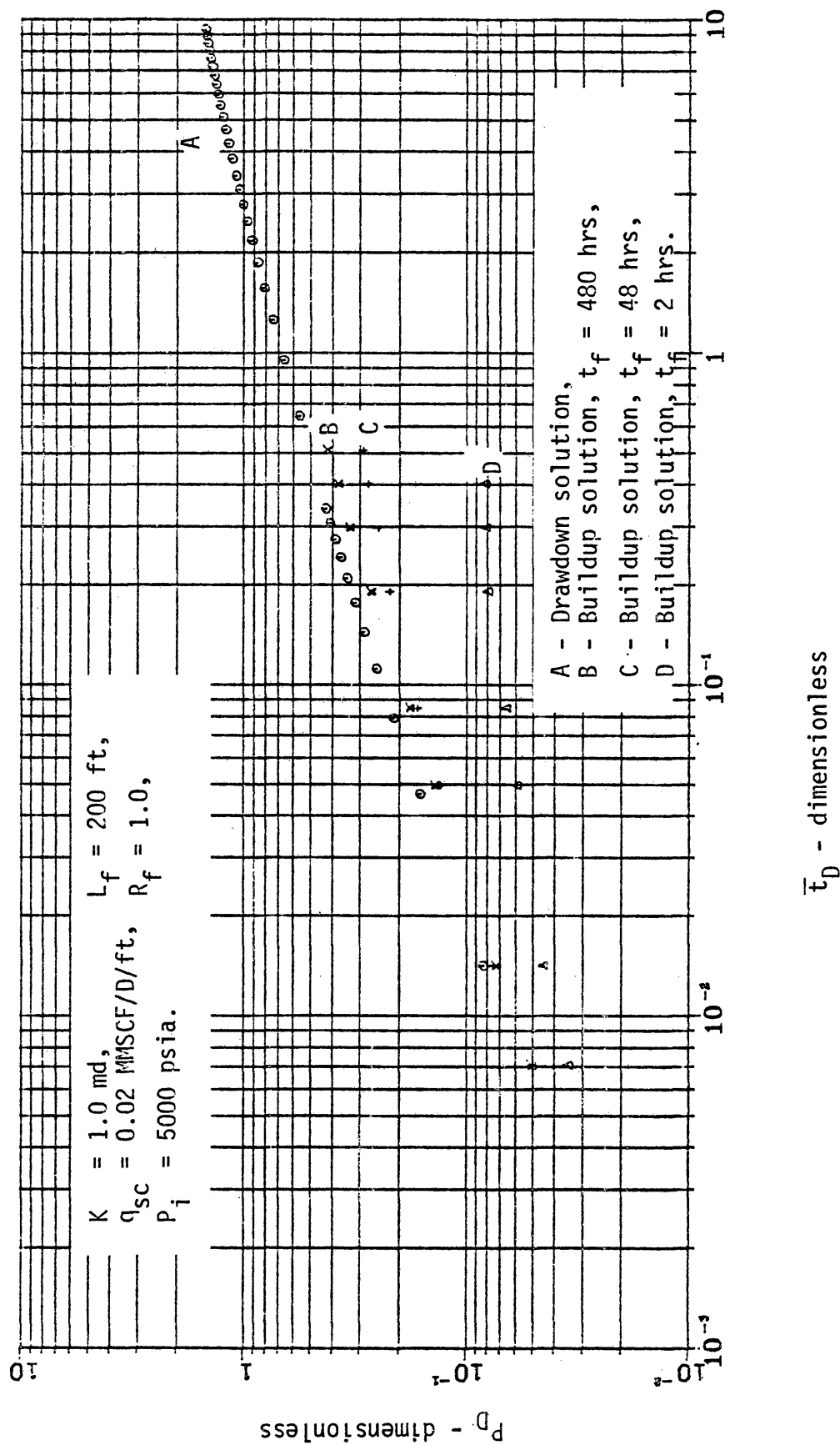


Figure 12. Actual Pressure Buildup Data Compared to Converted Drawdown Data Normally used for Type Curve Analysis.



t_D - dimensionless

Figure 13. Actual Pressure Buildup Data Compared to Converted Drawdown Data Normally used for Type Curve Analysis.

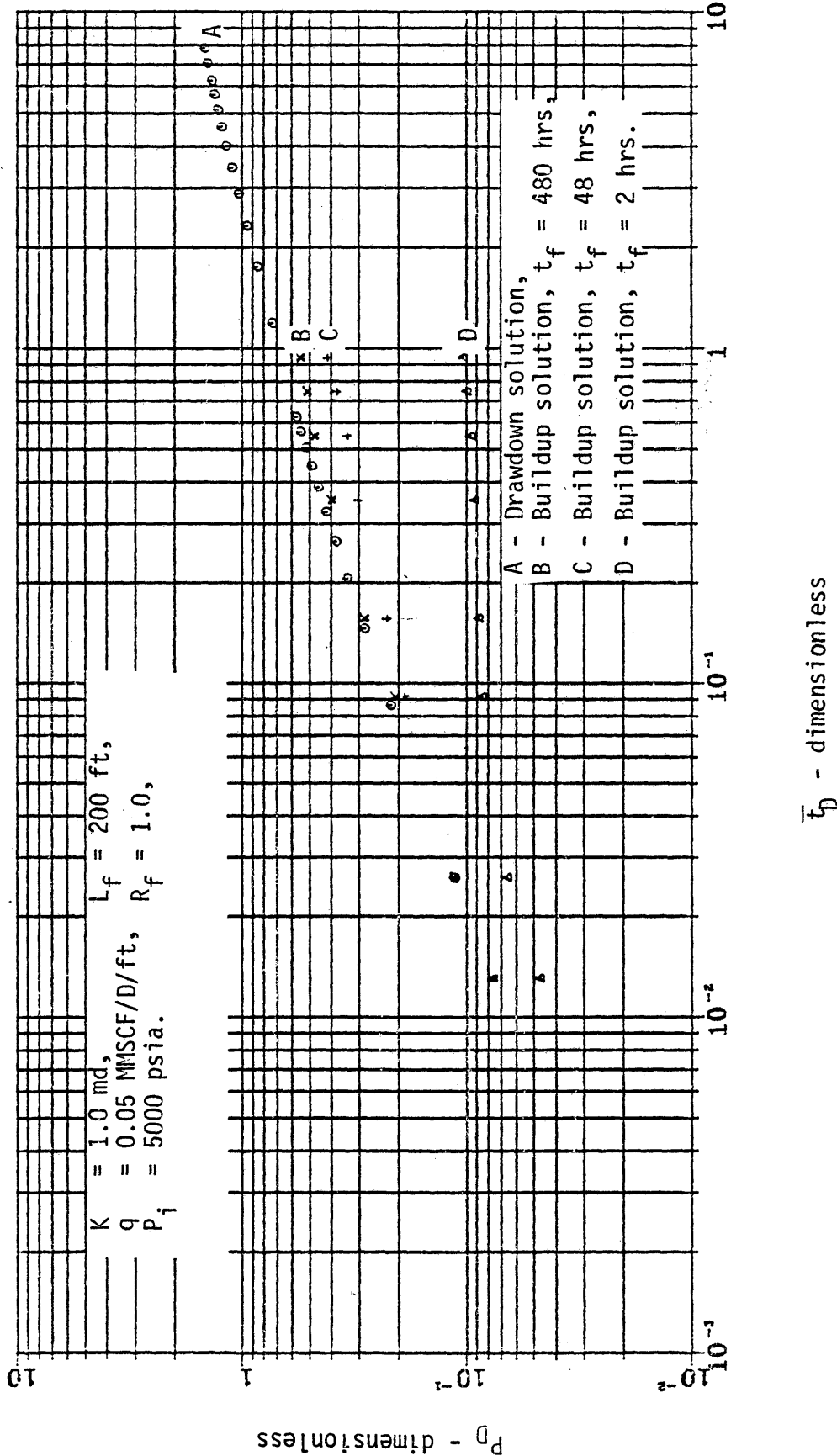
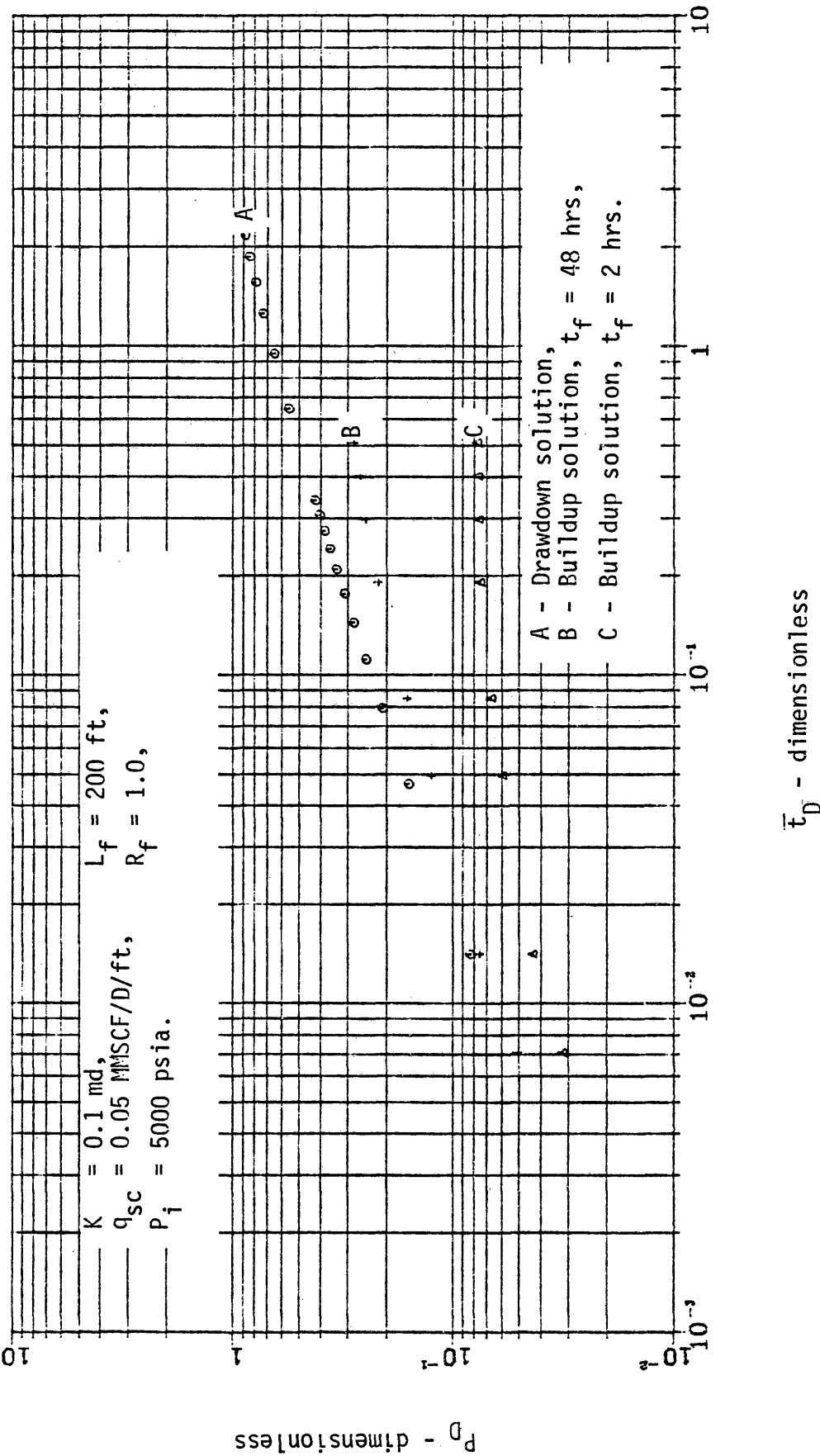


Figure 14. Actual Pressure Buildup Data Compared to Converted Drawdown Data Normally used for Type Curve Analysis.



D. Superposition and Pressure Buildup

Buildup theory has been based on the principle of superposition for constant fluid compressibility and viscosity. This theory leads to the use of the Horner plot for buildup curve analysis. The slope of the curve is used to calculate a well's flow capacity, Kh .

For constant flow rate at the surface, constant mass rate at the sand face, Figures 15 through 19 show the buildup solution based on superposition theory and the actual buildup solution generated by the model. It is noted that the two solutions are in close agreement when the flow time prior to the buildup is two hours.

It is also noted that the two solutions are in close agreement only at the early time of buildup when the flow times prior to the buildup are 48 and 480 hours. As the flow time preceding the buildup becomes larger, the length of the time of close agreement increases.

As the buildup time increases, the two solutions separate with the actual solution lower than the superposition solution.

The deviation in the two solutions because of changes in permeability are illustrated in Figures 15 through 18. It is noted that as the permeability decreases, the magnitude of the deviation between the two solutions increases with time because of the lower sand face pressure for lower permeability.

The deviation because of changes in flow rate are illustrated in Figures 16 and 18. It is noted that as the flow rate increases, the magnitude of the deviation between the two solutions increases because of the higher pressure drop caused by higher flow rates.

Figures 18 and 20 illustrate the effect of the initial reservoir

pressure on the separation between the two solutions. It is noted that the magnitude of the separation between the two solutions decreases as the initial reservoir pressure increases, which can be attributed to the larger variation of the time coefficient (μc) with $m(p)$ at low pressure.

For constant flow rate at the sand face Figures 21 through 23 show the difference between the two solutions, buildup solution based on superposition and the actual buildup solution. It is noted that the two solutions in close agreement during the early buildup time. Figures 21 and 22 illustrate the effect of changes in the initial sand face flow rate. As the initial flow rate increases, the magnitude of the separation between the two solutions increases because of less pressure drop at lower flow rates. Figures 19 and 21 illustrate the effect of the flow rate being constant at the sand face rather than being constant at the surface. It is noted that the magnitude of the separation between the two solutions is less in the case of constant flow rate at the sand face because of the higher observed pressure at the sand face. This higher pressure is the result of removing less mass from the reservoir in any time period when using constant rate at the sand face as compared to a constant rate at the surface.

At high initial reservoir pressure, Figures 16 and 23, less separation between the two solutions was observed in the case of constant flow rate at the sand face because of the higher observed pressure at the sand face.

Figures 24 through 35 present the pressure buildup data generated by the model using a variable (μc) in the time coefficient for both constant flow rate at the sand face and constant mass rate at the sand face as a function of $\log \frac{t_f + \Delta t}{\Delta t}$.

In each case the suspected straight line does not appear because of the variation in fluid properties with pressure and the changing of flow regime with time.

A straight line has been drawn for these figures and the formation flow capacity has been calculated from that straight line. It is noted that for all cases, the calculated formation flow capacity Kh is greater than the real value by more than 10 percent. The error is because of the variation of the quantity (μc) with pressure and the attempted superposition of two flow regimes.

Figures 24 through 28 show a semilog plot of p_{wf} as a function of $\frac{t_f + \Delta t}{\Delta t}$ when $t_f = 2.0$ hours. It is noted that an error of greater than 300 percent was found in the calculated value of Kh when using the standard Horner method. This error could be explained as a result of a non-radial flow in the system at the early times and the variation of fluid properties with pressure.

Figures 29 through 35 are semilog plots of p_{wf} as a function of $\frac{t_f + \Delta t}{\Delta t}$ when $t_f = 48$ hours and $t_f = 480$ hours.

It is noted that an error of greater than 50 percent was found in the calculation of the formation flow capacity Kh because of the non-radial flow in the system and the variation of fluid properties with time.

It is also noted that as the flow time prior to the buildup increases, the error in the calculation of Kh decreases because of the apparent radial flow begins to show in the system at the same time as the flow time increases the effect of the quantity (μc) on the calculation of Kh increases.

Figure 15. Superposition and actual buildup solutions -
Constant mass rate at the sand face.

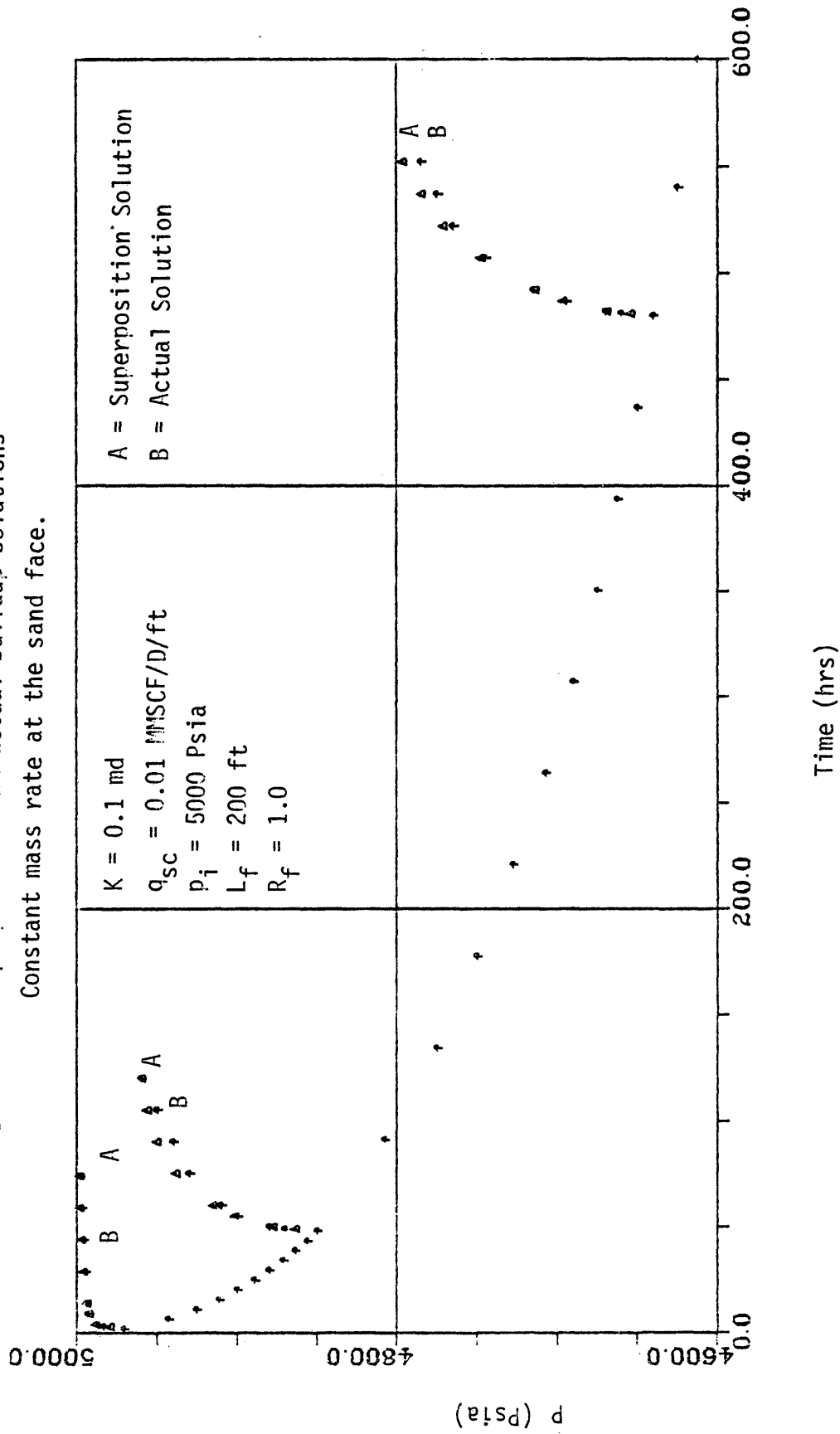


Figure 16. Superposition and actual buildup solutions -
Constant mass rate at the sand face.

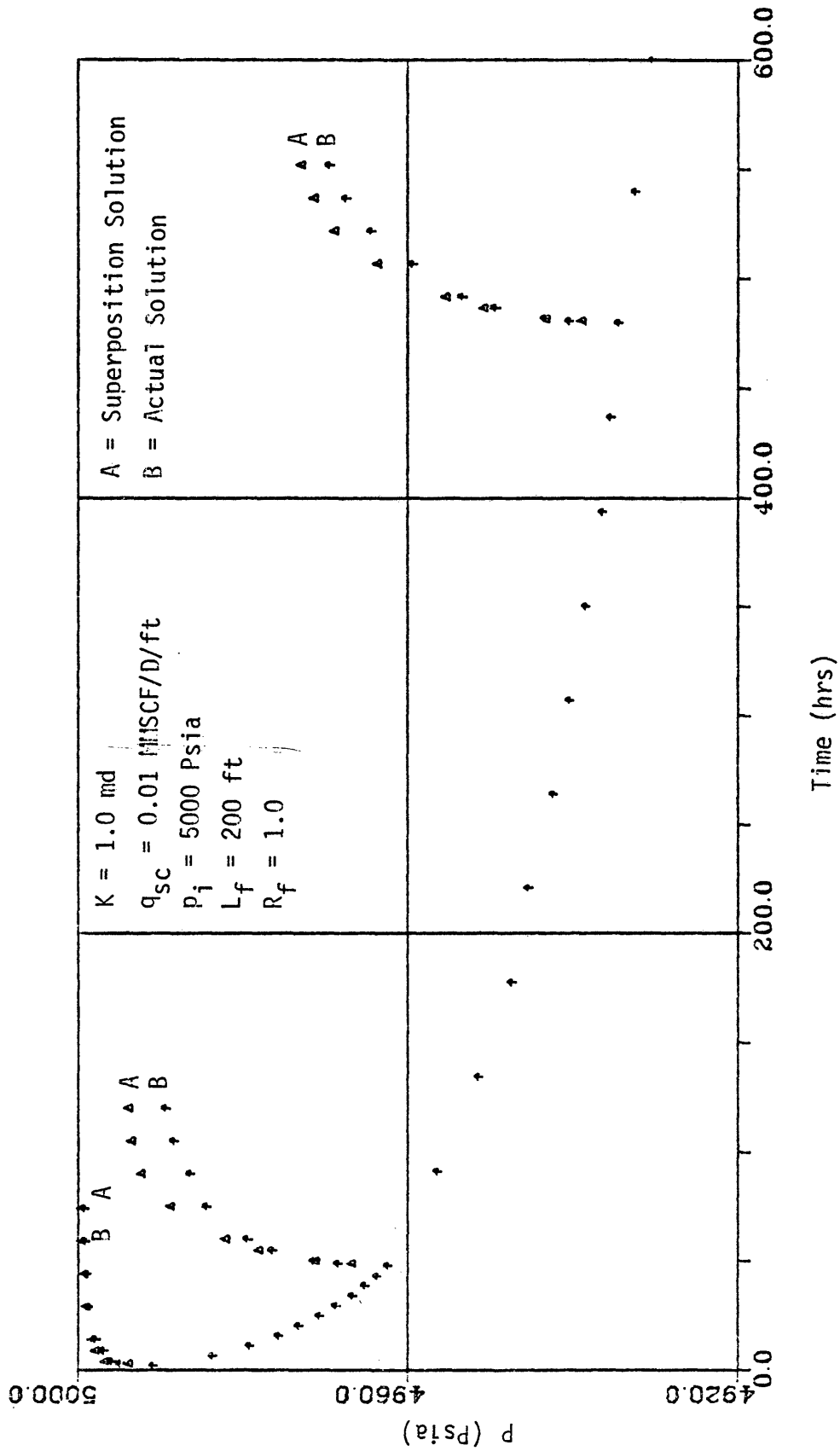


Figure 17. Superposition and actual buildup solutions -
Constant mass rate at the sand face.

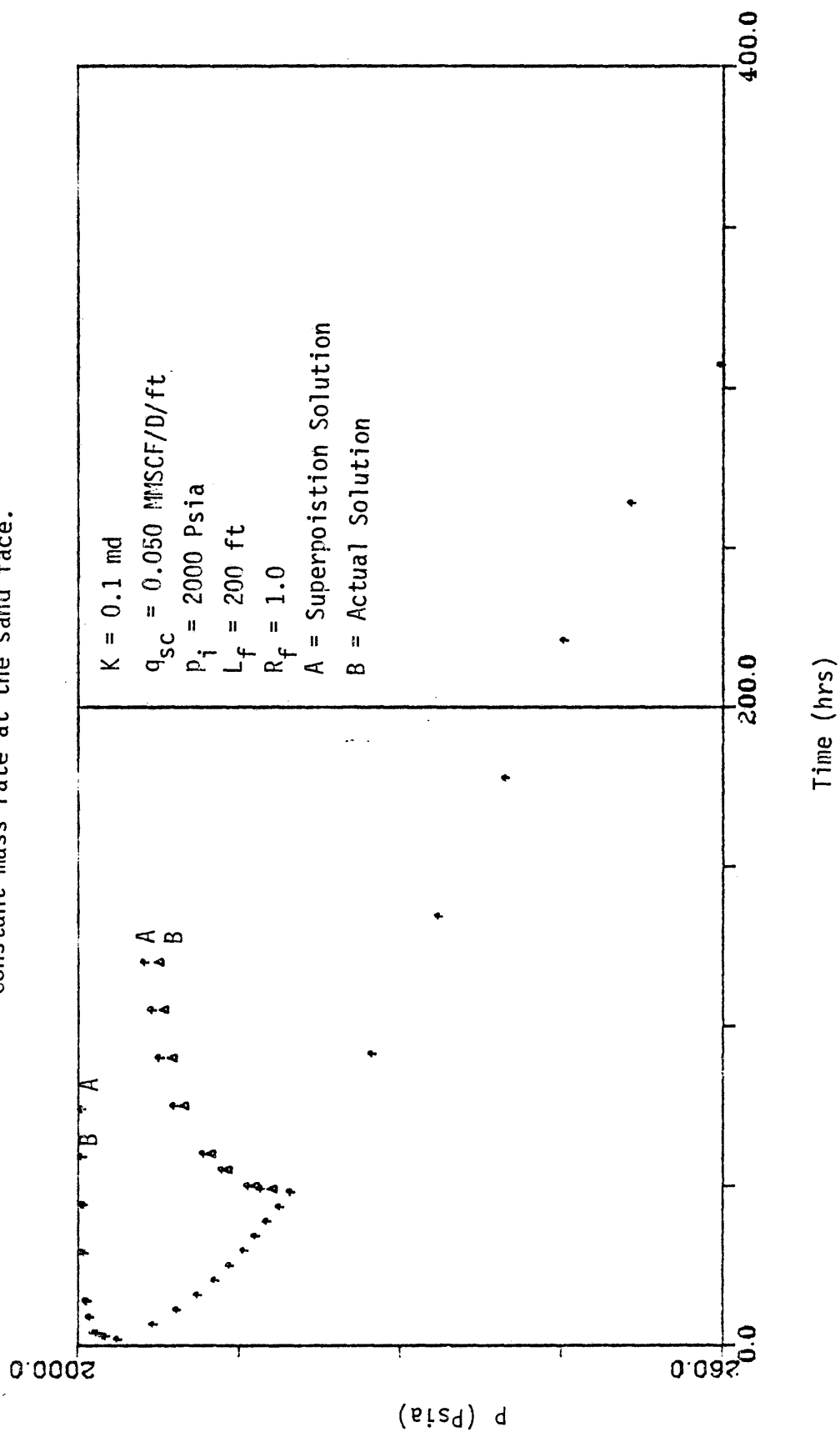


Figure 18. Superposition and actual buildup solutions -
Constant mass rate at the sand face.

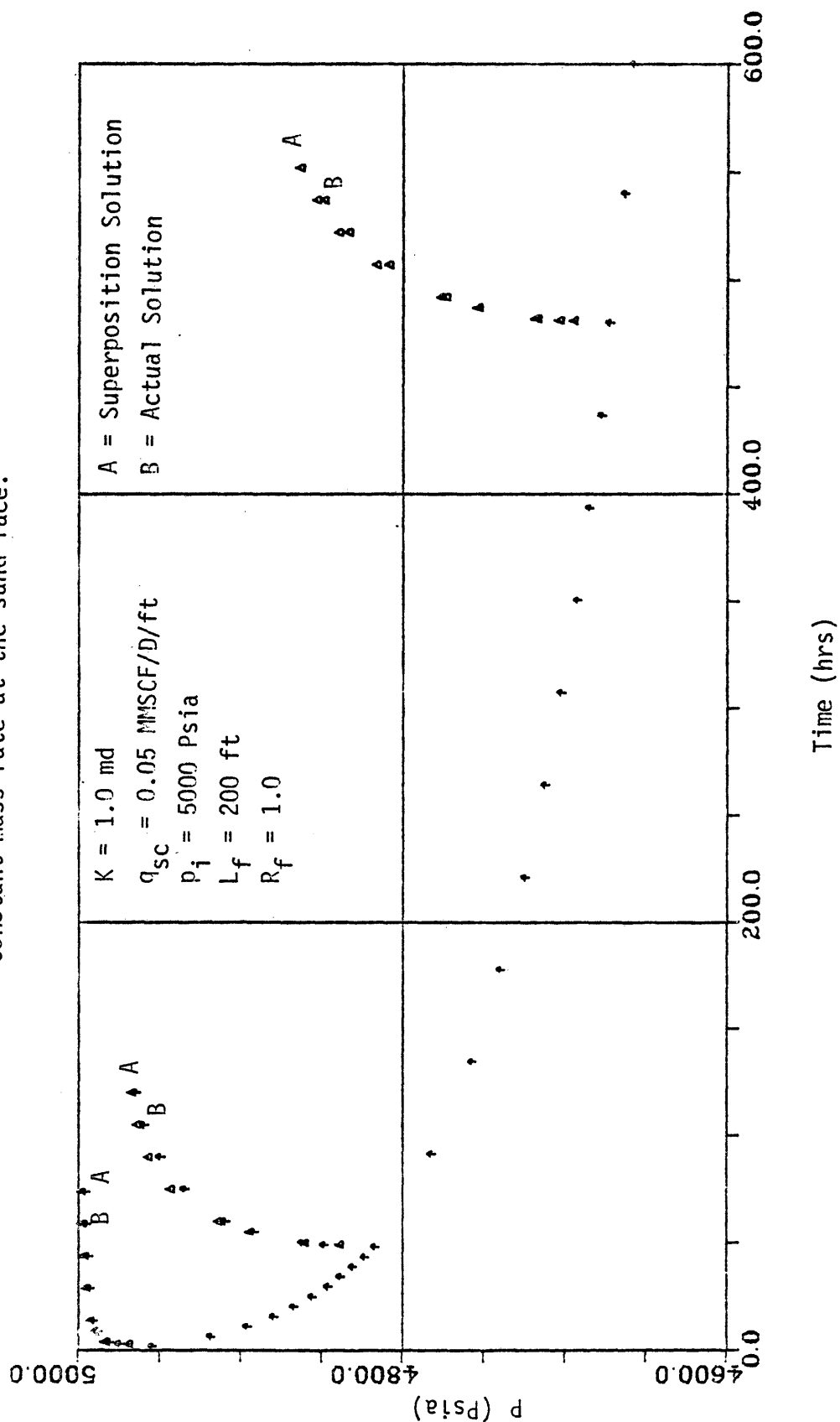


Figure 19. Superposition and actual buildup solutions -
Constant mass rate at the sand face.

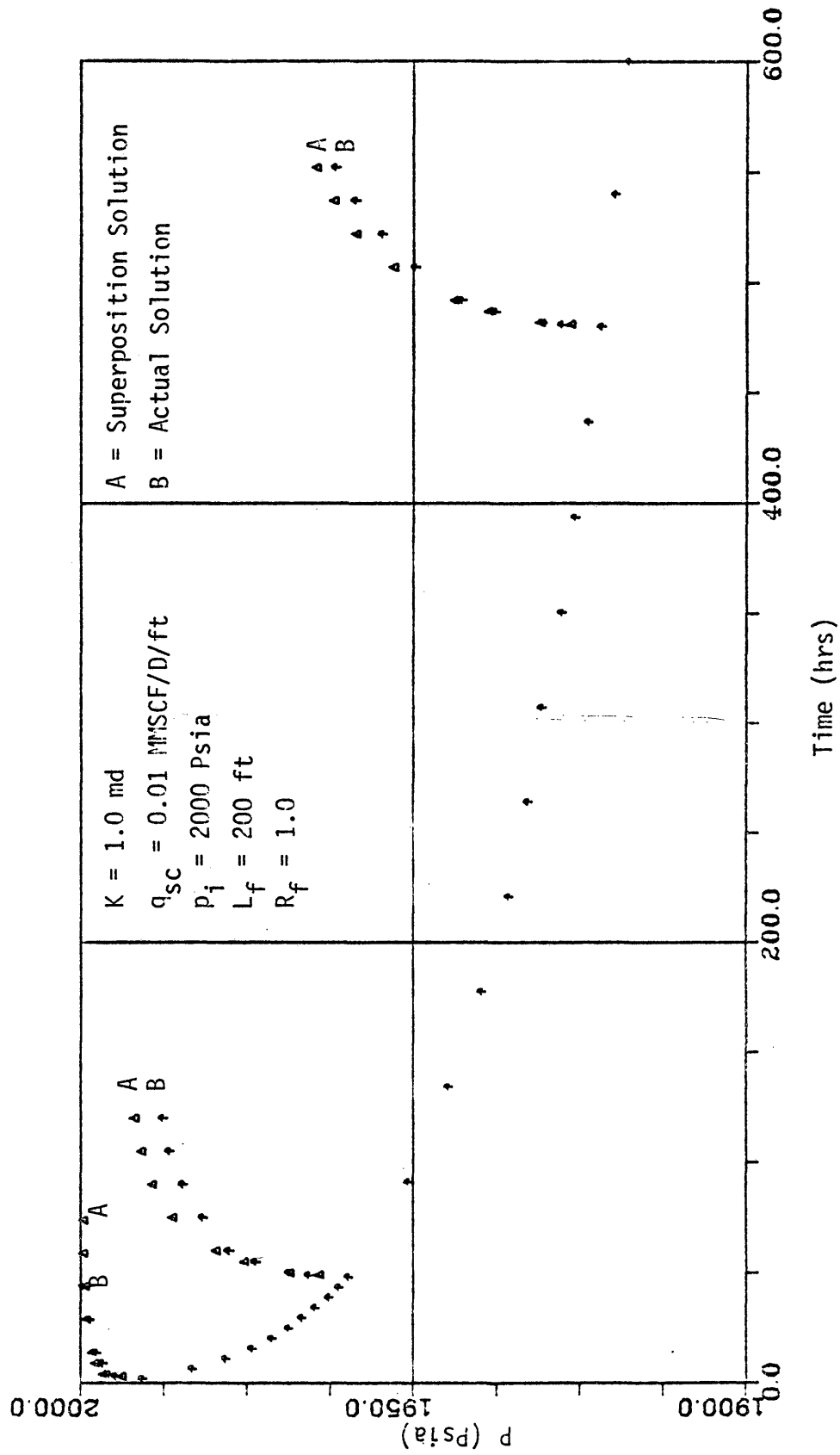


Figure 20. Superposition and actual buildup solutions -
Constant mass rate at the sand face.

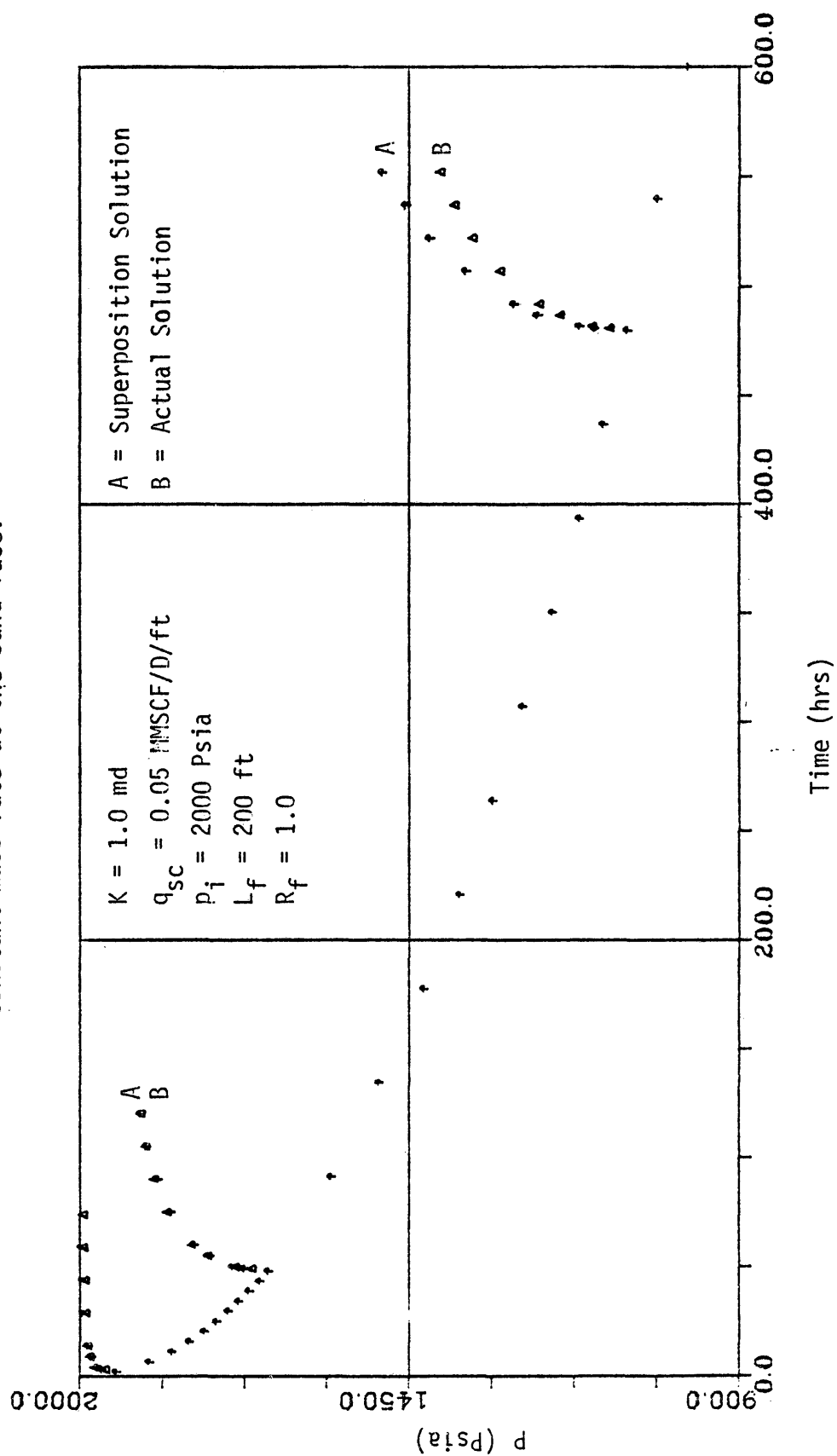


Figure 21. Superposition and actual buildup solutions -
Constant flow rate at the sand face.

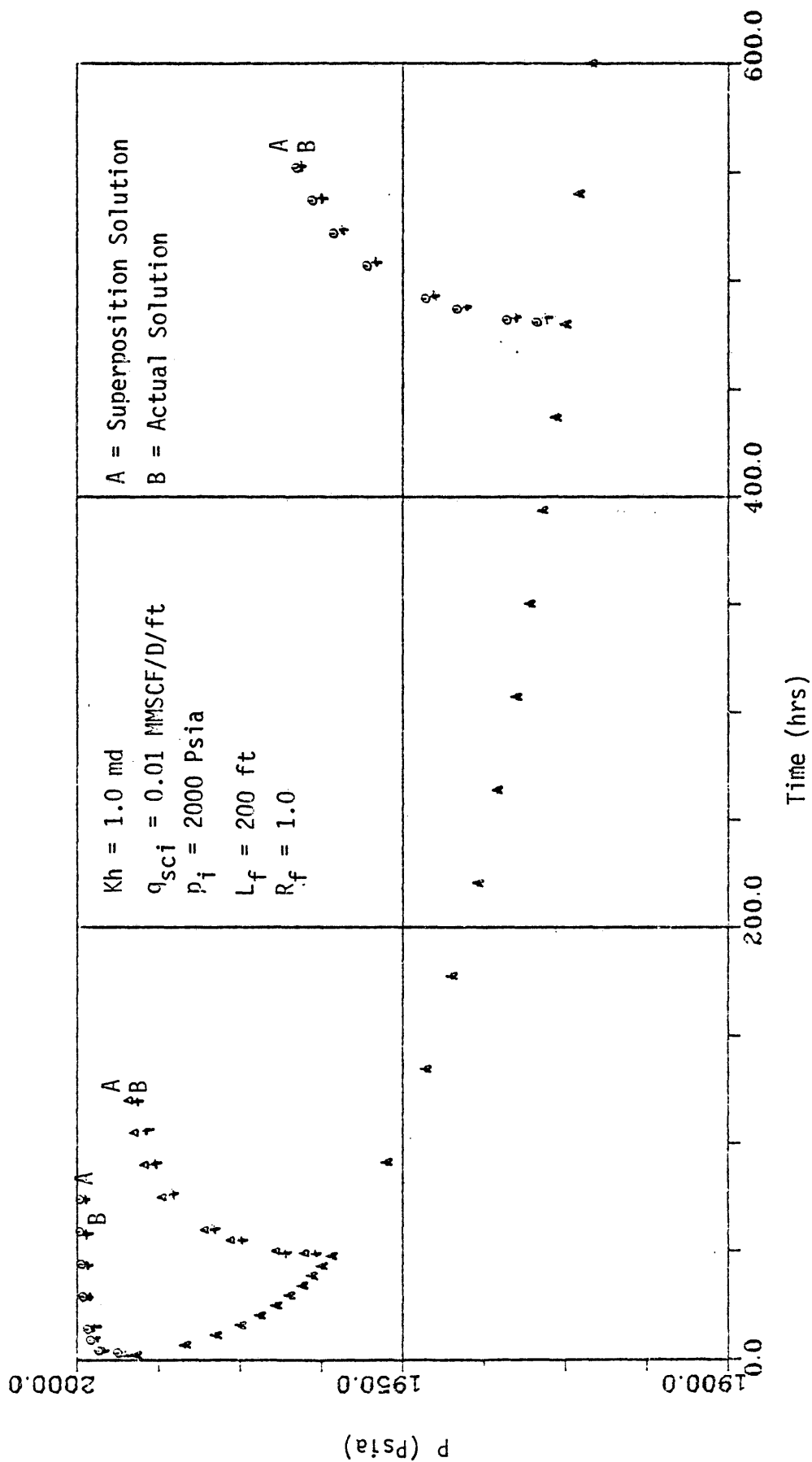


Figure 22. Superposition and actual buildup solutions -
Constant flow rate at the sand face.

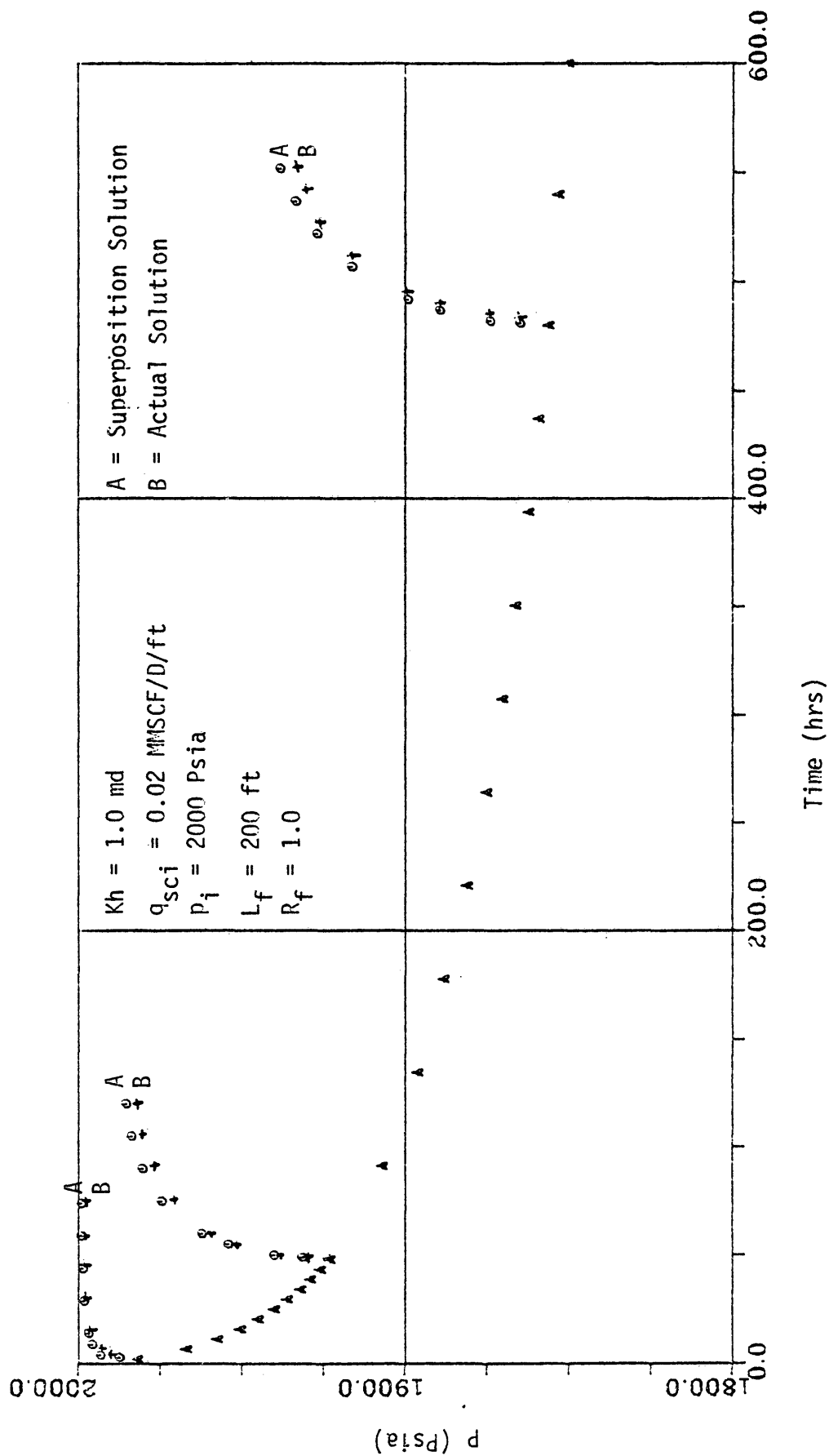


Figure 23. Superposition and actual buildup solutions -
Constant flow rate at the sand face.

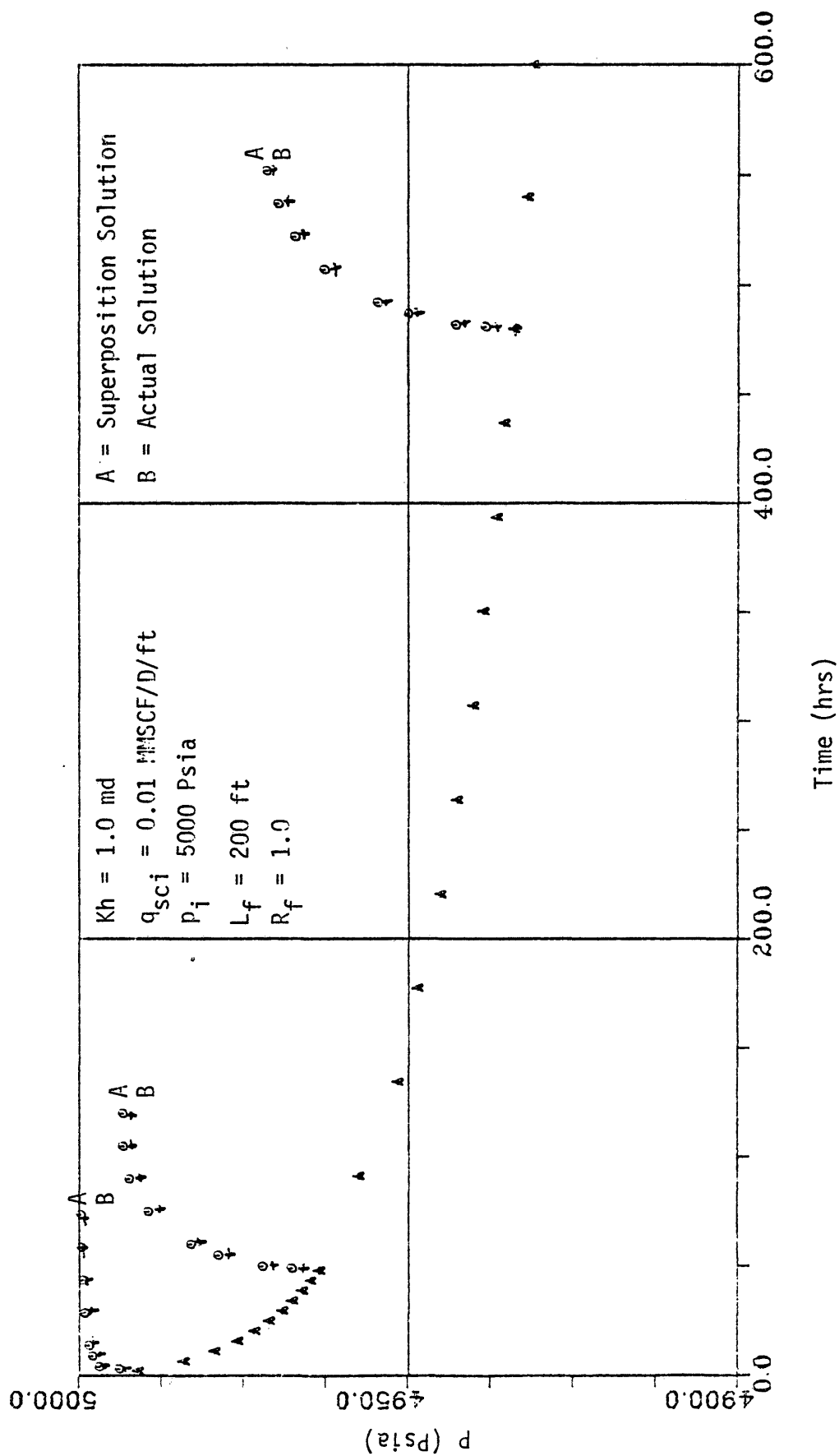


Figure 24. Horner plot - Constant mass rate at the sand face.

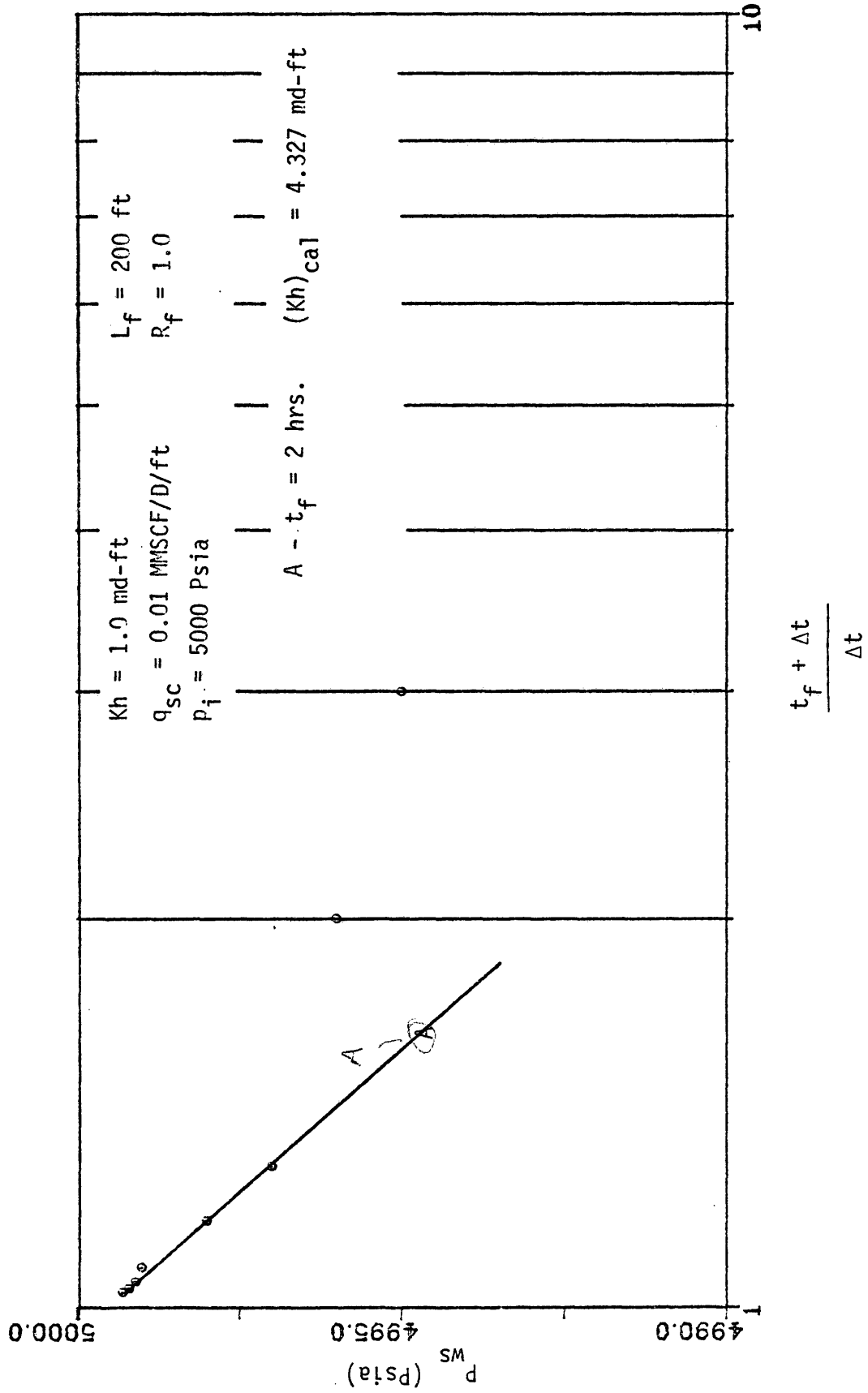


Figure 25. Horner plot - Constant mass rate at the sand face.

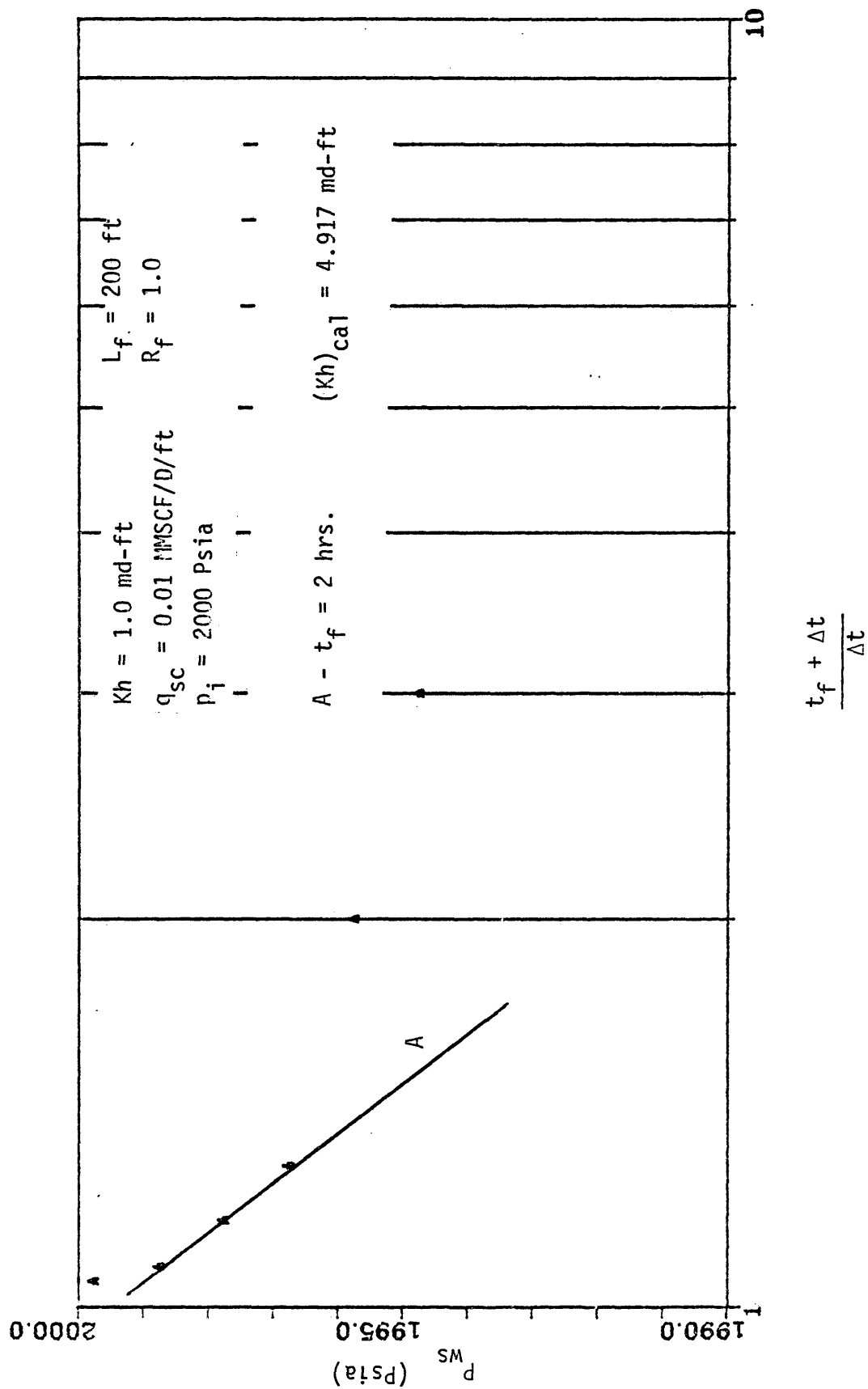


Figure 26. Horner plot - Constant mass rate at the sand face.

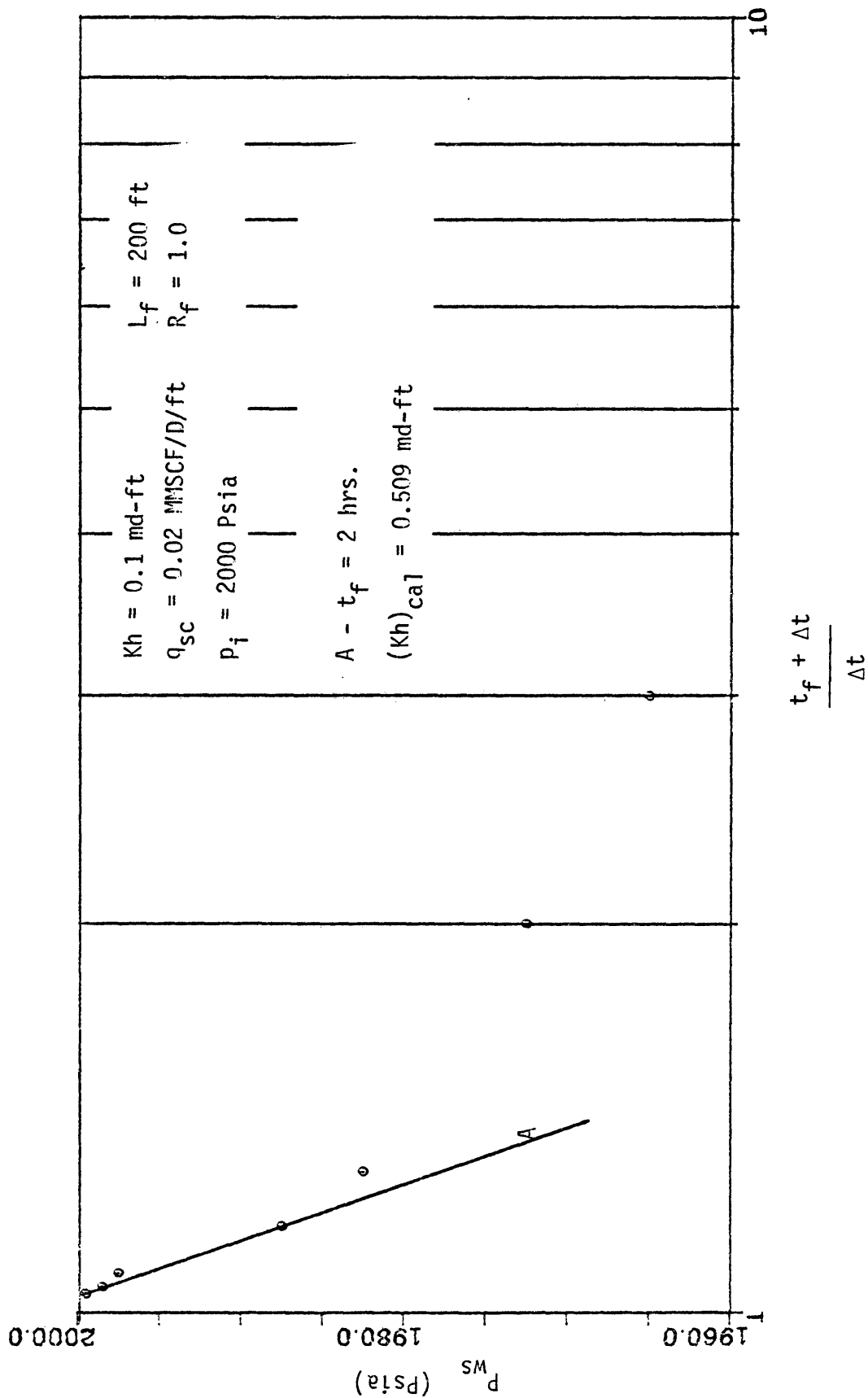


Figure 27. Horner plot - Constant mass rate at the sand face.

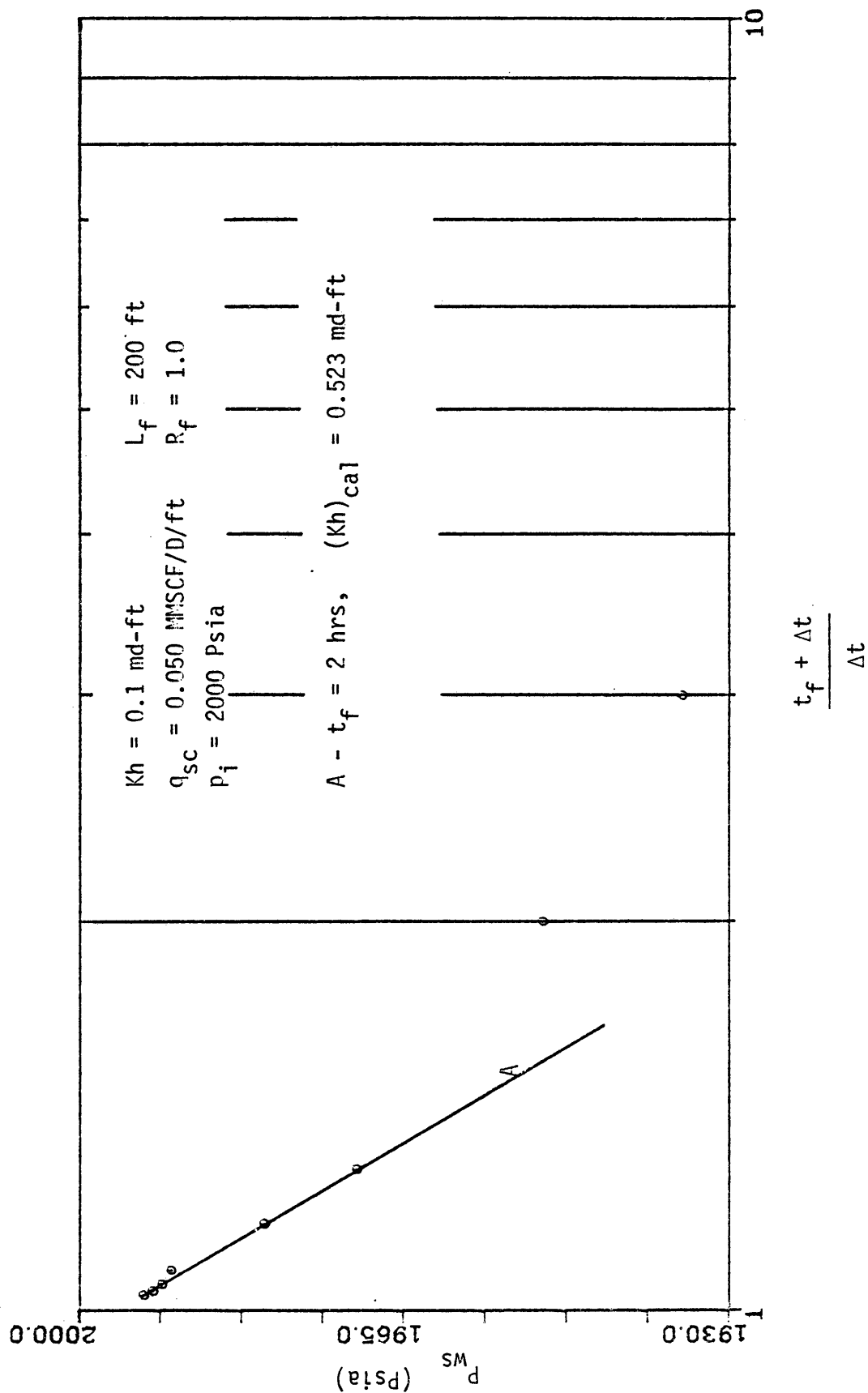


Figure 28. Horner plot - Constant flow rate at the sand face.

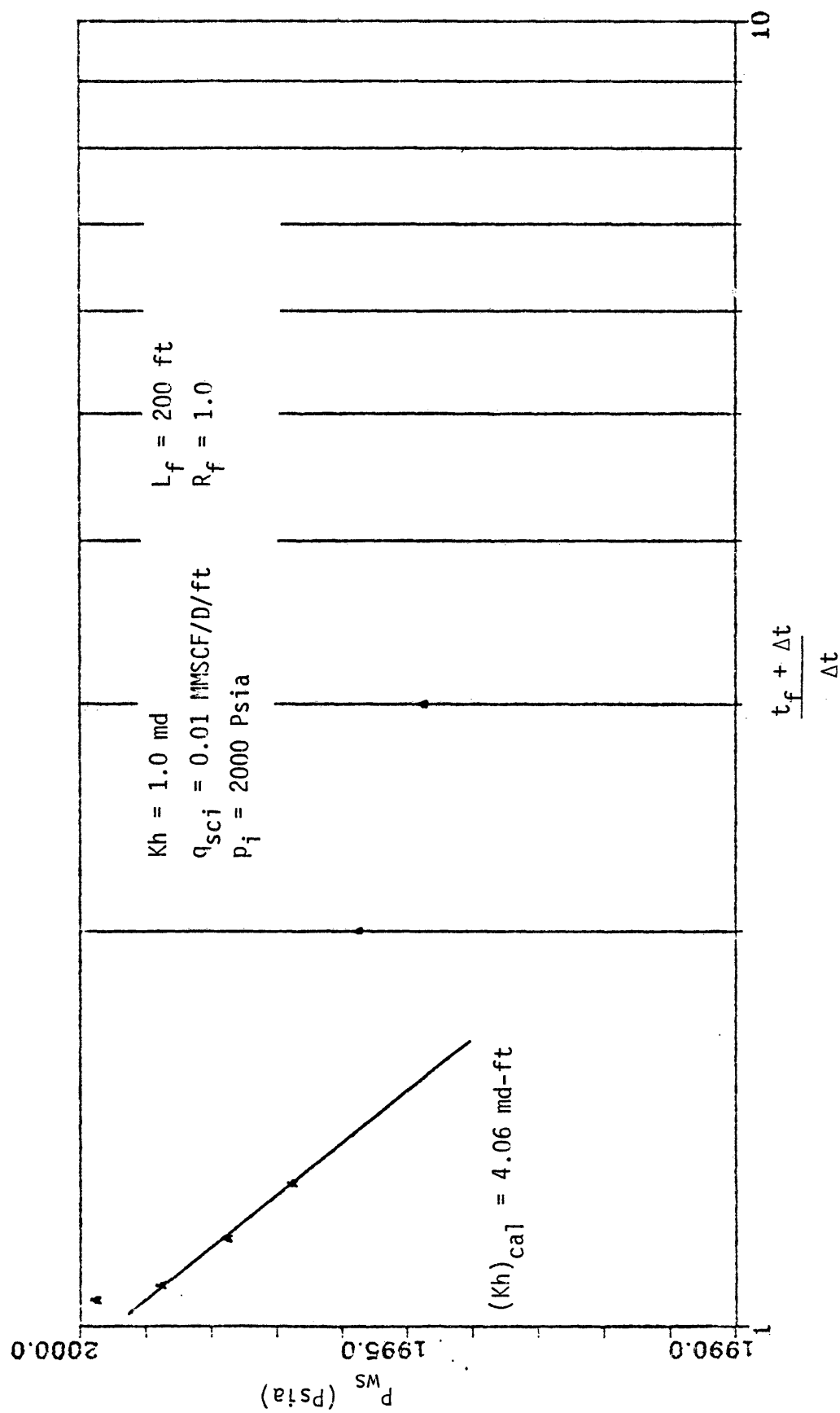


Figure 29. Horner plot - Constant mass rate at the sand face.

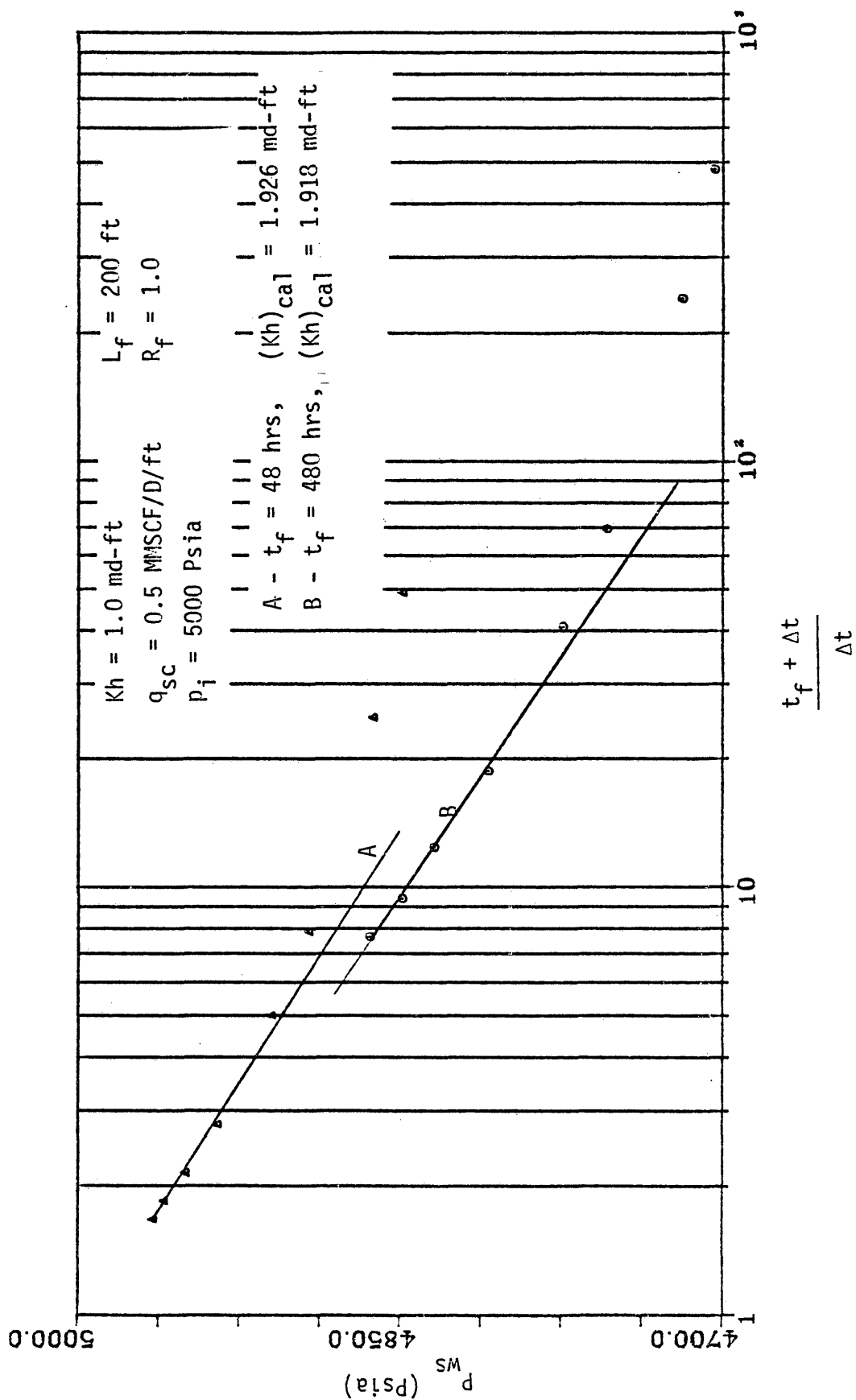


Figure 30. Horner plot - Constant mass rate at the sand face.

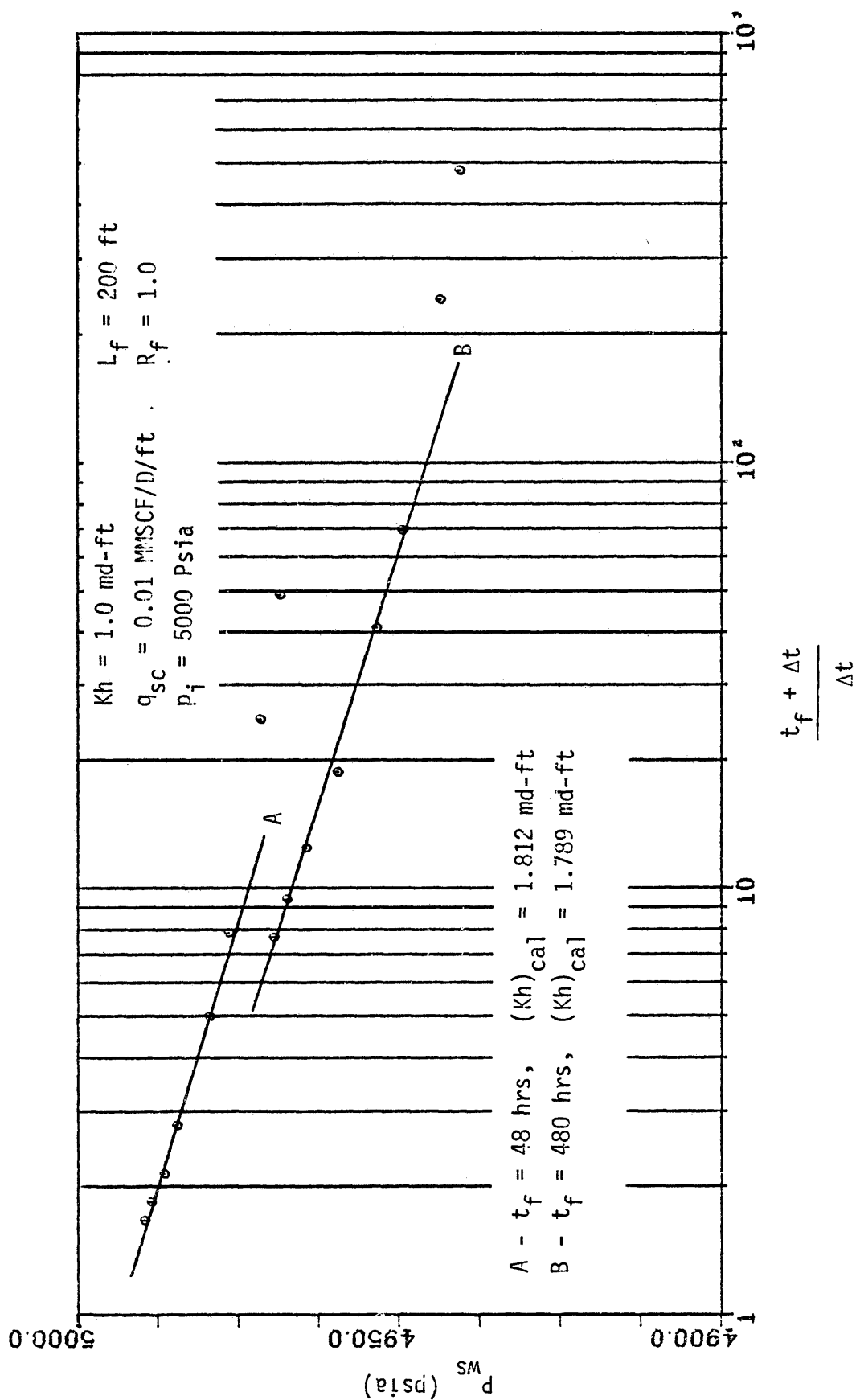


Figure 31. Horner plot - Constant mass rate at the sand face.

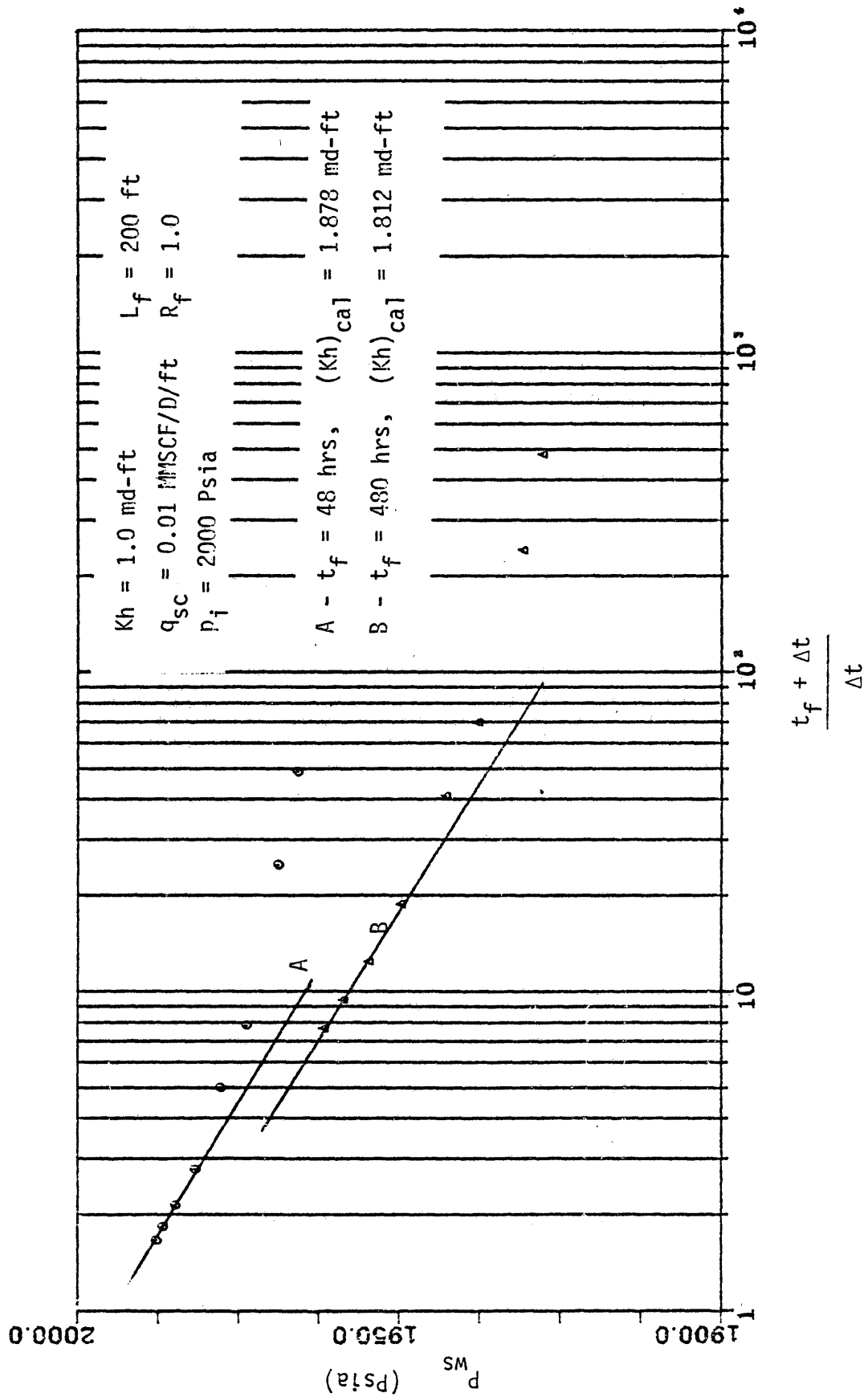


Figure 32. Horner plot - Constant mass rate at the sand face.

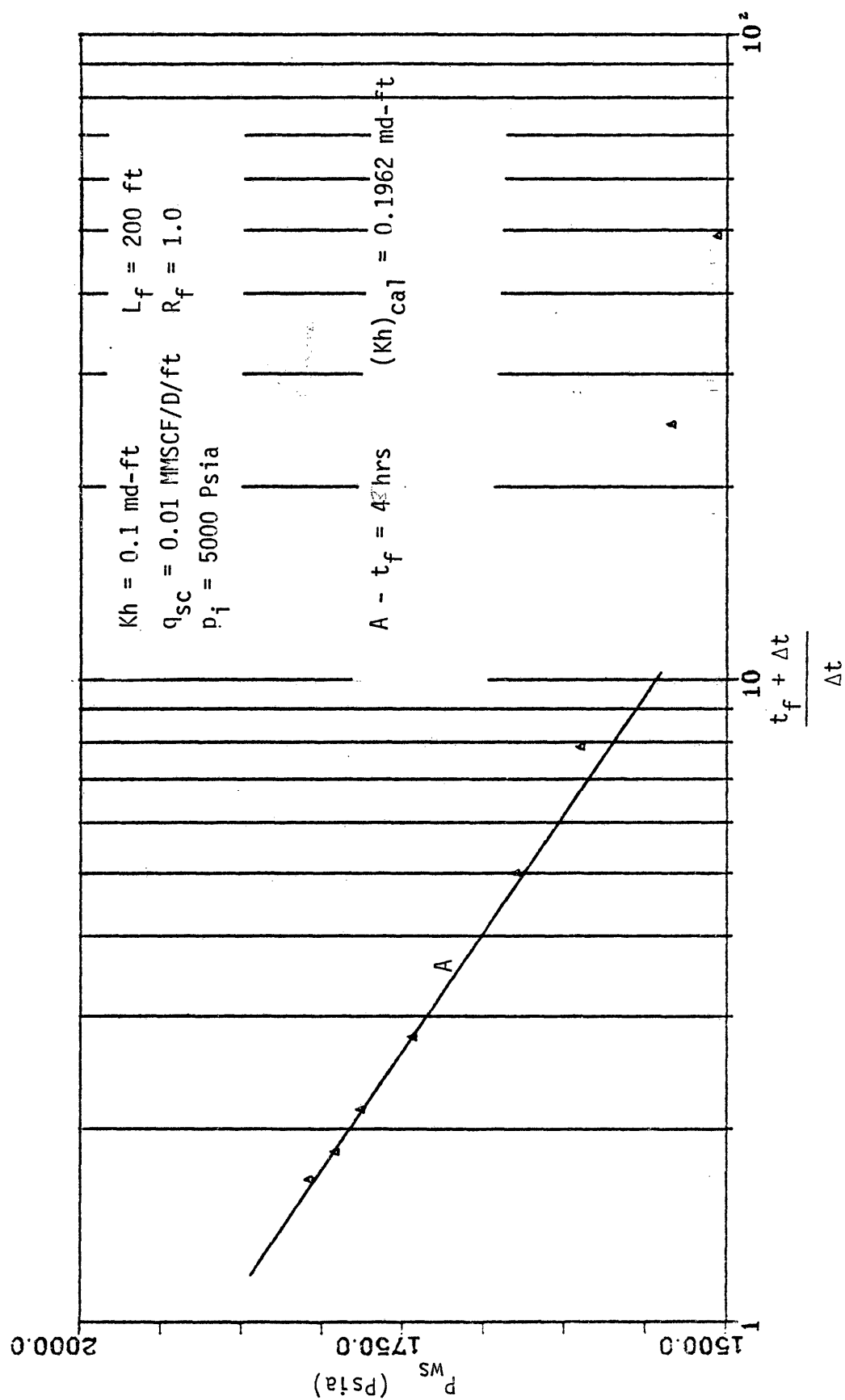


Figure 33. Horner plot - Constant flow rate at the sand face.

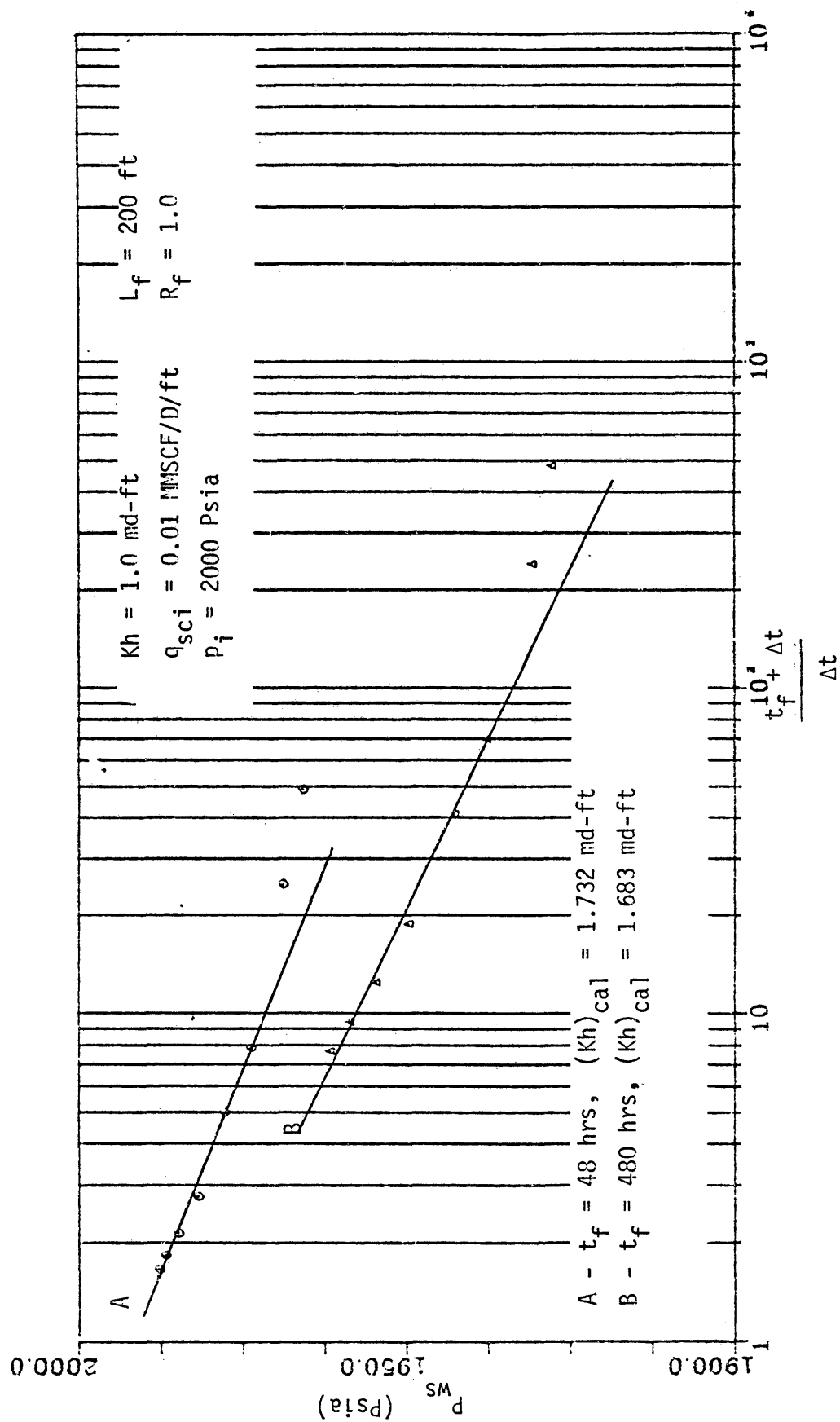


Figure 34. Horner plot - Constant flow rate at the sand face.

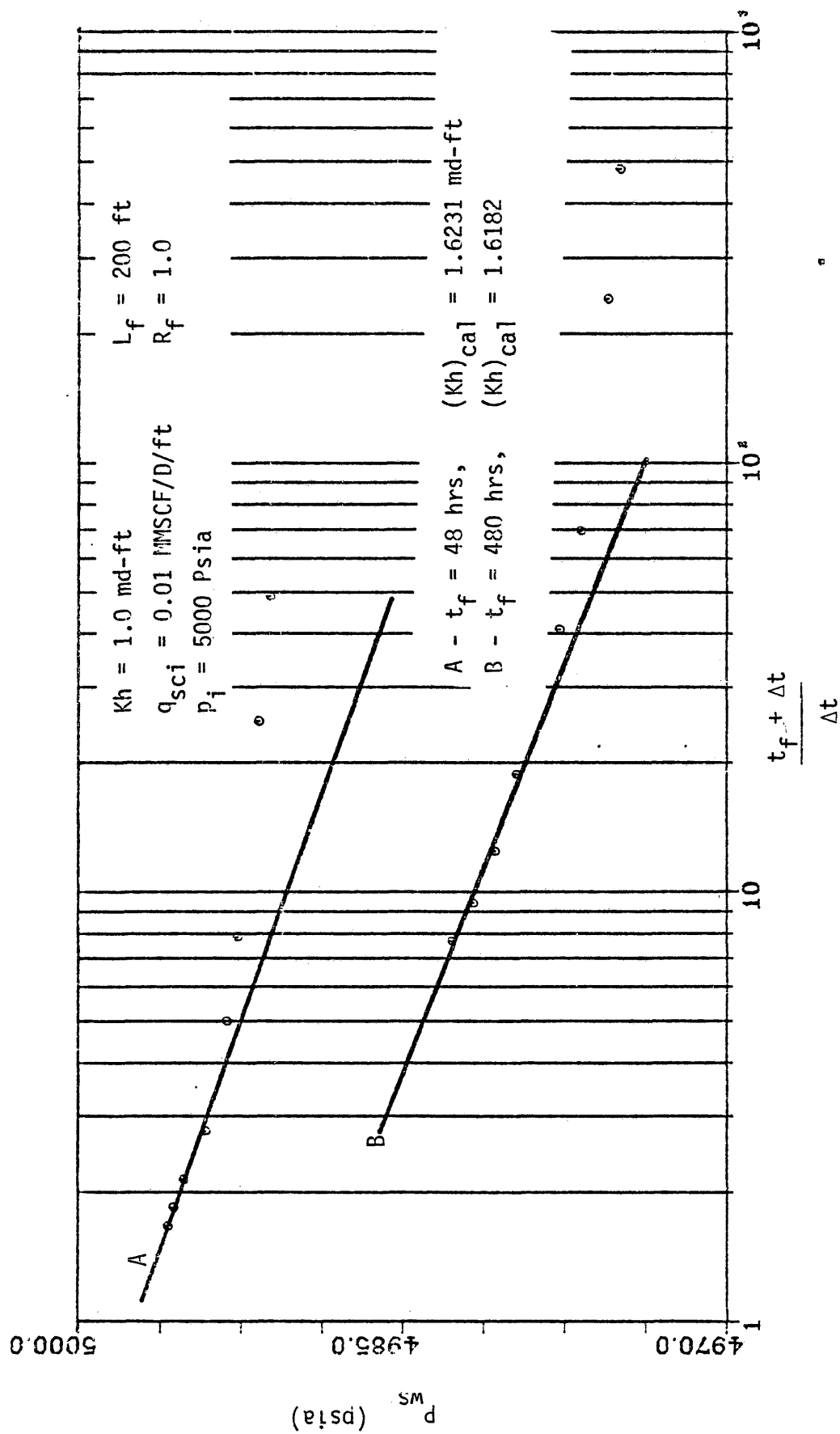
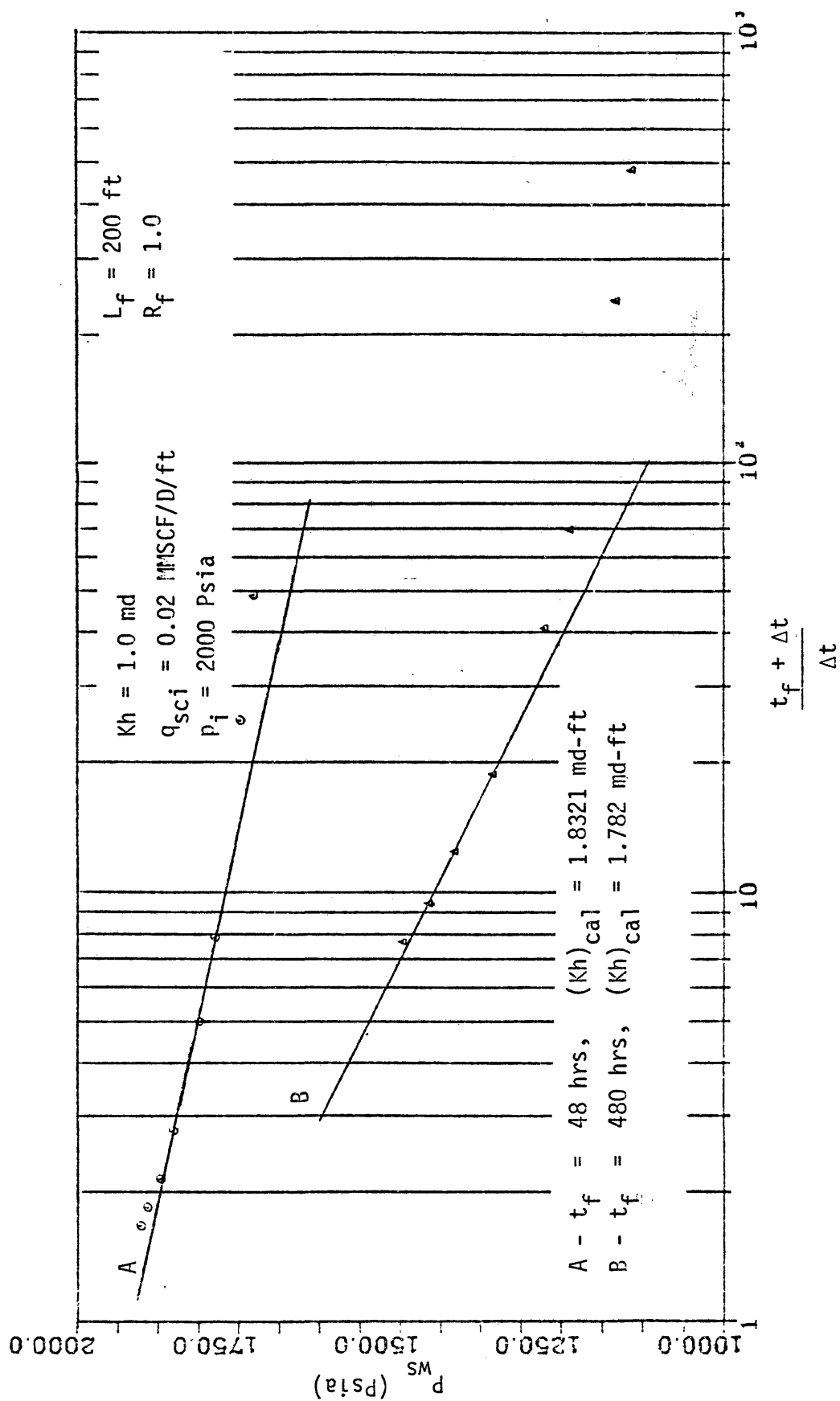


Figure 35. Horner plot - Constant flow rate at the sand face.



E. Short Time Solution

A short time solution for fluid flow into a vertical fracture of infinite conductivity was presented by Russel and Truitt⁴ when fluid compressibility and viscosity were held constant. At early times the system behaves as though all flow were normal to the face of the fracture, such that this period has been referred to as the linear flow period.

Solutions similar to those presented by Russel and Truitt, were made wherein the value of (μc) in the time coefficient was permitted to vary with pressure. The results of these solutions are presented in Figures 36 through 38 as a function of dimensionless variables for the flow of a real gas. The straight line portion of the curves in these figures was found to be fitted by Equation (44).

$$m_D = 1.772 \sqrt{t_{DL}} \quad . \quad . \quad . \quad . (44)$$

Equation 44 can be rearranged such that:

$$m_i - m_{wf} = \frac{1.772 q_{sc} p_{sc} T}{2(1.987 \times 10^{-5}) T_{sc} h \phi} \sqrt{\frac{1}{KL_f^2}} \sqrt{t/\mu c} \quad . \quad . \quad . \quad . (45)$$

A plot of $(m_i - m_{wf})$ as a function of $\sqrt{t/\mu c}$ during the linear flow period will result in a straight line of a slope which could be used to estimate the quantity (KL_f^2) .

From the computer solution, it is noted that the end of linear flow period, in terms of the new definition of dimensionless time, is not a constant which indicates the invalidity of type curve analysis during the linear flow period.

The quantity (KL_f^2) was calculated from the slope of the straight

line of Figures 36, 37 and 38, using Equation 45, and was found to be within 1 percent of the real value. It is noted that the fracture orientation does not affect the linear flow period because of the infinite conductivity of the fracture and the lack of any outer boundary effects.

Figures 37 and 38 illustrate the effect of the fracture orientation after the end of the linear flow period. It is noted that a lower pressure drop was observed when the fracture is symmetric around the wellbore. This behavior could be explained as the effect of the boundary on the flow behavior, which will be observed earlier in the case of an asymmetric fracture.

Figure 36. Effect of fracture position during the linear flow period.

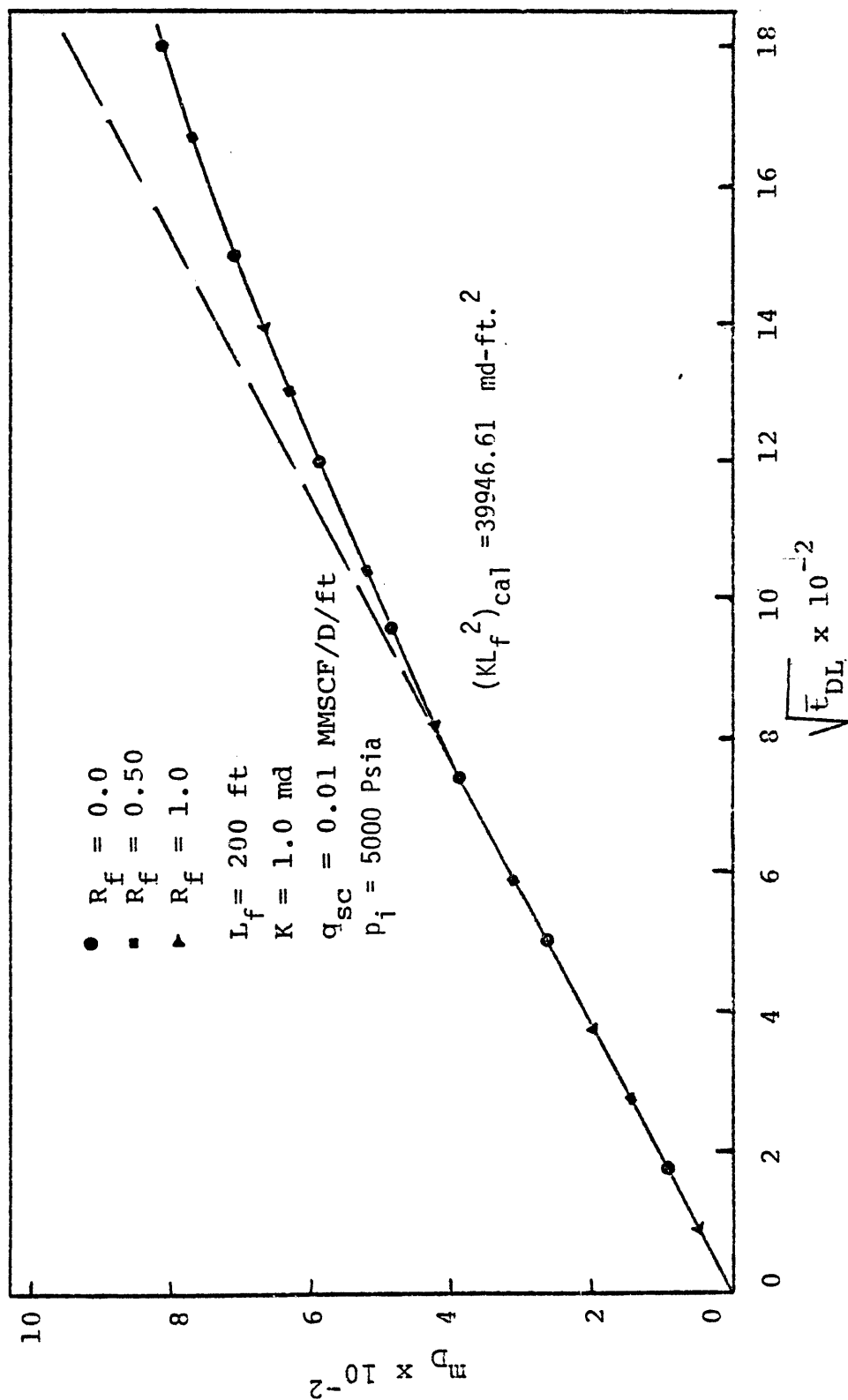


Figure 37. Effect of fracture position during the linear flow period.

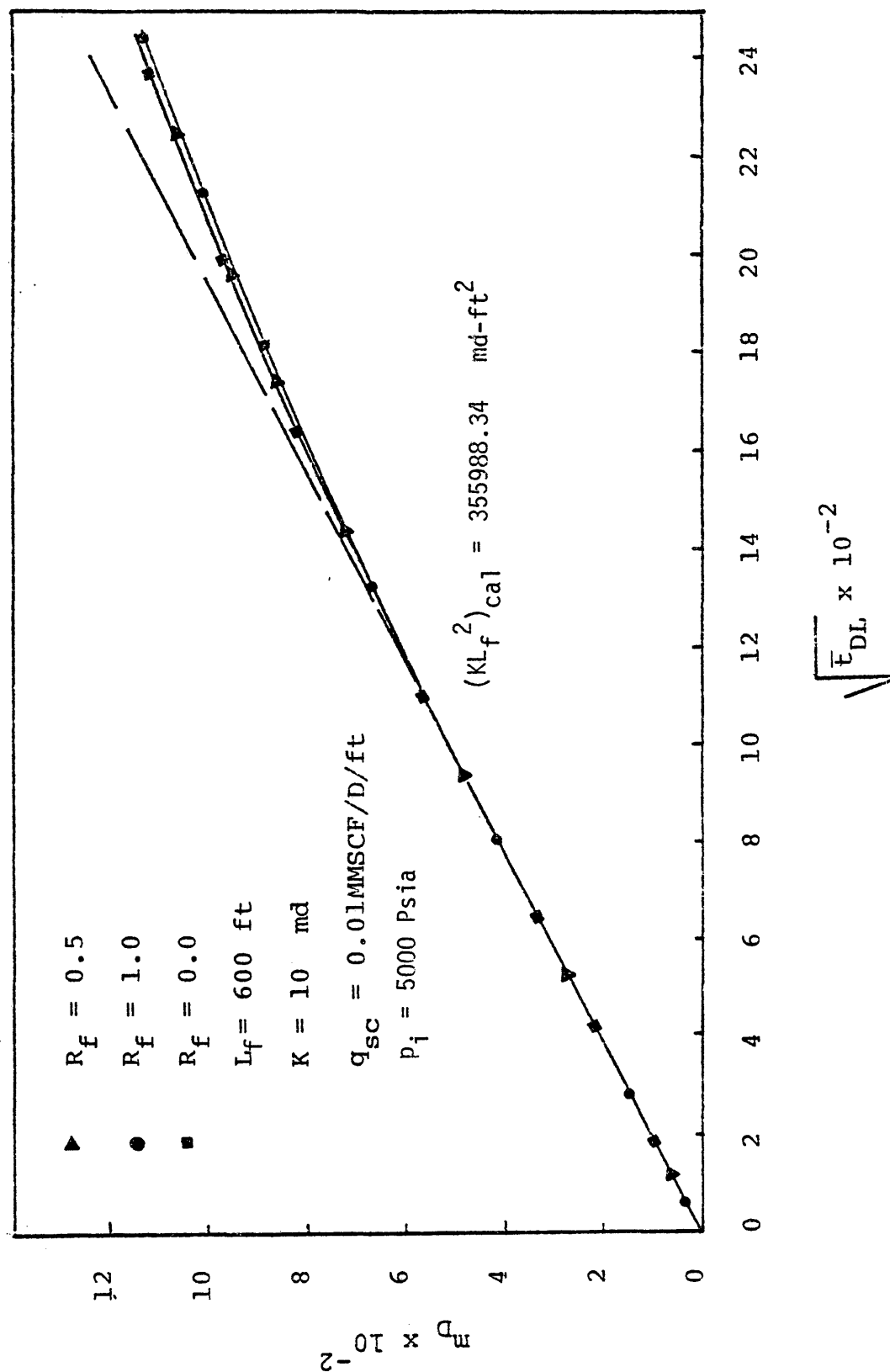
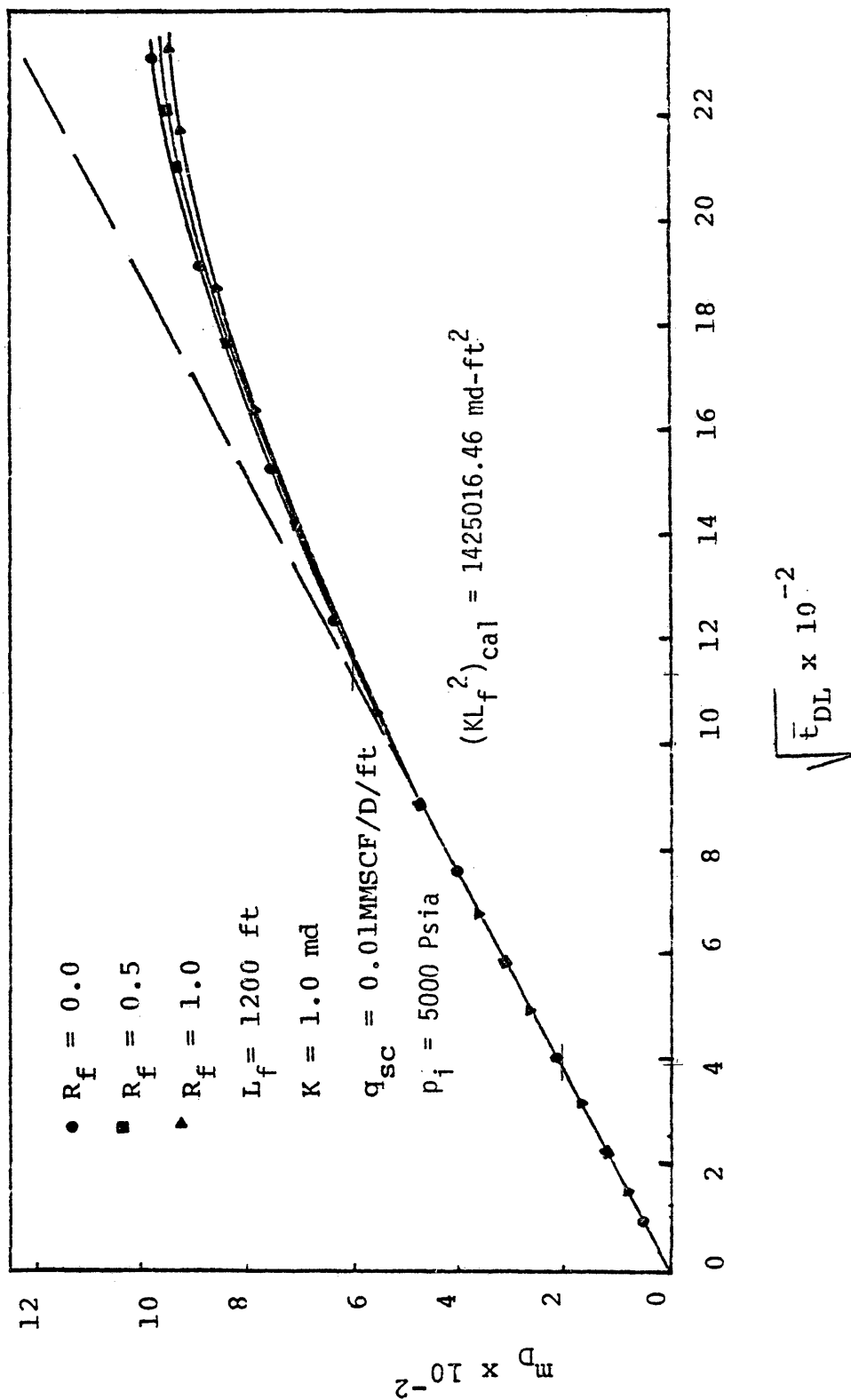


Figure 38. Effect of fracture position during the linear flow period.



F. Basic Drawdown Solution

For both constant mass rate at the sand face and constant flow rate at the sand face, semilog plots of the observed sand face pressure and the flowing time are presented in Figures 39 through 47.

It is noted from these figures that the desired straight line which is supposed to represent radial flow in the system does not exist. However, a line has been drawn to the extended time points which closely approach a straight line and the formation flow capacity determined from the slope of that line.

For constant mass rate at the sand face the formation flow capacity, Kh , was calculated using the following equation:⁵

$$Kh = \frac{57927 q_{sc} P_{sc} T}{2b T_{sc}}, \quad \dots (47)$$

where b is the slope of the straight line segment of p_{wf} as a function of flowing time in terms of the $m(p)$ function. The $m(p)$ values were calculated by taking two values of pressures on the straight line and calculating the two values of $m(p)$. The value of Kh is then calculated using Equation 47. This method of Kh determination has been used because it is observed from Figure (B-4) that a plot of the $m(p)$ function as a function of pressure can be represented by a straight line:

$$m(p) = a + bP, \text{ when } P \geq 3000 \text{ psia}$$

It is also noted that the $m(p)$ function as a function of pressure can be represented by a straight line within a limited range of pressure drop:

$$m(p) = \bar{a} + \bar{b}P, \text{ when } P_2 \leq P \leq P_1$$

$$\text{and } P_2 - P_1 \leq 400 \text{ psia}$$

Figure 43 represents a case where the pressure drop is greater than 400 Psia and hence this method cannot be used. In which case, both $m(p_{wf})$ as a function of flowing time and p_{wf} as a function of flowing time have been plotted and the formation flow capacity was calculated from both Figures 43 and 44. It is noted that a lower error was found in estimating the quantity (Kh) utilizing the plot of $m(p_{wf})$ as a function of flowing time rather than utilizing the plot of p_{wf} as a function of flowing time because of the non-linearity of $m(p)$ function with pressure at low pressure. It is noted that in all cases, the calculated Kh is within 9 percent error from the real value when the pressure drop was less than 400 psi. This error could be explained as a result of the variation of the quantity (μc) with pressure and the non-radial flow in the system. It is also noted that an error of 68 percent in the estimation of Kh when the pressure drop is high. The effect of changes in permeability is illustrated in Figures 40 and 41. It is noted that as the permeability increases the effect of (μc) on the evaluation of Kh decreases because of the smaller pressure drops observed at high permeability.

The effect of changes in flow rate is illustrated in Figures 39 and 40. It is noted that as the flow rate decreases the effect of (μc) on the evaluation of Kh decreases because of the high sand face pressure at low flow rate.

The effect of initial reservoir pressure is illustrated in Figures 40 and 42. It is noted that as the initial reservoir pressure decreases, the

effect of the quantity (μc) on the evaluation of Kh increases because of high variation of (μc) with $m(p)$ at low pressure.

Figure 43 presents a case of high flow rate with low reservoir permeability and 2000 Psia initial reservoir pressure. It is noted that a 68 percent error was found in the calculation of Kh utilizing $m(p_{wf})$ vs. t_f plot because of the variation of (μc) with $m(p)$ at low pressure and the non-radial flow in the system. It is noted that a 73 percent error was found in the calculation of Kh utilizing the p_{wf} vs. t_f plot because of the lower observed pressure at the sand face which will increase the effect of (μc) on the calculation of Kh because of the high variation of (μc) with $m(p)$ at low pressure and the non-linearity of $m(p)$ with pressure at low pressure.

For constant flow rate at the sand face the formation flow capacity, Kh , was evaluated using the following equation:⁵

$$Kh = \frac{57927 q_{sc} p_{sc} T Z \mu}{2b p_{wf} T_{sc}}, \quad \dots (48)$$

where the quantity $\left(\frac{q_{sc} p_{sc} T Z}{p_{wf} T_{sc}}\right)$ is constant equal to the flow rate at the sand face and b in this case is the slope of a semilog plot of sand face pressure as a function of flow time, psi/hrs.

It is noted that in all cases of constant flow rate at the sand face the calculated Kh are within 7 percent error from the real value when the viscosity (μ), in Equation 48, is evaluated at the average pressure of the apparent straight line.

The effect of changes in flow rate for constant flow rate at the sand face is illustrated in Figures 45 and 46. It is noted that as the flow rate increases, the effect of (μc) on the evaluation of Kh increases because of the low observed sand face pressure at high flow rate.

Figures 45 and 47 show the effect of the initial reservoir pressure. It is noted that as the initial reservoir pressure increases the effect of (μc) on the evaluation of Kh decreases because of the low variation of (μc) with $m(p)$ at high pressure.

Figures 40 and 42 represent a constant flow rate at the surface, were compared with Figures 45 and 47 which represent a constant flow rate at the sand face. It is noted that a better estimate of Kh was found in the case of constant flow rate at the sand face because of less pressure drop which decreased the effect of (μc) on the apparent straight line.

Figure 39. Semilog plot of (p_{wf}) as a function of flow time -
Constant mass rate at the sand face.

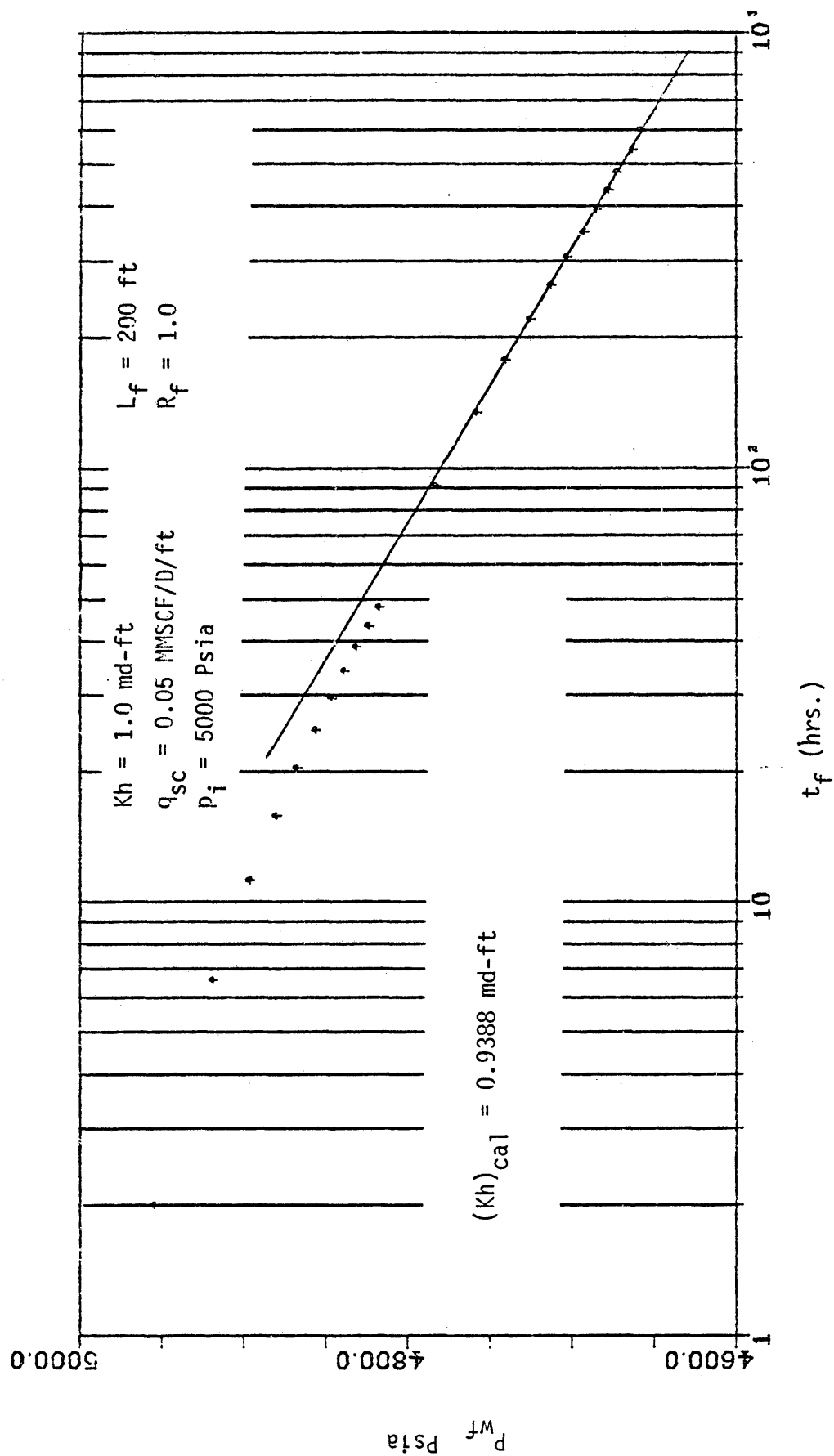


Figure 40. Semilog plot of (p_{wf}) as a function of flow time -
Constant mass rate at the sand face.

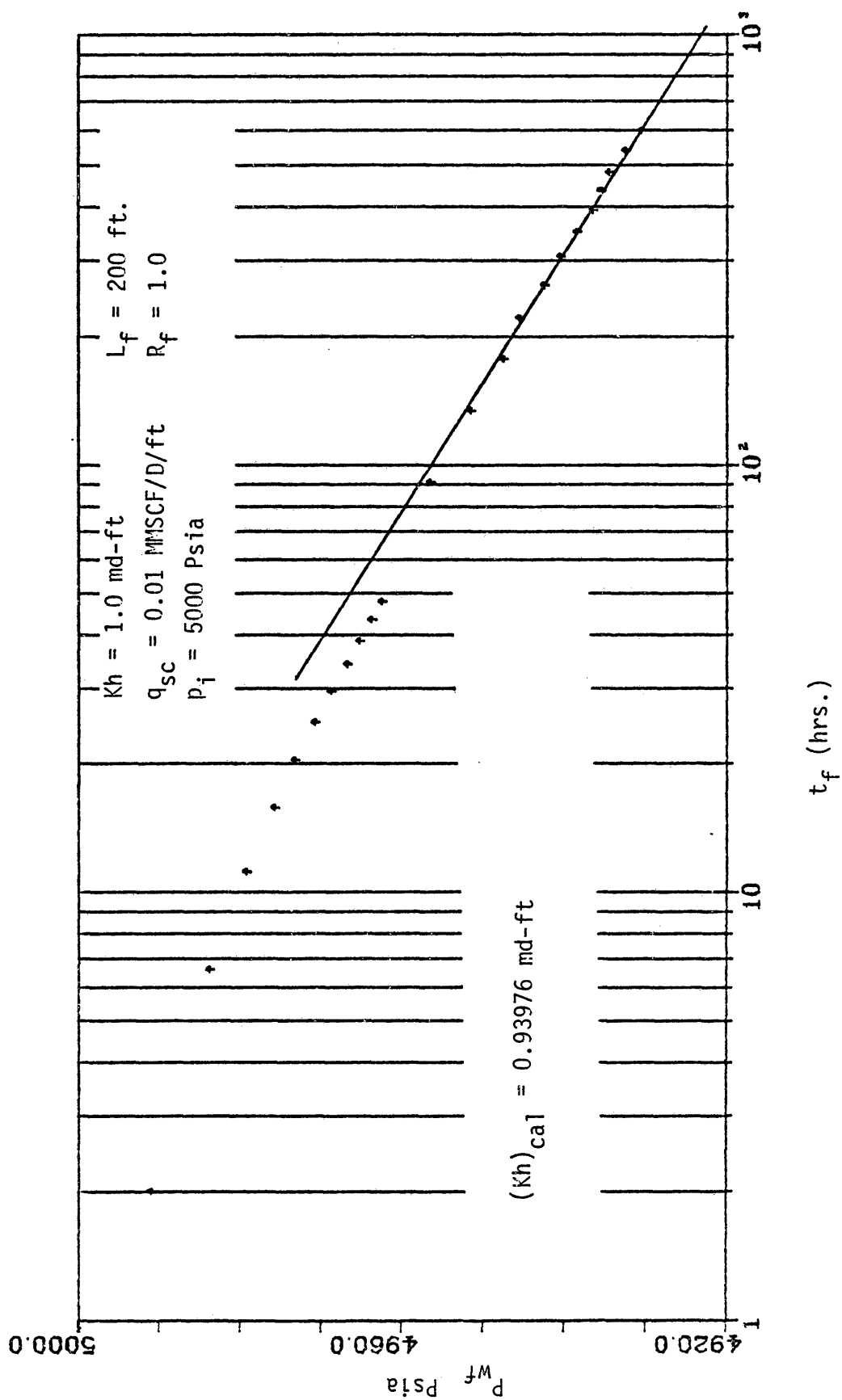


Figure 41. Semilog plot of (p_{wf}) as a function of flow time -
Constant mass rate at the sand face.

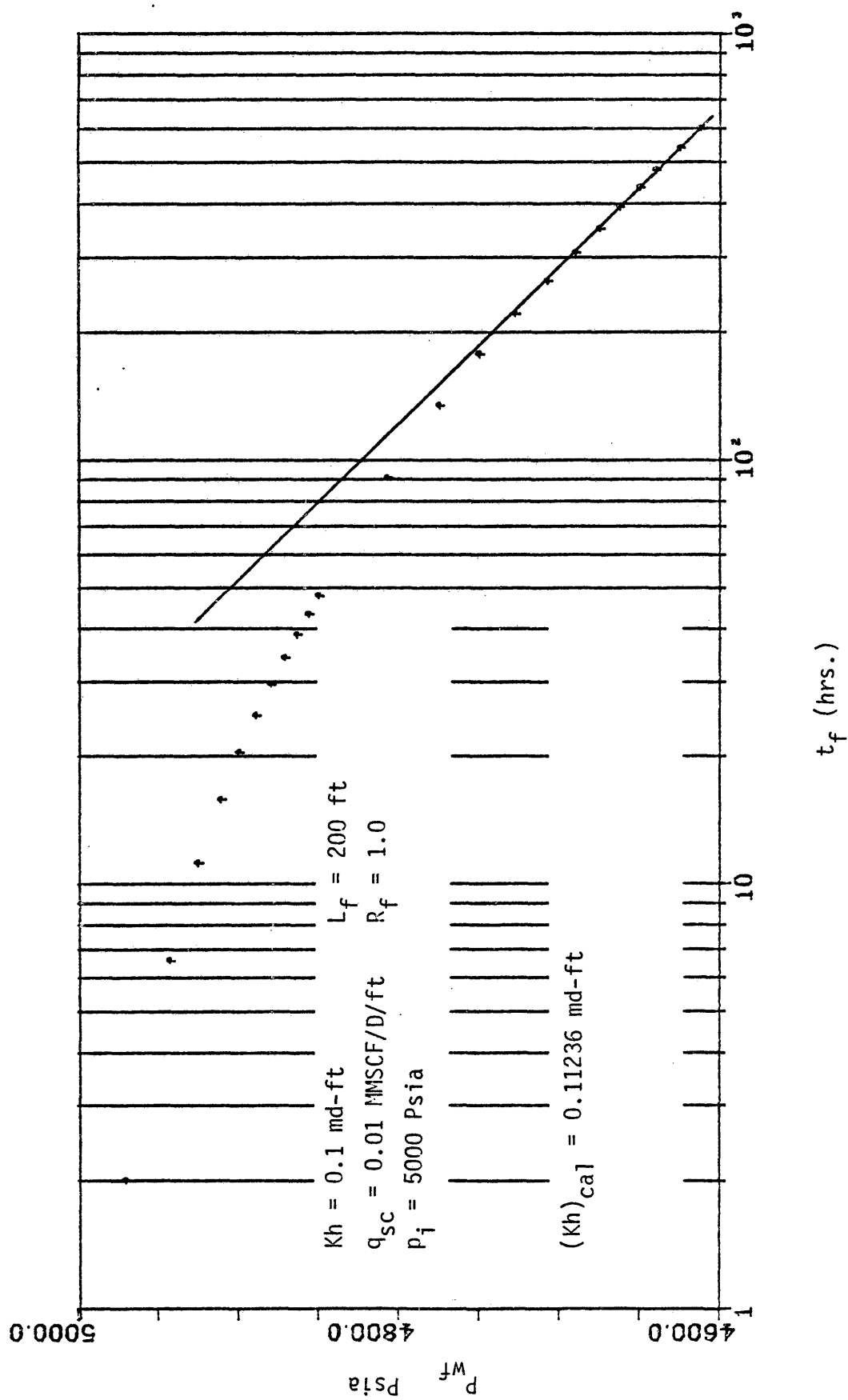


Figure 42. Semilog plot of (p_{wf}) as a function of flow time -
Constant mass rate at the sand face.

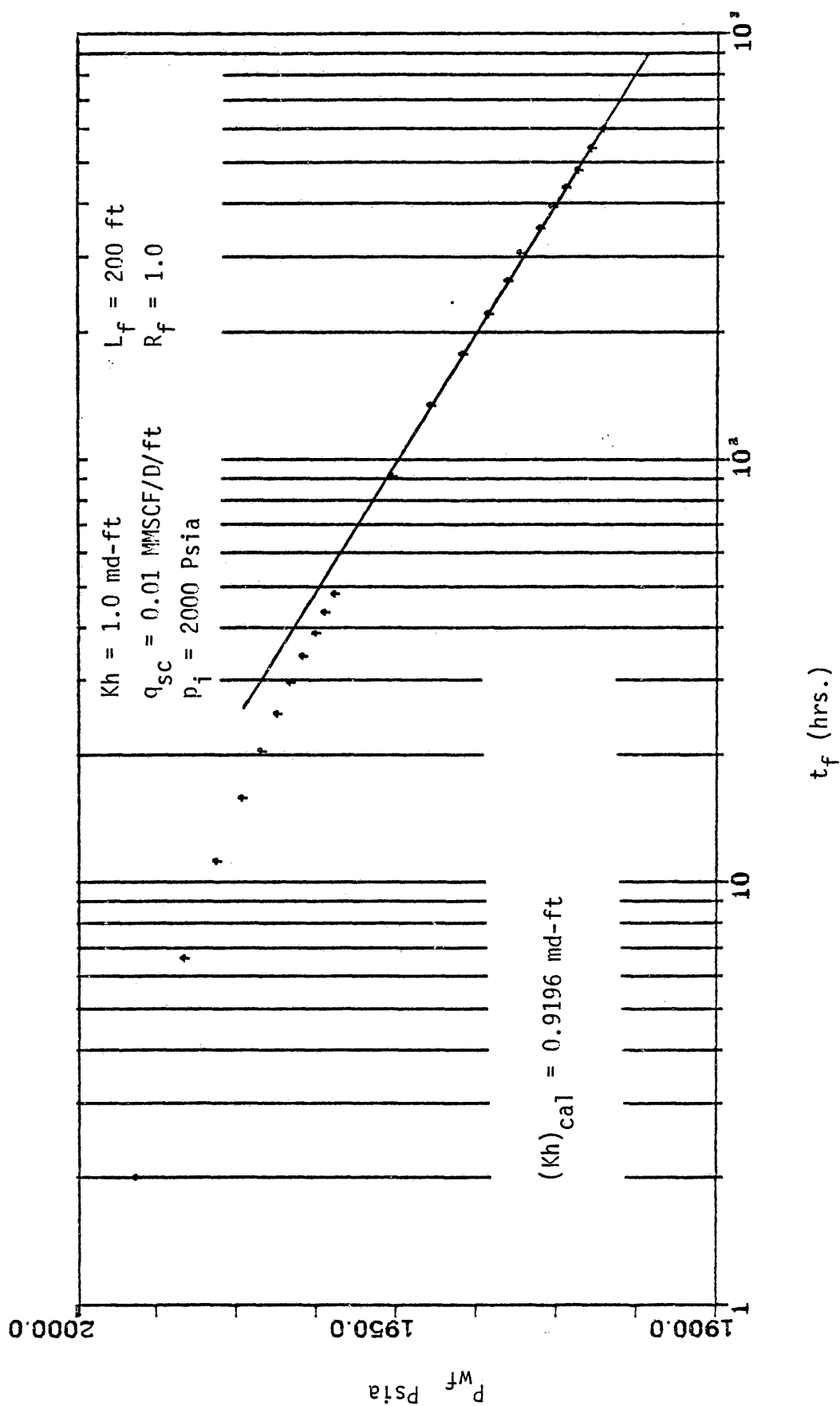


Figure 43. Semilog plot of (p_{wf}) as a function of flow time -
Constant mass rate at the sand face.

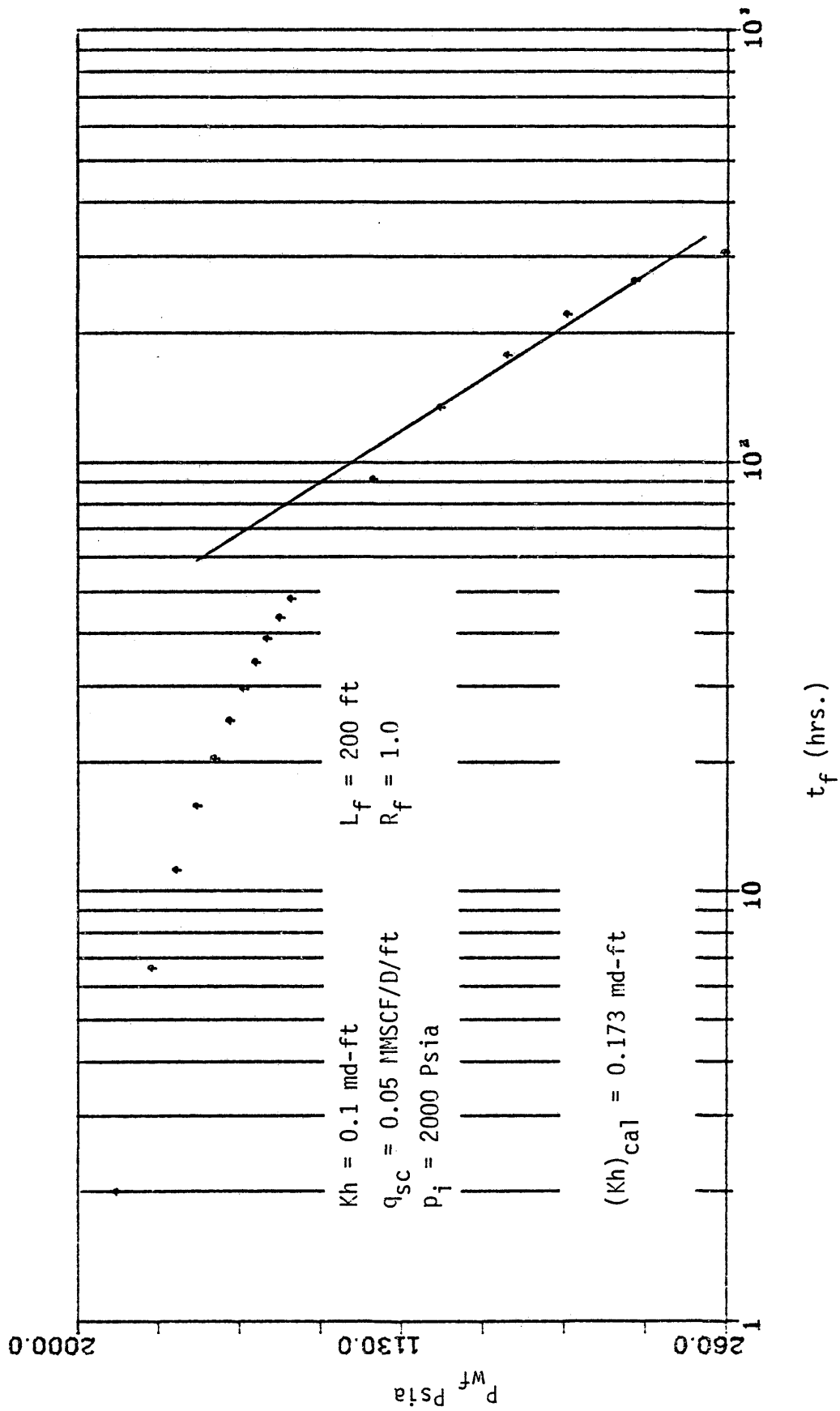


Figure 44. Semilog plot of (p_{wf}) as a function of flow time -
Constant mass rate at the sand face.

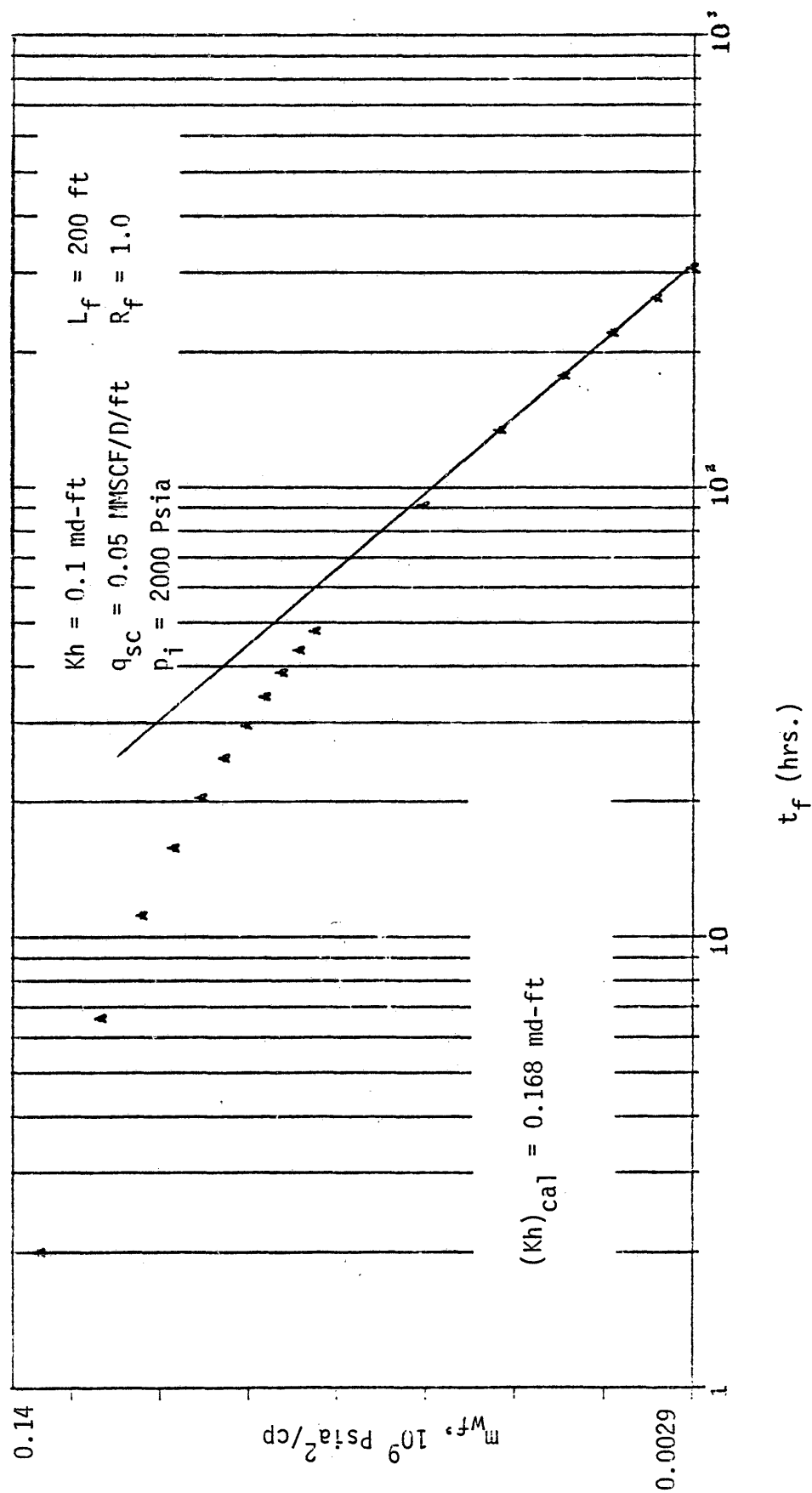


Figure 45. Semilog plot of (p_{wf}) as a function of flow time -
Constant flow rate at the sand face.

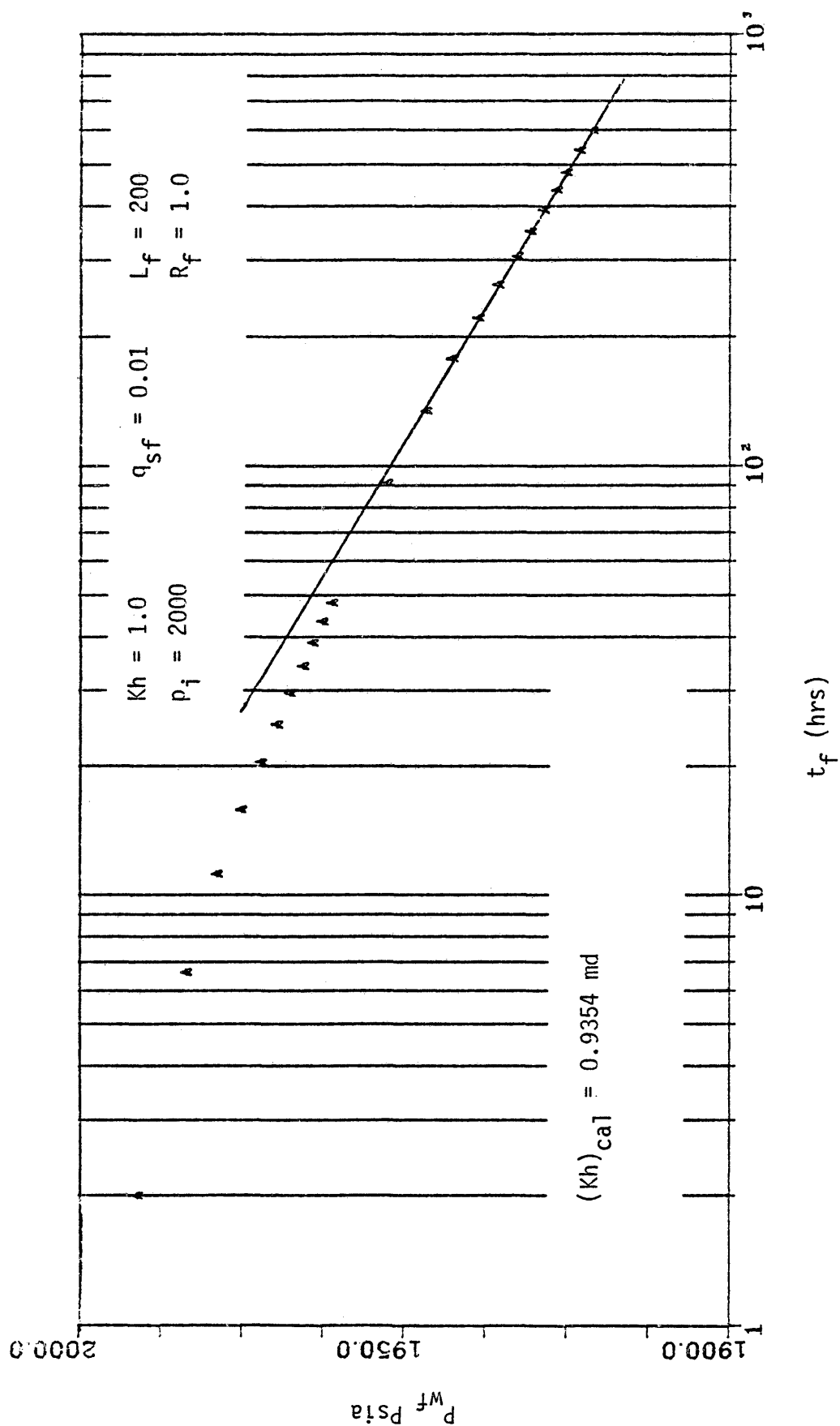


Figure 46. Semilog plot of (p_{wf}) as a function of flow time -
Constant flow rate at the sand face.

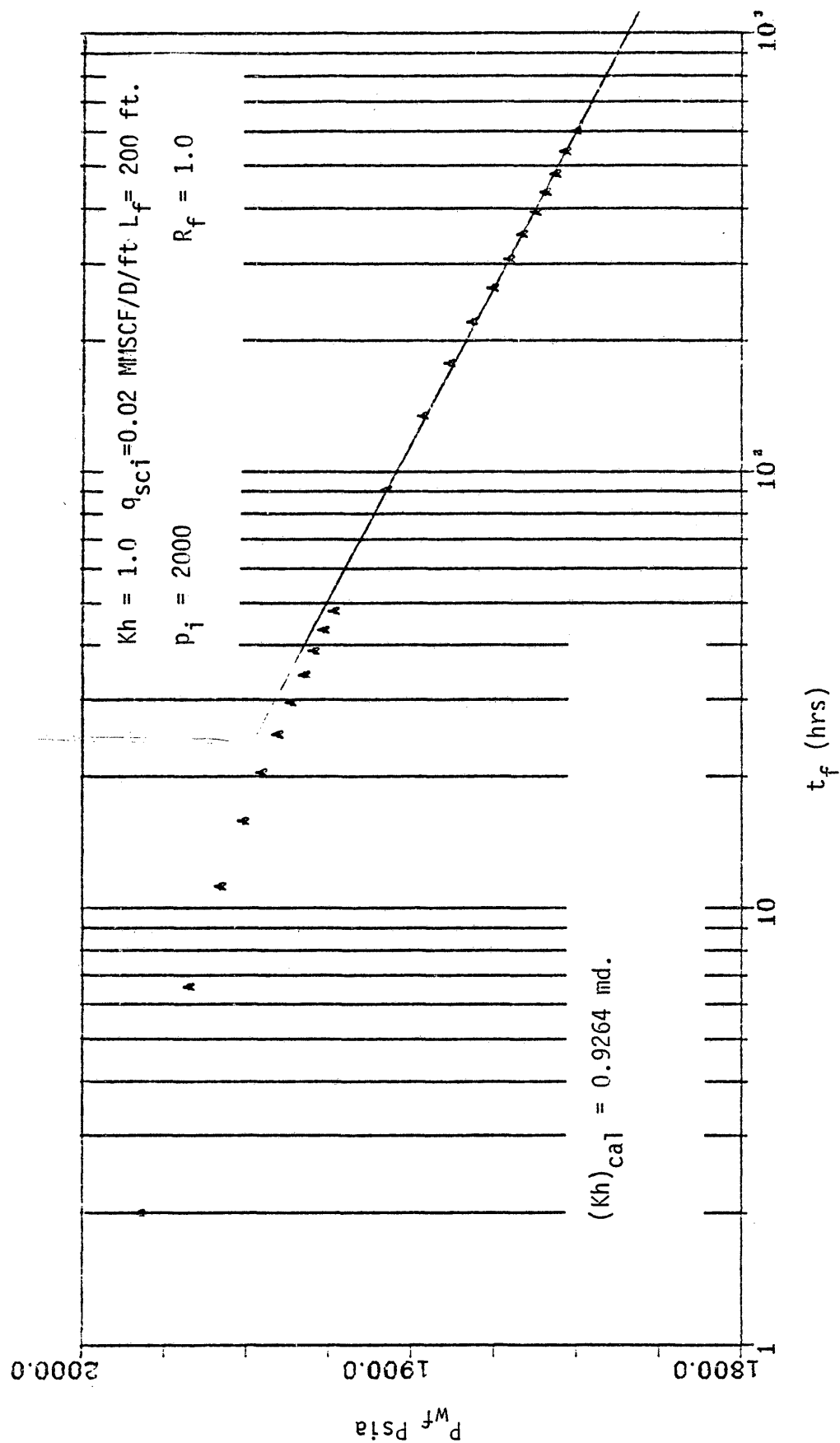
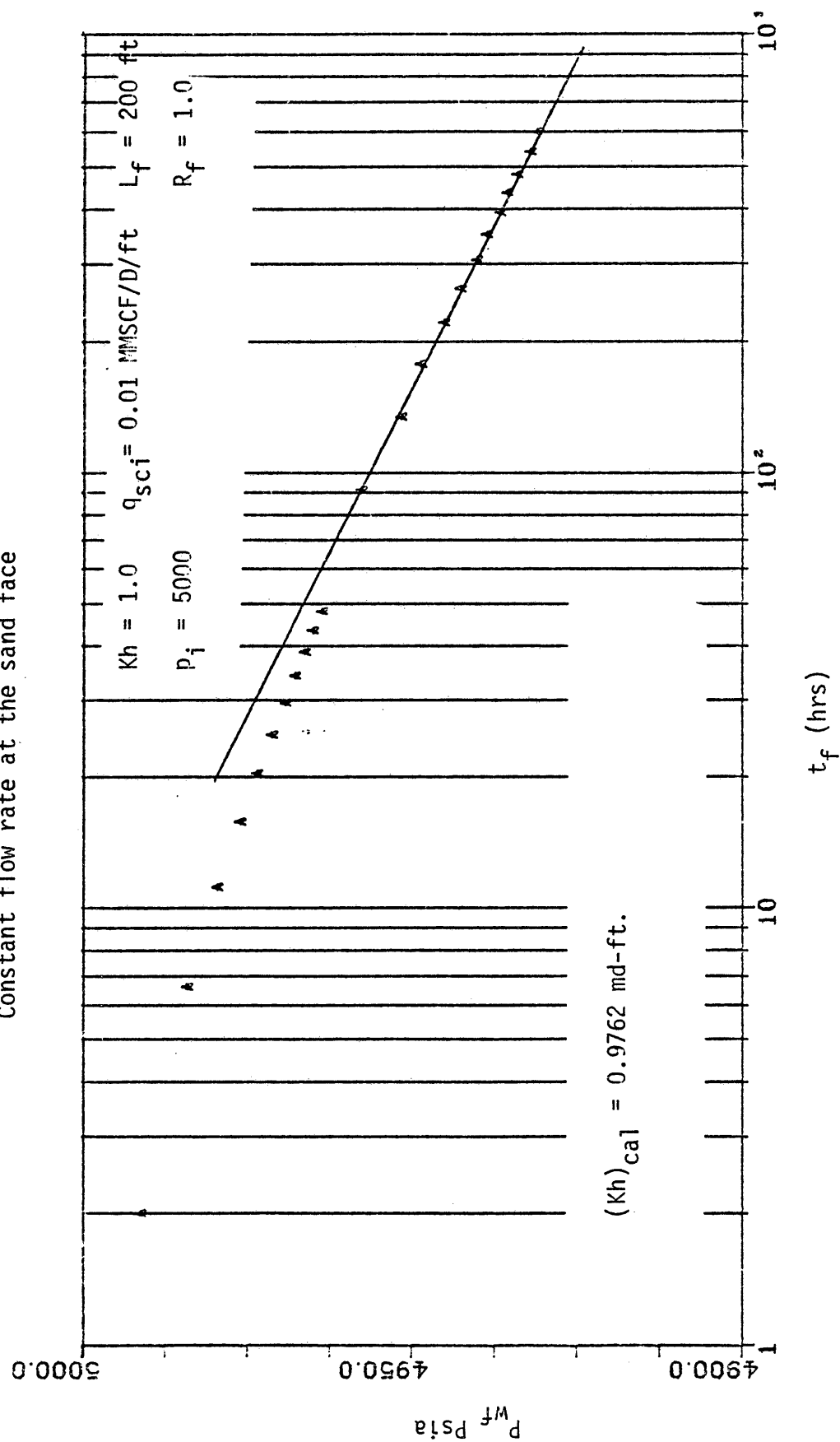


Figure 47. Semilog plot of (p_{wf}) as a function of flow time -
Constant flow rate at the sand face



G. Calculation of Fracture Length

Type curve analysis⁵ by assuming that the "linear" portion of the curve always terminated at the same dimensionless time, has been used to calculate the formation flow capacity and the hydraulic fracture length. As a result of this study, which indicates that the "linear" portion does not terminate at the same dimensionless time, the standard or the modified definition, thus preventing the use of type curve analysis for fractured gas reservoirs. Hence, it is suggested that the following procedures be used to calculate fracture length and formation permeability from a pressure drawdown test:

- (1) Calculate the quantity (KL_f^2) using "linear" flow period data as explained in section E;
- (2) Calculate the formation flow capacity (Kh) using "radial" flow period data as explained in section F; and
- (3) Having the values of (KL_f^2) and (Kh) the value of L_f , fracture length, can be calculated.

Table 5 shows the calculated values of L_f using the above steps. It is noted that in all cases the calculated values of L_f are within 1.0 percent of the actual values.

At the completion of this study, a preliminary report was published on a government contract, ET-78-C-08-1557, by Intercomp Resource Development Engineering Inc. The tentative results published in this report are in complete agreement with the results of this study.

TABLE 6

Fracture Length Calculation

Figure	K Actual md	L _f Actual ft	K Calculated md	KL _f ² Calculated md-ft ²	L _f Calculated ft
3536	1.0	200	0.9862	39946.61	201.263
3637	1.0	600	0.9743	355988.34	604.461
3738	1.0	1200	0.9692	1425016.46	1217.50
			% Error in K	% Error in L _f	
			1.38	0.6315	
			2.57	0.7435	
			3.08	1.046	

CONCLUSIONS

As a result of the data generated by the model and its evaluation, the following is concluded:

1. The $m(p)$ function fails to linearize the flow equation of real gas in porous media;
2. Type curve analysis appears to be invalid for fractured gas reservoirs because the dimensionless quantities are not independent of the variation of fluid properties with pressure and the flow regimes with time;
3. The "linear" flow period can be evaluated for a good estimate of KL_f^2 by plotting m_{wf} or p_{wf} as a function of $\sqrt{t/\mu c}$ where (μc) is evaluated at p_{wf} ;
4. A reasonable value of Kh can be obtained from the apparent straight line section of a plot of m_{wf} or p_{wf} against $\log t$, thus permitting the value of L_f to be calculated;
5. For a given fracture length the fracture position does not affect the slope obtained during the "linear" flow period because of the infinite conductivity of the fracture and the infinite acting of the system;
6. The superposition principle was found to be invalid in fractured gas wells because of the multiple flow regimes with different physical behavior. With larger pressure drops the variation in fluid properties also invalidates the principle of superposition;
7. Type curve analysis for buildup data on fractured gas reservoirs

- is invalid because of the failure of superposition;
8. The Horner plot is an invalid method of evaluating buildup test data in fractured gas wells because it is based on superposition;
 9. The pressure obtained during an initial drawdown test on a fractured gas well is the only data that gives reasonable values of flow capacity and fracture length;
 10. The fracture length cannot be calculated from the "linear" flow period curve alone, but must be combined with data obtained from "radial" flow period.
 11. The "linear" flow period obtained during a pressure buildup test, after an extended flow period, is approximately correct, but the "radial" portion of the buildup curve is incorrect.

RECOMMENDATIONS FOR FURTHER RESEARCH

Areas for further research are recommended below as topics of research into the field of fractured gas reservoirs:

- (1) Asymmetric fracture with finite conductivity;
- (2) Asymmetric fracture with finite and infinite conductivity with turbulent flow into and/or around the fracture;
- (3) Asymmetric fracture with partial penetration;
- (4) Asymmetric fracture with the above conditions with inclined fractures.

NOMENCLATURE

$A_{i,j}$	Arbitrary defined term, see Equation (19) for definition
$B_{i,j}$	Arbitrary defined term, see Equation (20) for definition
$C_{i,j}$	Arbitrary defined term, see Equation (21) for definition
$D_{i,j}$	Arbitrary defined term, see Equation (22) for definition
$G_{i,j}$	Arbitrary defined term, see Equation (23) for definition
FA	Arbitrary defined term, see Equation (15) for definition
b	Slope
c	Gas Compressibility
D	Arbitrary defined term, see Equation (B-11) for definition
d	Total derivative
E	Arbitrary defined term, see Equation (B-12) for definition
F	Arbitrary defined term, see Equation (B-13) for definition
G	Gas specific gravity (Air = 1.0)
h	Reservoir thickness
Ln	Natural logarithm, base e
Log	Common logarithm, base 10
L_f	Total vertical fracture length
L_{f1}	Right length of the fracture
L_{f2}	Left length of the fracture
m	Real-gas pseudo-pressure
m_w	Bottom-hole real-gas pseudo-pressure, general

m_{wf}	Bottom-hole real-gas pseudo-pressure flowing
m_{ws}	Bottom-hole real-gas pseudo-pressure static
m_i	Initial real-gas pseudo-pressure
m_D	Dimensionless real-gas pseudo-pressure
M	Gas molecular weight
MSCF/D/ft	Thousand standard cubic feet per day per ft.
n	Total number of moles
P	Pressure
P_D	Dimensionless pressure
P_c	Pseudo-critical pressure
P_r	Pseudo-reduced pressure
P_{sc}	Pressure at standard condition (14.7 psia)
P_1	Pressure, lower limit of integration for m
P_2	Pressure, upper limit of integration for m
q	Volumetric production rate
q_{sci}	Initial flow rate
q_D	Dimensionless flow rate
R	Universal gas constant (10.72)
R_f	Ratio of two fracture lengths
RHS	Right-hand side of equation
r_w	Wellbore radius
t	Time
t_D	Dimensionless time

\bar{t}_D	Modified dimensionless time
T	Temperature of reservoir
T_{sc}	Temperature at standard condition (520°F)
T_c	Pseudo-critical temperature
T_r	Pseudo-reduced temperature
V	Velocity
V_p	Pore volume
W	Mass Production
x,y	Cartesian space coordinates
X,Y	Cartesian space coordinates
x_f	One-half fracture length, $L_f/2$
Z	Gas deviation factor
∇	Divergence operator
Δ	Finite-difference increment
μ	Gas viscosity
ρ	Gas density
ϕ	Porosity
∂	Partial derivative
Φ	Flow potential

Subscripts and Superscripts

c	Critical
D	Dimensionless
e	External

f	Fracture
i	Initial condition
i	Discrete index of x-direction
j	Discrete index of y-direction
K	Index of iterations at a time step
n	Discrete index of time-step level
r	Pseudo-reduced
sc	Surface, standard conditions
w	Wellbore
x,y	Direction in Cartesian coordinates
t	Time

APPENDICES

APPENDIX A

MATHEMATICAL DEVELOPMENT

In studying flow of any kind -- heat flow, fluid flow, or electric flow -- the mathematics describing the process are obtained by applying a conservation principle which states that some physical quantity is neither created nor destroyed.

Continuity Equation

The Continuity Equation is the mathematical expression of the law of conservation of mass. The equation can be developed by considering the mass flow of fluid through a cubic element of space having dimensions Δx , Δy and unit height with its edges parallel to the X, Y axes, Figure (A-1). For this cube, a mass balance may be written in the form

$$\text{mass in} - \text{mass out} = \text{mass change} \quad . . \text{ (A-1)}$$

At the (x) face of the cube, the fluid velocity and density are V_x and ρ_x , respectively. At the $(x + \Delta x)$ face of the cube, the velocity and density are $V_{x+\Delta x}$ and $\rho_{x+\Delta x}$, respectively.

The fluid velocity and density at the (y) face can be similarly defined as V_y, ρ_y and at the $(y + \Delta y)$ face, the velocity and density are $V_{y+\Delta y}$ and $\rho_{y+\Delta y}$. Furthermore, let the amount of mass released be (W) expressed in mass per unit time per unit volume.

This is the equation of continuity in rectangular coordinates, including a generation term.

Equation (A-1) can be used to formulate differential equations which describe fluid movement within porous media. To do this it is necessary to have a law of flow which can be used to evaluate the velocity terms in Equation (A-2) and an equation of state which describes the dependence of fluid density on pressure.

Darcy's Law

Darcy's law can be used to define the velocities as

$$V_x = - (K_x/\mu) \frac{\partial \Phi}{\partial x}, \text{ and}$$

$$V_y = - (K_y/\mu) \frac{\partial \Phi}{\partial y}$$

Where K is the permeability which may be different in the two coordinate directions,

μ is the fluid viscosity, and

Φ is the flow potential.

The flow potential may be expressed as

$$\Phi = P + \rho gh,$$

where g is the acceleration due to gravity,

P is the pressure,

h is the vertical distance, and

ρ is the fluid density.

Since the x-y plane is horizontal, the only potential which will contain the gravitational term will be the one in the z direction.

With these definitions, the conservation of mass can be stated from Equation (A-1) as follows:

The amount of mass entering the element during a time interval, Δt , is

$$\rho_x V_x \Delta y \Delta t + \rho_y V_y \Delta x \Delta t$$

The amount of mass leaving the element during this time is

$$\rho_{x+\Delta x} V_{x+\Delta x} \Delta y \Delta t + \rho_{y+\Delta y} V_{y+\Delta y} \Delta x \Delta t$$

During this time an amount of mass

$$W(x,y) \Delta x \Delta y \Delta t$$

is released from the element.

The amount of excess of in-flow over out-flow and the release of mass from the element, accumulation of mass, is

$$(\phi_{x,y,t+\Delta t} \rho_{x,y,t+\Delta t} - \phi_{x,y,t} \rho_{x,y,t}) \Delta x \Delta y \Delta t$$

where ϕ is the porosity.

Substituting these expressions into Equation (A-1), dividing through by $\Delta x \Delta y \Delta t$, and taking the limits as Δx , Δy and Δt are allowed to approach zero gives

$$\frac{\partial}{\partial x} (\rho V)_x + \frac{\partial}{\partial y} (\rho V)_y - W(x,y,t) = - \frac{\partial}{\partial t} (\rho \phi) . \quad . . (A-2)$$

Therefore, the velocities may be defined as

$$v_x = -(K_x/\mu) \frac{\partial P}{\partial x}, \text{ and}$$

$$v_y = -(K_y/\mu) \frac{\partial P}{\partial y}.$$

Substituting these expressions for velocity into Equation (A-2) gives

$$\frac{\partial}{\partial x} \left(\frac{\rho K}{\mu} \frac{\partial P}{\partial x} \right) + \frac{\partial}{\partial y} \left(\frac{\rho K}{\mu} \frac{\partial P}{\partial y} \right) - W(x,y,t) = \frac{\partial}{\partial t} (\phi \rho). \quad \text{. . (A-3)}$$

This equation has two dependent variables, pressure and density. It is necessary to eliminate one of the variables to obtain a solution to the equation. To do this, we must have a relationship between density and pressure, provided by an equation of state. The equation of state which is chosen will depend upon the type of fluid under consideration. As a result, the differential equation resulting from substitution of the equation of state in Equation (A-3) will have a different form, depending upon the type of fluid.

Equation of State

The density of a real gas can be expressed as

$$\rho = \frac{M}{ZRT} P,$$

where

M is the molecular weight,

R is the gas constant,

T is the absolute temperature, and

Z is the gas deviation factor.

Substituting into Equation (A-3), neglecting the source term, gives:

$$\frac{\partial}{\partial x} \left(\frac{K}{\mu} \frac{P}{Z} \frac{\partial P}{\partial x} \right) + \frac{\partial}{\partial y} \left(\frac{K}{\mu} \frac{P}{Z} \frac{\partial P}{\partial y} \right) = \frac{\partial(\phi P/Z)}{\partial t} \quad \text{. . (A-4)}$$

The right-hand side of Equation (A-4) can be simplified by assuming that the porosity ϕ is independent of time, in which case the result would be

$$\frac{\partial}{\partial x} \left(\frac{K}{\mu} \frac{P}{Z} \frac{\partial P}{\partial x} \right) + \frac{\partial}{\partial y} \left(\frac{K}{\mu} \frac{P}{Z} \frac{\partial P}{\partial y} \right) = \phi \frac{\partial(P/Z)}{\partial t} \quad \text{. . (A-5)}$$

Real Gas Potential

Al-Hussainy et al (1966) have defined the real-gas pseudo-pressure as (excluding their factor of two)

$$m = \int_{P_1}^{P_2} \frac{P'}{\mu Z} dp' \quad \text{. . (A-6)}$$

then

$$\frac{\partial m}{\partial x} = \frac{\partial m}{\partial p} \frac{\partial P}{\partial x} = \frac{P}{\mu Z} \frac{\partial P}{\partial x} \quad \text{. . (A-7)}$$

$$\frac{\partial m}{\partial y} = \frac{\partial m}{\partial p} \frac{\partial P}{\partial y} = \frac{P}{\mu Z} \frac{\partial P}{\partial y} \quad \text{. . (A-8)}$$

$$\text{and } \frac{\partial m}{\partial t} = \frac{\partial m}{\partial P} \frac{\partial P}{\partial t} = \frac{P}{\mu Z} \frac{\partial P}{\partial t} \quad \text{. . (A-9)}$$

The right-hand side of Equation (A-5) can be written as

$$\begin{aligned}
 \phi \frac{\partial(P/Z)}{\partial t} &= \phi \left(\frac{1}{Z} \frac{\partial P}{\partial t} + P \frac{\partial(1/Z)}{\partial t} \right) \\
 &= \phi \left(\frac{1}{Z} + P \frac{\partial(1/Z)}{\partial P} \right) \frac{\partial P}{\partial t} \\
 &= \phi \frac{P}{Z} \left(\frac{1}{P} - \frac{1}{Z} \frac{dZ}{dP} \right) \frac{\partial P}{\partial t} .
 \end{aligned}
 \quad \dots (A-10)$$

Substituting Equations (A-7), (A-8), (A-9), (A-10), and (A-11) into Equation (A-5) and using the definition of the isothermal gas compressibility, $c = \left(\frac{1}{P} - \frac{1}{Z} \left(\frac{\partial Z}{\partial P} \right) \right)_T$, one obtains

$$\frac{\partial}{\partial x} \left(K \frac{\partial m}{\partial x} \right) + \frac{\partial}{\partial y} \left(K \frac{\partial m}{\partial y} \right) = \phi \mu c \frac{\partial m}{\partial t} , \quad \dots (A-11)$$

This equation can be written as

$$\nabla (\nabla m) = \frac{\phi \mu c}{K} \frac{\partial m}{\partial t} , \quad \dots (A-12)$$

which is Equation 10 of the text.

Finite Differences

By definition, as Δx approaches zero the derivative of a function $g(x)$ can be approximated by

$$\frac{dg(x)}{dx} = \frac{g(x+\Delta x) - g(x)}{\Delta x} + o\Delta(x) . \quad \dots (A-13)$$

where $o\Delta(x)$ represents the truncation error.

For practical application the term $o\Delta(x)$ is omitted and the derivative

of a function is approximated by

$$\frac{dg(x)}{dx} \approx \frac{g(x+\Delta x) - g(x)}{\Delta x} \quad \dots (A-14)$$

Use of the definition given by Equation (A-14) permits Equation (A-11) to be converted to finite-difference form for unequally spaced intervals in the following manner:

The first application of Equation (A-14) to Equation (A-11) yields, for block (i,j) (see Figure (A-3)):

$$\begin{aligned} & \frac{\frac{m_{i+1,j} - m_{i,j}}{X_{i+1} - X_i} - \frac{m_{i,j} - m_{i-1,j}}{X_i - X_{i-1}}}{X_{i+\frac{1}{2}} - X_{i-\frac{1}{2}}} \\ & + \frac{\frac{m_{i,j+1} - m_{i,j}}{Y_{j+1} - Y_j} - \frac{m_{i,j} - m_{i,j-1}}{Y_j - Y_{j-1}}}{Y_{j+\frac{1}{2}} - Y_{j-\frac{1}{2}}} \\ & = \frac{\phi}{K} (\mu c)_{i,j} \frac{m_{i,j}^{n+1} - m_{i,j}^n}{\Delta t} \quad \dots (A-15) \end{aligned}$$

The time level at which to evaluate the m's on the left-hand side and (μc) on the right-hand side of Equation (A-15) is set at n^* for now, resulting in

$$(\text{Left-hand side})^{n^*} = \phi (\mu c)_{i,j}^{n^*} \frac{m_{i,j}^{n+1} - m_{i,j}^n}{\Delta t} \quad \dots (A-16)$$

where

i = spatial index in x direction,

j = spatial index in y direction,

$i+\frac{1}{2},j$ = the representative value between blocks i,j and $i+1,j$

$i,j+\frac{1}{2}$ = the representative value between blocks i,j and $i,j+1$

$$X_{i+\frac{1}{2}} = X_i + \frac{X_{i+1} - X_i}{2},$$

$$X_{i-\frac{1}{2}} = X_i - \frac{X_i - X_{i-1}}{2},$$

$$X_{j+\frac{1}{2}} = Y_j + \frac{Y_{j+1} - Y_j}{2},$$

$$Y_{j-\frac{1}{2}} = Y_j - \frac{Y_j - Y_{j-1}}{2},$$

n = time level at beginning of time step,

$n+1$ = time level at end of time step,

n^* = time level where $n^* = n$ or $n^* = n + \frac{1}{a}$ for $a \geq 1$, and

Δt = size of time step, $t^{n+1} - t^n$.

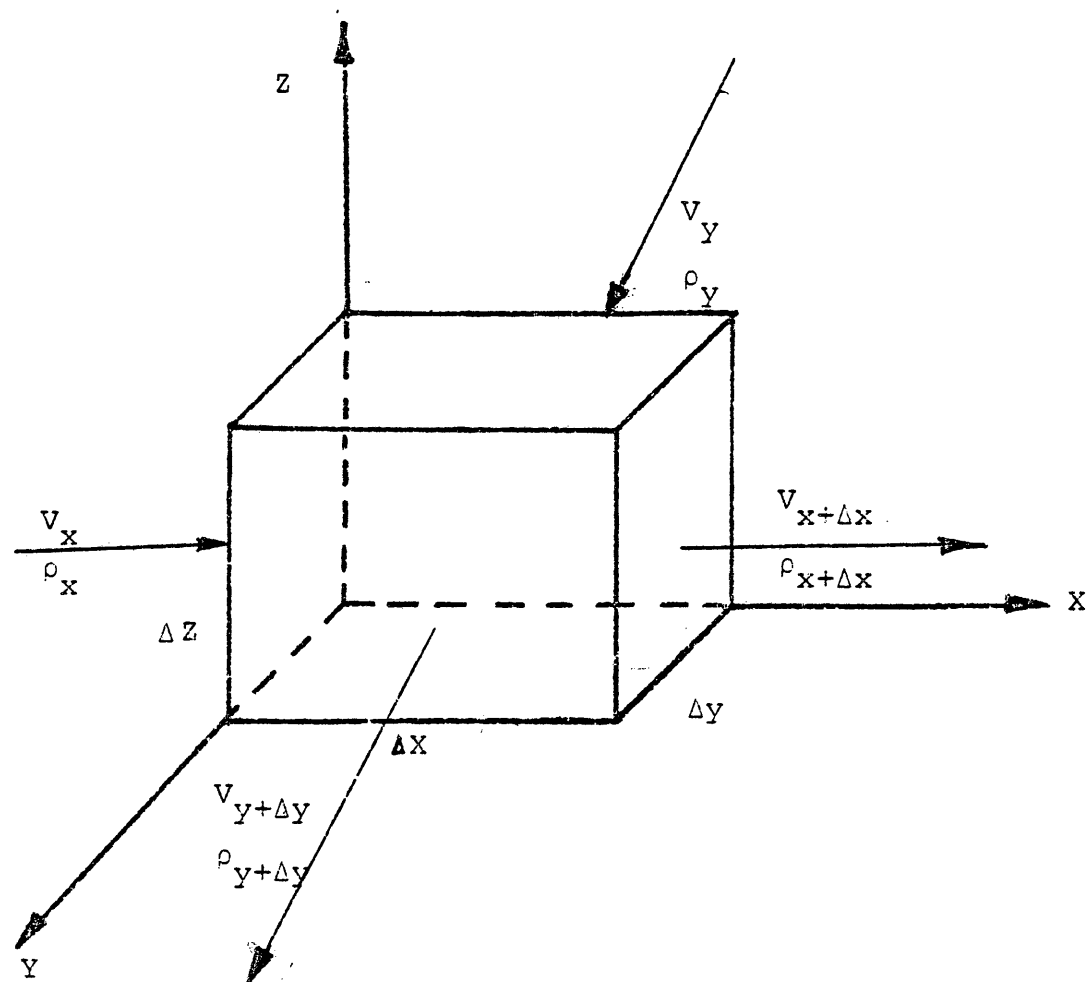


Figure (A-1)
Cubic Elemental Volume of Flow System

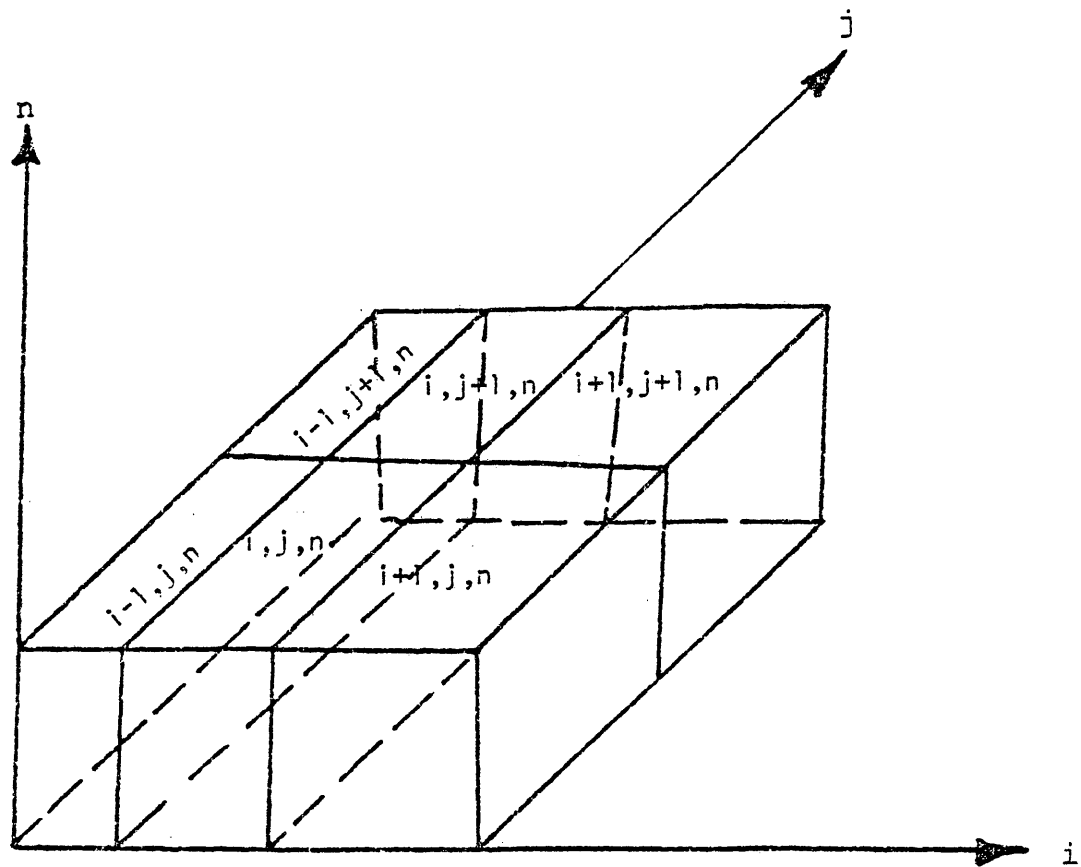


Figure (A-2)

Schematic of Reservoir Model

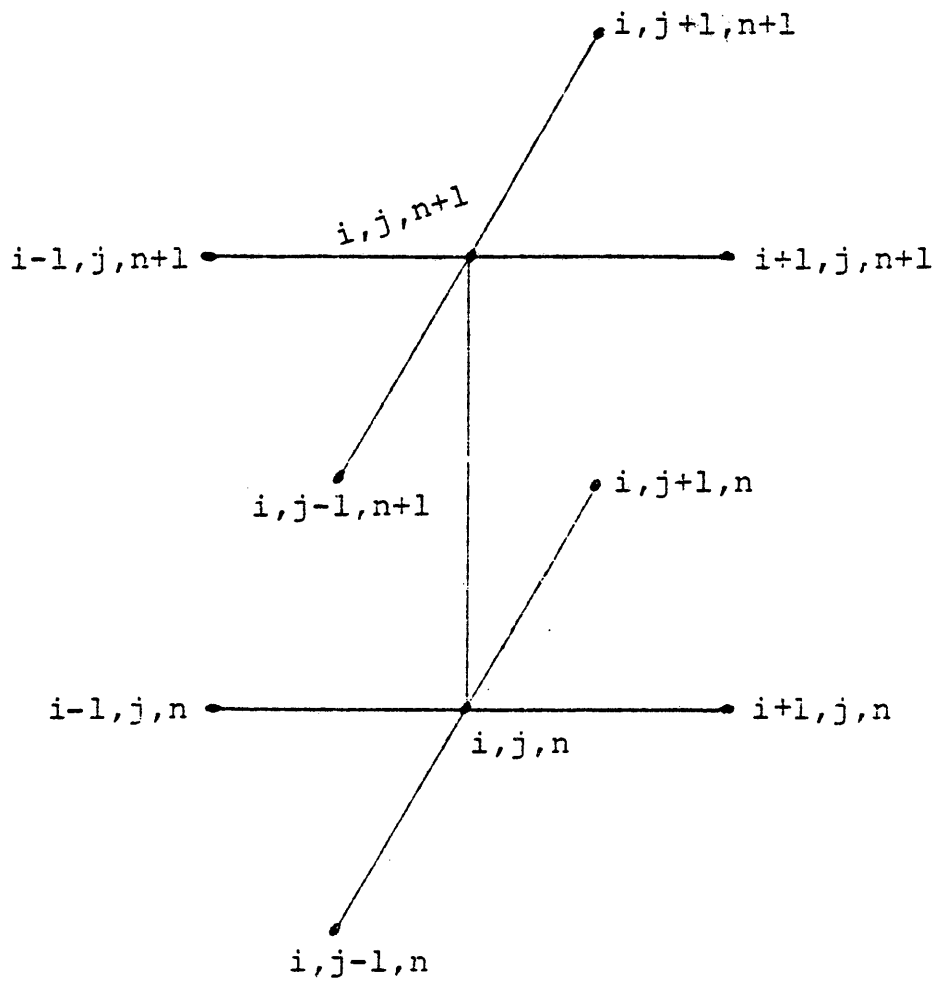


Figure (A-3)
Space-Time Grid Index System

APPENDIX B

HANDLING OF PRESSURE AND TEMPERATURE DEPENDENT VARIABLESPseudo-Critical Pressure and Temperature

Experimental results on abundant research formed the basis for a chart (Katz et al, 1959, p. 112)³⁷ relating pseudo-critical temperature and pressure to gas specific gravity G , from which was derived the relations

$$T_c = 170.2513 + 313.21386 G \quad . . (B-1)$$

$$P_c = 701.9310 - 49.28498 G \quad . . (B-2)$$

Where

T_c = pseudo-critical temperature
degrees R,

P_c = pseudo-critical pressure, psia,

G = gas specific gravity (air = 1.0).

Gas Deviation Factor

Although the Standing-Katz deviation factor charts are easy to use in manual computations, digital computer programming involving compressibility factors requires tedious programming and storage of tabulated compressibility data. This difficulty can be avoided by use of the Benedict,⁵⁷ Rubin, Webb equation of state fitted by Dranchuk and Abou-Kassem (1975).

$$\begin{aligned}
Z = & 1 + (A_1 + \frac{A_2}{T_r} + \frac{A_3}{T_r^3} + \frac{A_4}{T_r^4} + \frac{A_5}{T_r^5}) \rho_r \\
& + (A_6 + \frac{A_7}{T_r} + \frac{A_8}{T_r^2}) \rho_r^2 \\
& - A_9 (\frac{A_7}{T_r} + \frac{A_8}{T_r^2}) \rho_r^5 \\
& + A_{10} (1 + A_{11} \rho_r^2) \frac{\rho_r^2}{T_r^3} \exp(-A_{11} \rho_r^2) \quad \dots (B-3)
\end{aligned}$$

Where

$$\rho_r = \frac{0.27 P_r}{Z T_r} \quad \dots (B-4)$$

$$A_1 = 0.3265$$

$$A_2 = -1.0700$$

$$A_3 = -0.5339$$

$$A_4 = 0.01569$$

$$A_5 = -0.05165$$

$$A_6 = 0.5475$$

$$A_7 = -0.7361$$

$$A_8 = 0.1844$$

$$A_9 = 0.1056$$

$$A_{10} = 0.6134$$

$$A_{11} = 0.7210$$

ρ_r = reduced density

T_r = reduced temperature

P_r = reduced pressure

Z = gas compressibility factor

Gas Compressibility

The isothermal compressibility of a real gas is defined as:

$$c = \frac{1}{P} - \frac{1}{Z} \left(\frac{\partial Z}{\partial P} \right)_T \quad \dots (B-5)$$

Since Z is usually expressed as a function of pseudo-reduced pressure,

it is convenient to define a pseudo-reduced compressibility, thus

$$c_r = c P_c = \frac{1}{P_r} - \frac{1}{Z} \left(\frac{\partial Z}{\partial P_r} \right)_{T_r} \quad \dots (B-6)$$

using Equations (B-3) and (B-4) along with Equation (B-6) gives:

$$c_r = \frac{1}{P_r} - \frac{.027}{Z^2 T_r} \frac{(\partial Z / \partial \rho_r)_{T_r}}{1 + \rho_r / Z (\partial Z / \partial \rho_r)_{T_r}} \quad \dots (B-7)$$

Where

$$\begin{aligned} \left(\frac{\partial Z}{\partial \rho_r} \right)_{T_r} = & \left(A_1 + \frac{A_2}{T_r} + \frac{A_3}{T_r^3} + \frac{A_4}{T_r^4} + \frac{A_5}{T_r^5} \right) \\ & + 2 \left(A_6 + \frac{A_7}{T_r} + \frac{A_8}{T_r^2} \right) \rho_r \\ & - .5 A_9 \left(\frac{A_7}{T_r} + \frac{A_8}{T_r^2} \right) \rho_r^4 \\ & - 2 A_{11} A_{10} \rho_r (1 + A_{11} \rho_r^2) \frac{\rho_r^2}{T_r^3} \exp(-A_{11} \rho_r^2) \\ & + \exp(-A_{11} \rho_r^2) \left(\frac{2 \rho_r A_{10}}{T_r^3} \right) (1 + A_{11} \rho_r^2 + \frac{\rho_r^2}{T_r^3} (2 A_{11} \rho_r) \dots (B-8) \end{aligned}$$

Equations (B-6), (B-7) and (B-8) were used to calculate c .

Where

- c = isothermal gas compressibility, psia^{-1} ,
- T_r = reduced temperature,
- P_r = reduced pressure,
- ρ_r = reduced density,
- Z = gas compressibility factor.

Gas Viscosity

58

Lee et al (1966) reported the following empirically derived equations for calculating gas viscosity (μ , cp)

$$M = 28.966G \quad . . (B-9)$$

$$\rho = \frac{0.0160184MP}{ZRT} \quad . . (B-10)$$

$$D = \frac{(7.77 \text{ to } .063M) T^{1.5}}{122.4 + 12.9M + T} \quad . . (B-11)$$

$$E = 2.57 + \frac{1914.5}{T} + 0.0095M \quad . . (B-12)$$

$$F = 1.11 + 0.04E \quad . . (B-13)$$

$$\mu = \frac{D e^{E\rho^F}}{1000} \quad . . (B-14)$$

Where

M = gas Molecular Weight, Ib/mole,

ρ = gas density, Ib/cu.ft.,

D, E, F = intermediate values,

μ = gas viscosity, cp.

Numerical Integration of Real-Gas Pseudo-Pressure

Al-Hussainy et al (1966) have defined the real-gas pseudo-pressure as (excluding their factor of two)

$$m = \int_{P_1}^{P_2} 2 \frac{P}{\mu Z} dP \quad . . (B-15)$$

Where

m = real-gas pseudo-pressure,

P_1 = the lower pressure at which $m(p)$ is evaluated,

P_2 = the upper pressure at which $m(p)$ is evaluated,

μ = gas viscosity, cp,

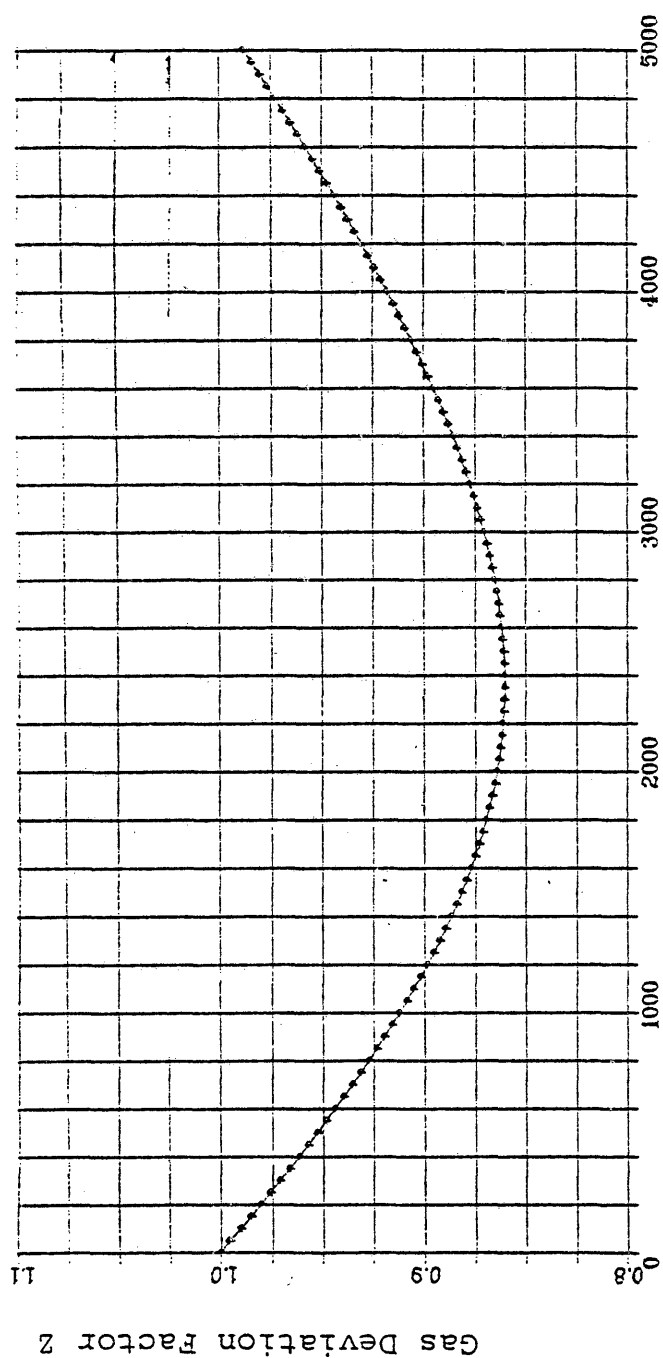
Z = gas compressibility factor,

P = pressure, psia.

Romberg's method of numerical integration was used to integrate Equation (B-15).

Interpolation Technique

The numerical model interpolated linearly between table values for pressure and real-gas pseudo-pressure and also between table values for real-gas pseudo-pressure and (μc) .



Pressure, psia

Figure B-1. The Relation of the Deviation Factor Z Function With Pressure for a 0.7 Gravity Gas at a Temperature of 200°F.

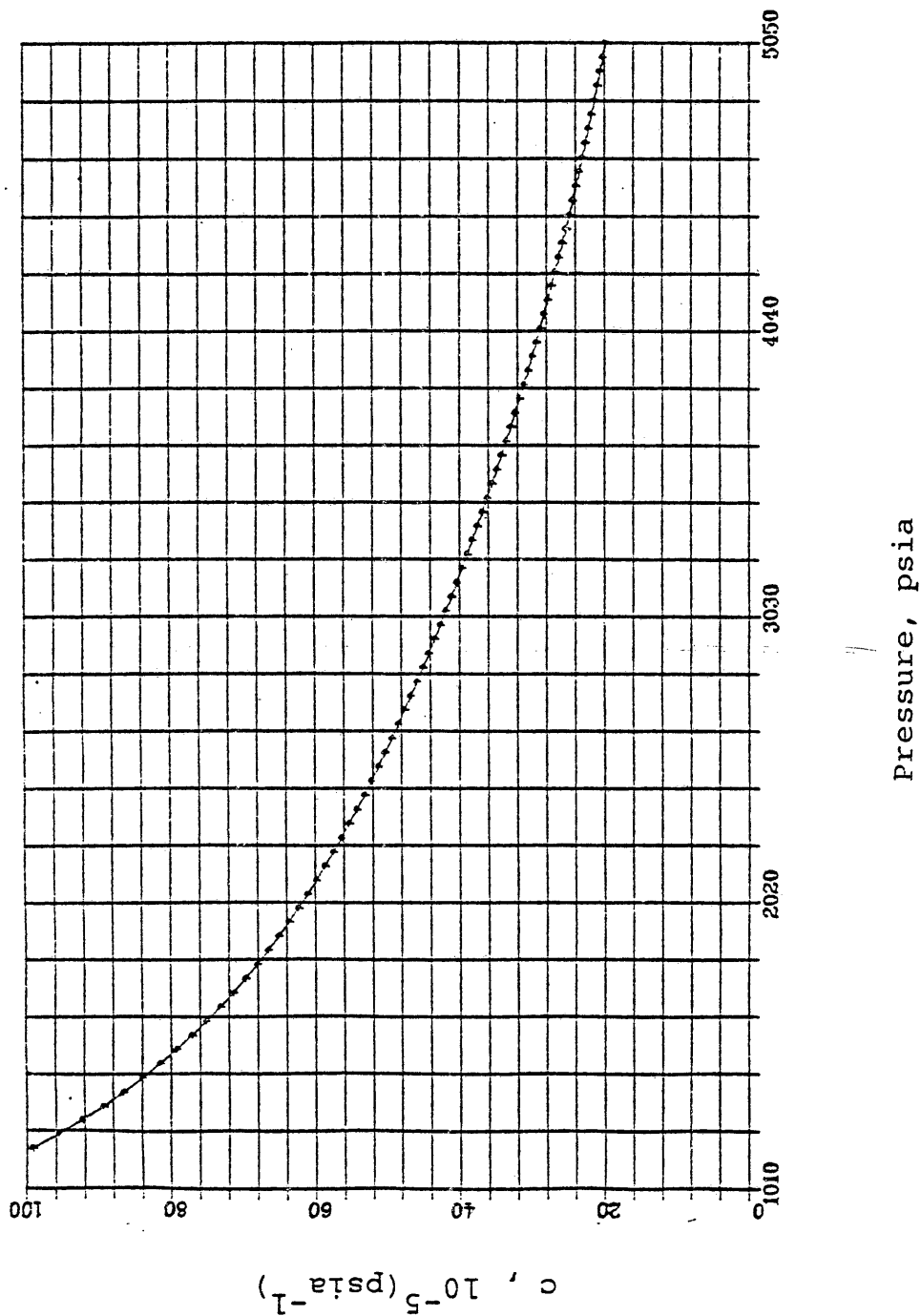


Figure B-2. The Relation of the Compressibility Function
with Pressure for a 0.7 Gravity Gas at a
Temperature of 200°F.

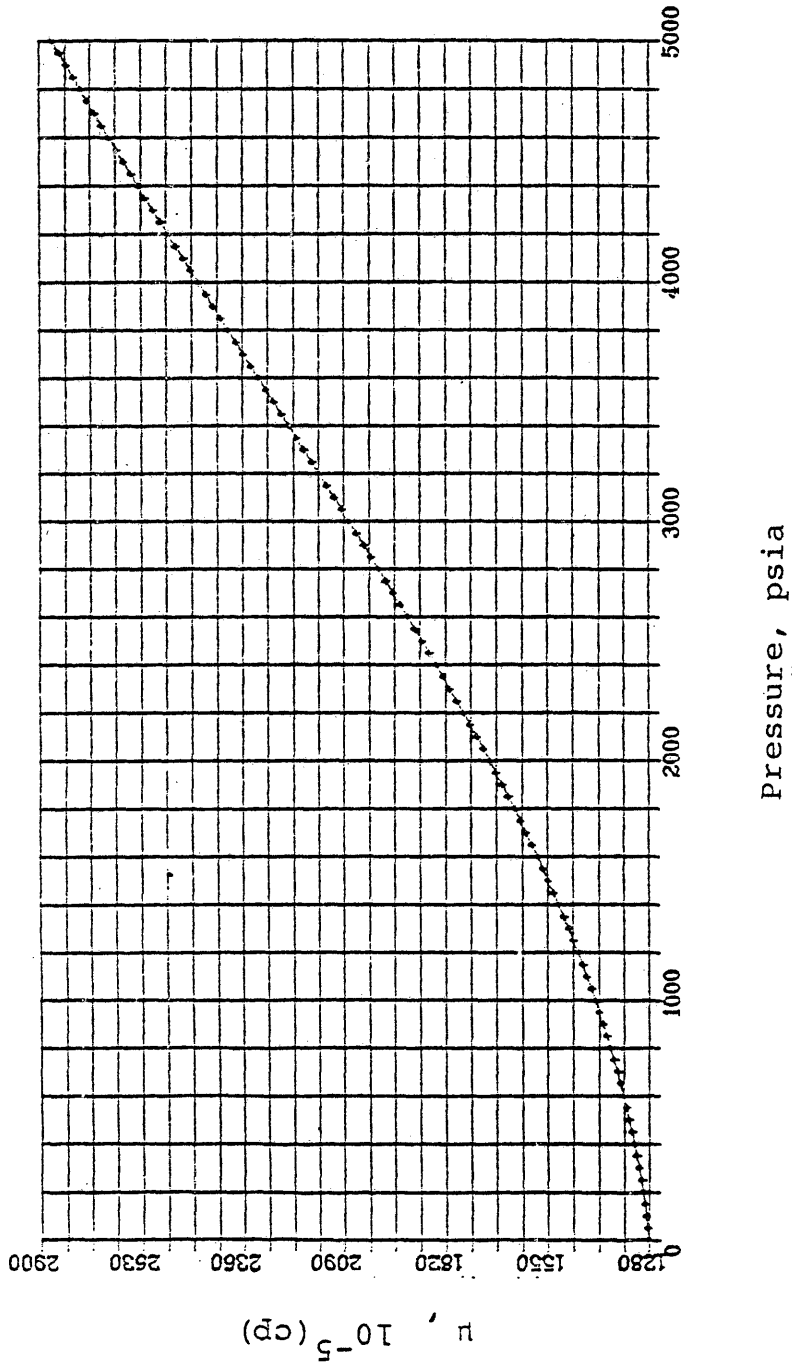


Figure B-3. The Relation of the Viscosity
Function with Pressure for 0.7
Gravity Gas at a
Temperature of 200°F.

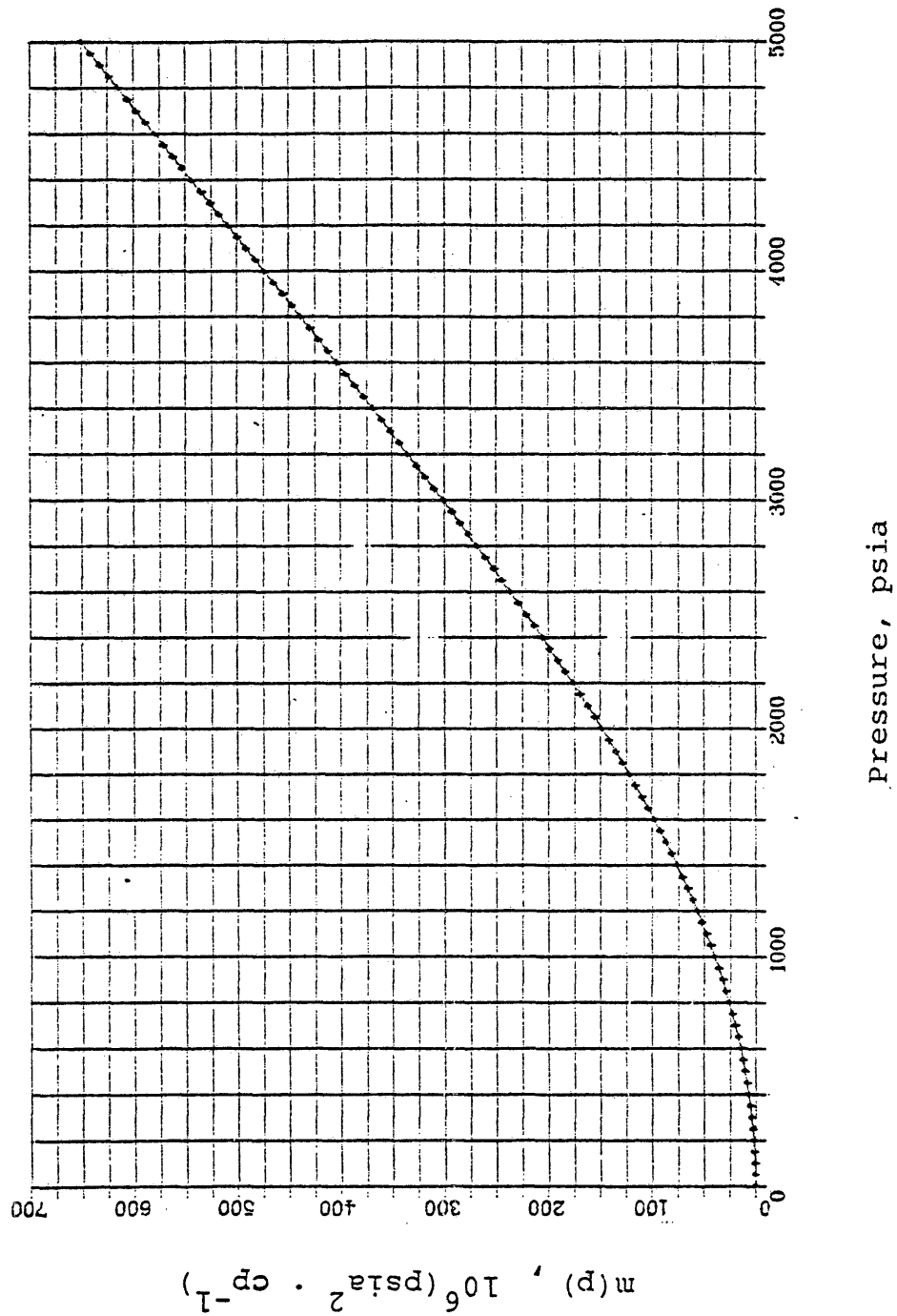


Figure B-4. The Relation of the $m(P)$ Function with Pressure for a 0.7 Gravity Gas at a Temperature of 200°F.

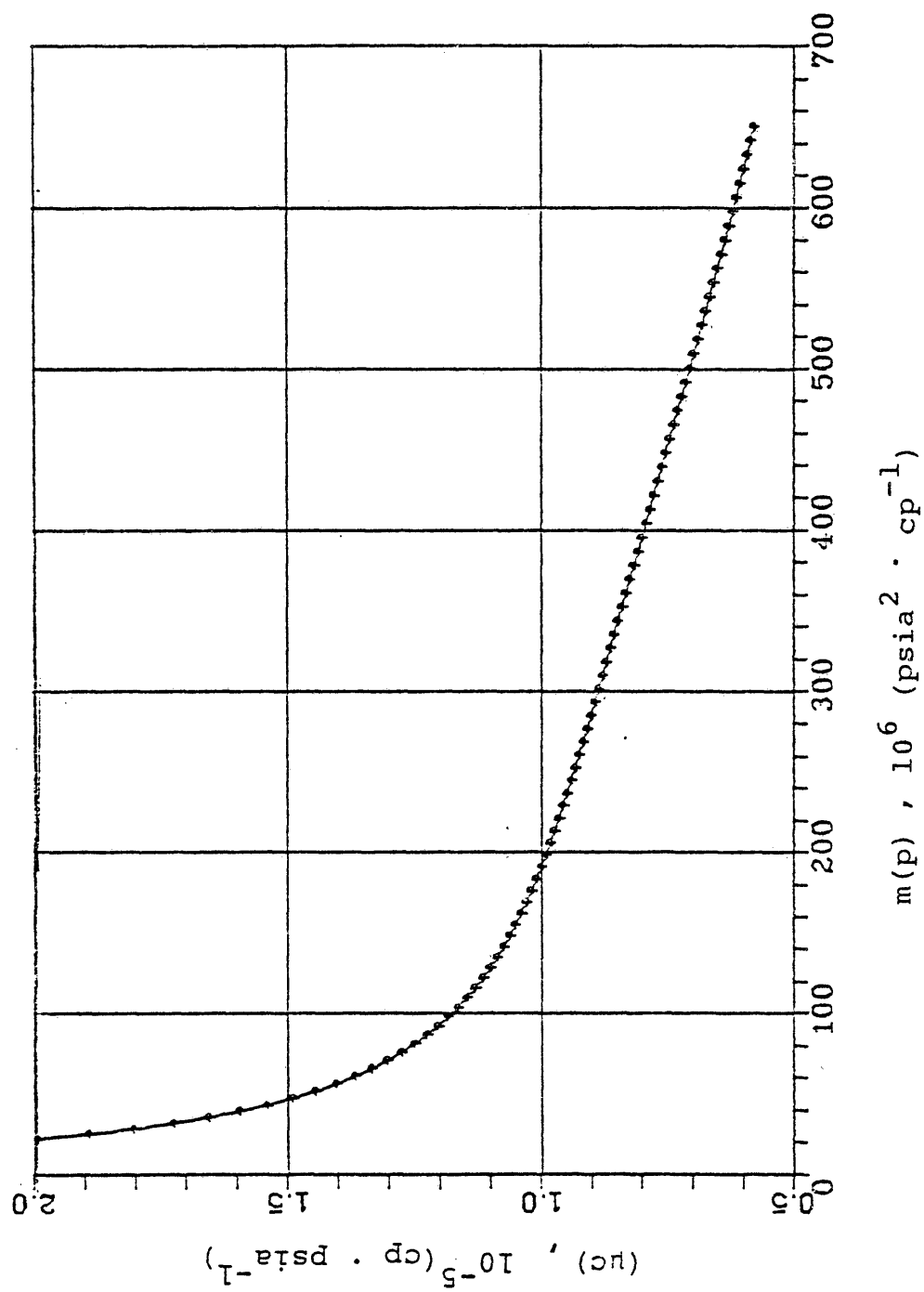
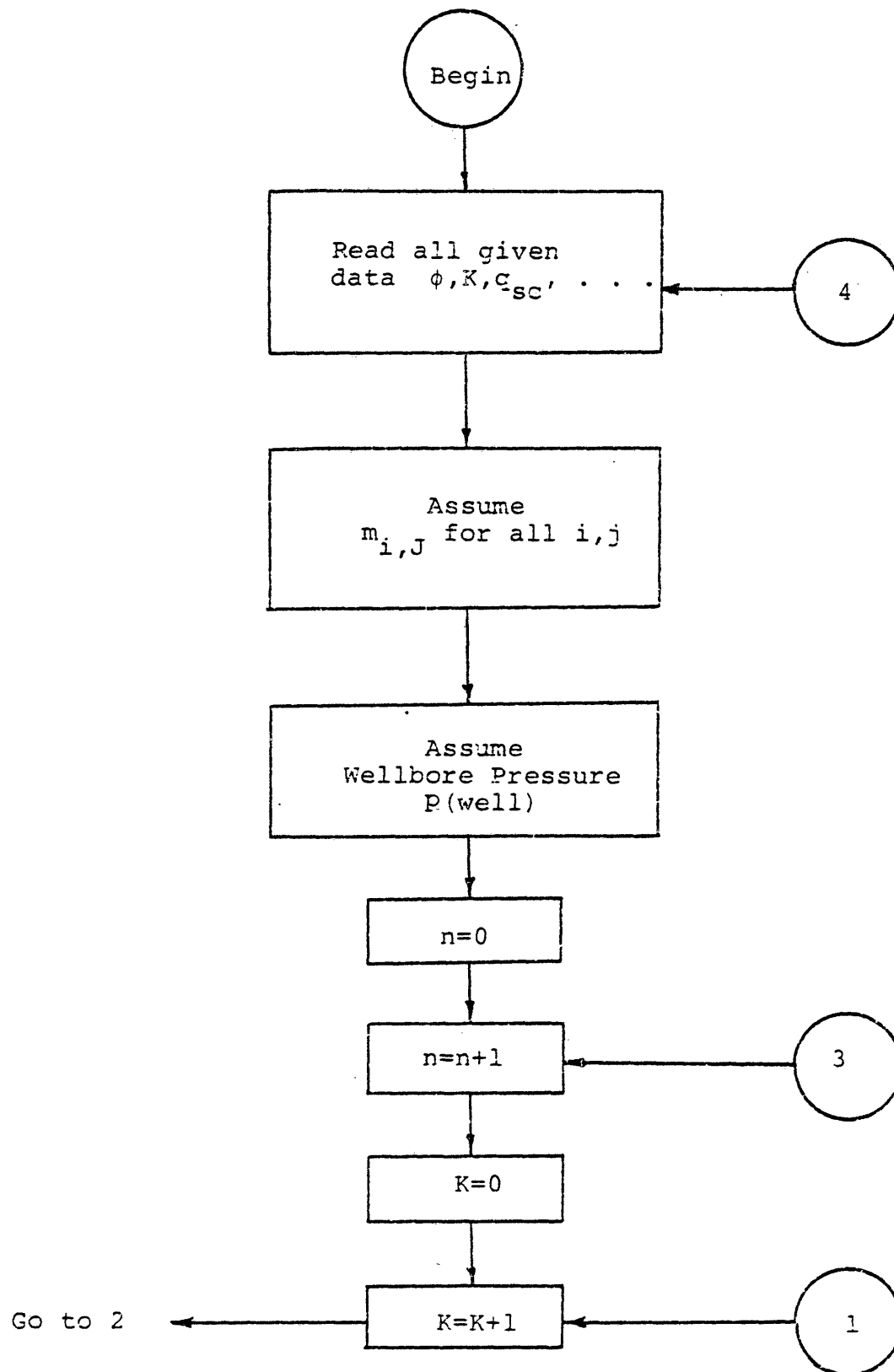


Figure B-5. The Relation of (μC) Function with $m(p)$ for a 0.7 Gravity Gas at a Temperature of 200°F.

APPENDIX C
FLOW DIAGRAM OF NUMERICAL MODEL
Figure C-1-Flow Chart of Numerical Model



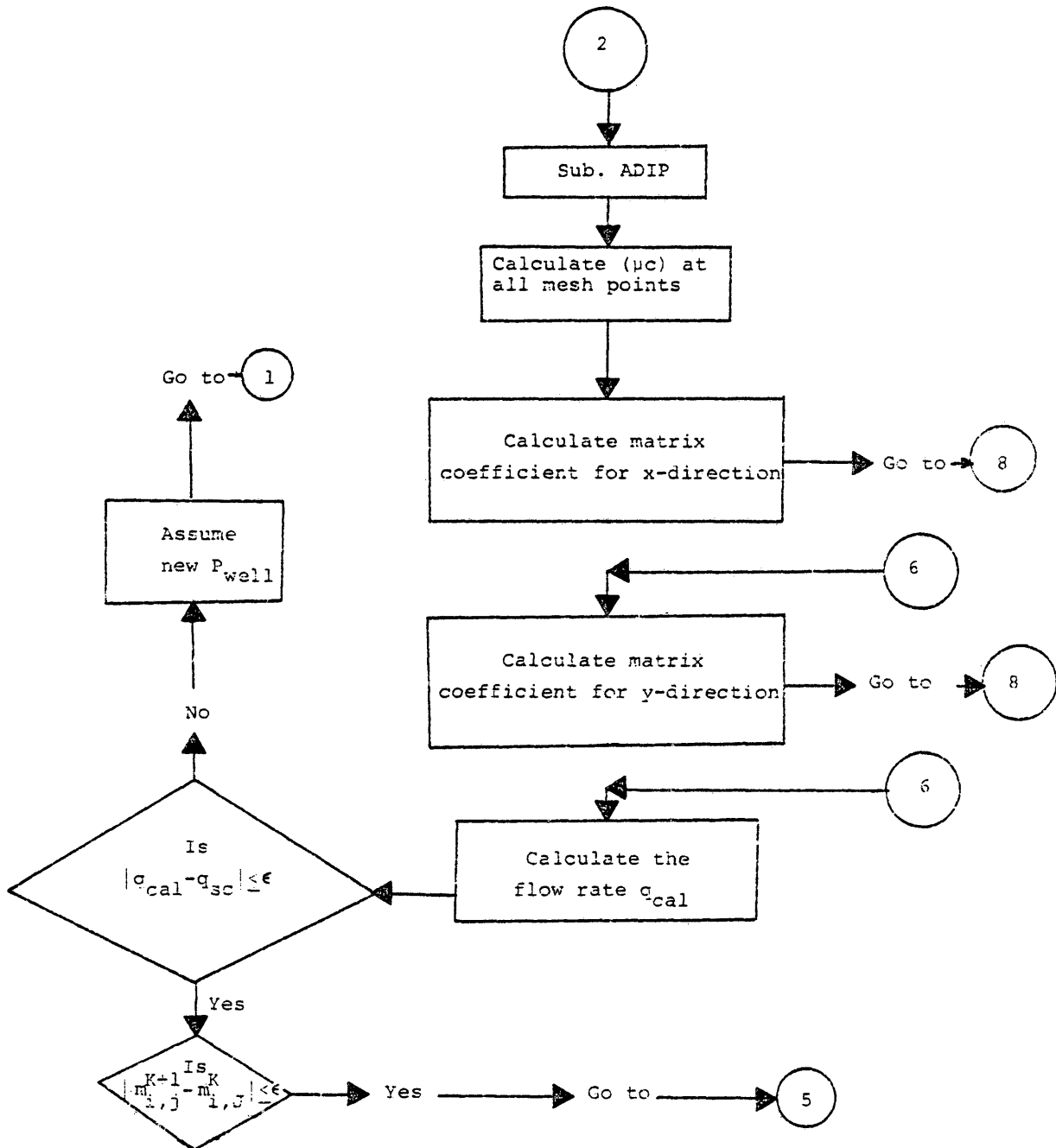


Figure C-2-Flow Chart of Numerical Model (con't)

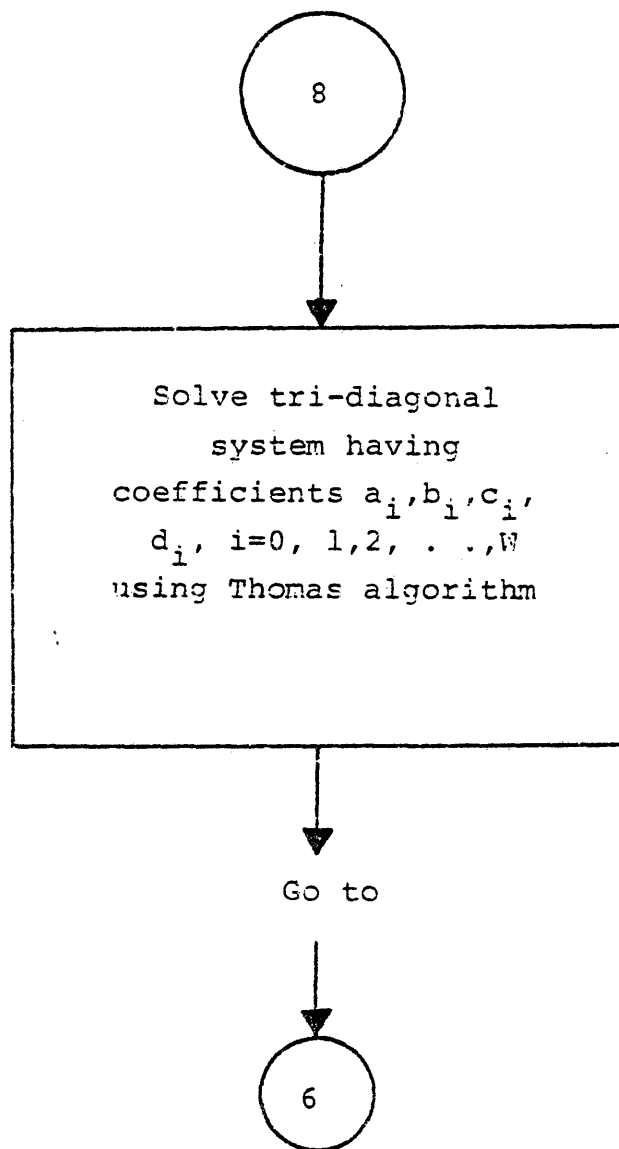


Figure C-3-Flow Chart of Numerical Model (con't)

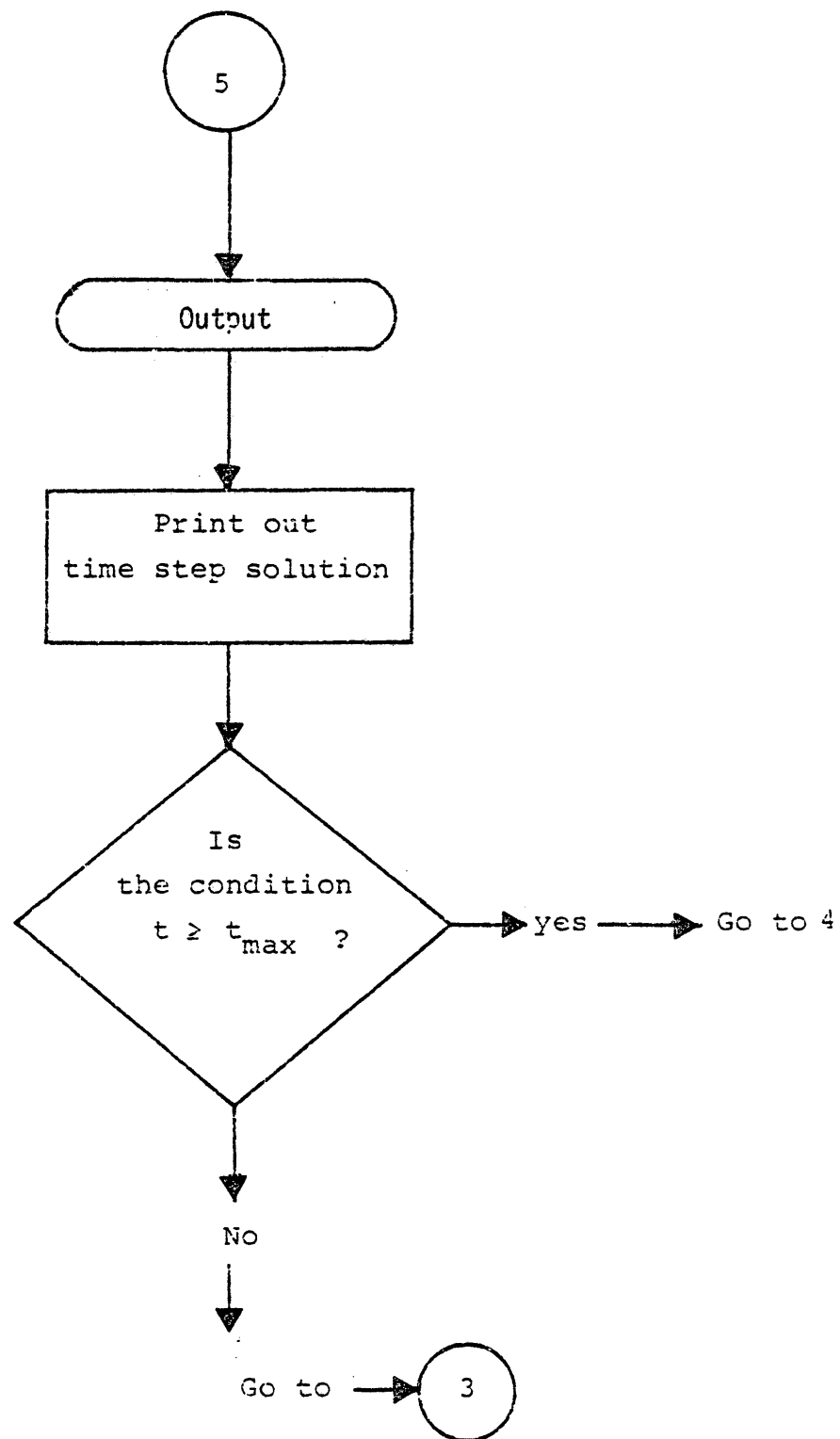


Figure C-4-Flow Chart of Numerical Model (con't)

BIBLIOGRAPHY

1. Bass, D.M.: A Study of the Factors Which Affect the Results of Short-Term Multi-Rate Gas Well Tests: Ph.D. Dissertation, Texas A & M University (1971).
2. McGuire, W.J. and Sikora, V.J.: "The Effect of Vertical Fractures on Well Productivity", Trans. AIME (1960) 218, 401.
3. Prats, M.: "Effect of Vertical Fractures on Reservoir Behavior-Incompressible Fluid Case", Trans. AIME (1961) 222, 105.
4. Russell, D.G. and Truitt, N.E.: "Transient Pressure Behavior in Vertically Fractured Reservoirs", Trans. AIME (1964) 231, 1159.
5. Gringarten, A.C., Ramey, H.J., Jr. and Raghaven, R.: "Unsteady-State Pressure Distributions Created by a Well with a Single Infinite - Conductivity Vertical Fracture", Soc. Pet. Eng. J. (Aug. 1974) 347-360.
6. Wattenbarger, R.A. and Ramey, H.J., Jr.: "Well Test Interpretation in Vertically Fractured Gas Wells", J. Pet. Tech. (May, 1969) 625-632.
7. Al-Hussainy, R., Ramey, H.J., Jr., and Crawford, P.B.: "The Flow of Real Gases Through Porous Media", Trans., AIME (1966) Vol. 237, 624.
8. Al-Hussainy, R., and Ramey, H.J., Jr.: "Application of Real Gas Flow Theory to Well Testing and Deliverability Forecasting", Trans., AIME (1966) Vol. 237, 637.
9. Muskat, M.: The Flow of Homogeneous Fluids Through Porous Media, McGraw-Hill Book Co., Inc., New York (1937).

10. Mueller, T.D., and Witherspoon, P.A.: "Pressure Interference Effects Within Reservoirs and Aquifers", Trans., AIME (1965) Vol. 234, 471.
11. Horner, D.R.: "Pressure Build-up in Wells", Proceedings of the Third World Petroleum Congress (II), (1951), The Hague, 503.
12. Miller, C.C., Dyes, A.B., and Hutchinson, C.A., Jr.: "The Estimation of Permeability and Reservoir Pressure from Bottom Hole Pressure Build-up Characteristics", Trans., AIME (1950) Vol. 189, 91.
13. van Everdingen, A.F. and Hurst, W.: "The Application of the LaPlace Transformation to Flow Problems in Reservoirs", Trans., AIME (1949) Vol. 186, 305.
14. van Everdingen, A.F.: "The Skin Effect and Its Influence on the Productive Capacity of a Well", Trans., AIME (1953) Vol. 198, 171.
15. Hurst, W.: "Establishment of the Skin Effect and Its Impediment to Fluid Flow Into a Well Bore", The Petroleum Engineer, October, 1953, B-6.
16. Matthews, C.S., Brons, F., and Hazebroek, P.: "A Method for Determination of Average Pressure in a Bounded Reservoir", Trans. AIME (1954) Vol. 204, 35.
17. Matthews, C.S.: "Analysis of Pressure Build-up and Flow Test Data", Journal of Petroleum Technology, September, 1961, 862.
18. Matthews, C.S., and Russell, D.G.: "Pressure Build-up and Flow Tests in Wells", S.P.E. Monograph Series, Vol. 1, Society of Petroleum Engineers, Dallas, Texas (1967).
19. Prats, M., Hazebroek, P., and Strickler, W.R.: "Effect of Vertical Fractures on Reservoir Behavior - Compressible Fluid Case", Trans., AIME (1962) Vol. 225, 87.

20. Prats, M., and Levine, J.S.: "Effect of Vertical Fractures on Reservoir Behavior - Results on Oil and Gas Flow", Trans., AIME (1965) Vol. 228, 1119.
21. Scott, J.O.: "The Effect of Vertical Fractures on Transient Pressure Behavior of Wells", Trans., AIME (1963) Vol. 228, 1365.
22. Rawlins, E.L., and Schellhardt, M.A.: "Back-Pressure Data on Natural Gas Wells and Their Application to Production Practices", Monograph 7, U.S. Bureau of Mines (1935).
23. Hetherington, C.R., MacRoberts, D.T., Huntington, R.L.: "Unsteady Flow of Gas Through Porous Media", Trans., AIME (1942) Vol. 146, 166.
24. MacRoberts, D.T.: "Effects of Transient Conditions in Gas Reservoirs", Trans., AIME (1949) Vol. 186, 36.
25. Bruce, D.G., Peaceman, D.W., Rachford, H.H. and Rice, J.: "Calculations of Unsteady-State Gas Flow Through Porous Media", Trans., AIME (1953) Vol. 198, 79.
26. Van Kirk, C.W.: "Effect of Pressure-Dependent Variables in Gas-Well Numerical Simulation and Gas-Well Testing" Doctor of Philosophy Thesis, Colorado School of Mines, (1972).
27. Van Poolen, H.K., Breitenbach, E.A. and Thurnau, D.H.: "Treatment of Individual Wells and Grids in Reservoir Modeling", Soc. Pet. Eng. J. (Dec., 1968) 341-346.
28. Breitenbach, E.A., Thurnau, D.H. and Van Poolen, H.K.: "The Fluid Flow Simulation Equations", SPE paper 2020 presented at the Symposium on Numerical Simulation of Reservoir Performance in Dallas, Texas, April 22-23, 1968.

29. McKinley, R.M.: "Wellbore Transmissibility from Afterflow - Dominated Pressure Build-up Data", J. Pet. Tech. (July, 1971) 863-872.
30. Gringarten, A.C., Ramey, H.J., Jr. and Raghaven, R.: "Applied Pressure Analysis for Fractured Wells", J. Pet. Tech. (July, 1975) 887-892.
31. Ramey, H.J., Jr.: "Short-Time Well Test Data Interpretation in the Presence of Skin Effect and Wellbore Storage", J. Pet. Tech. (Jan., 1970) 97-104.
32. Aronofsky, J.S. and Porter, J.D.: "Unsteady Radial Flow of Gas Through Porous Media: Variable Viscosity and Compressibility", Journal of Applied Mechanics (1956) Vol. 23, 128.
33. Dykstra, H.: "Calculated Pressure Build-up for a Low Permeability Gas-Condensate Well", Trans., AIME (1961) Vol. 222, 1131.
34. Douglas, J., Peaceman, D.W., and Rachford, H.H., Jr.: "Calculation of Unsteady-State Gas Flow Within a Square Drainage Area", Trans., AIME (1955) Vol. 204, 190.
35. Smith, R.V.: "Unsteady-State Gas Flow into Gas Wells", Trans., AIME (1961) Vol. 222, 1151.
36. Swift, F.W. and Kiel, O.G.: "The Prediction of Performance Including the Effect of Non-Darcy Flow", Trans., AIME (1962) Vol. 225, 791.
37. Katz, D.L., Cornell, D., Kobayashi, R., Poettman, F.H., Vary, J.A., Elenbaas, J.R., and Weinaug, C.F.: Handbook of Natural Gas Engineering, McGraw-Hill Book Co., Inc., New York (1959).
38. Bird, R.B., Stewart, W.E., and Lightfoot, E.N.: Transport Phenomena, John Wiley and Sons, Inc., New York (1960).
39. Carslaw, H.S. and Jaeger, J.C.: Conduction of Heat in Solids, 2nd Ed., Oxford U. Press, London (1959).

40. Richtmeyer, R.D.: Difference Methods for Initial Value Problems, Interscience Publishers, New York, NY (1957).
41. Peaceman, D.W. and Rachford, H.H., Jr.: "The Numerical Solution of Parabolic and Elliptic Differential Equations", J. Soc. Ind. Appl. Math. (1955) Vol. 3, 28.
42. Fox, L.: Numerical Solution of Ordinary and Partial Differential Equations, Addison-Wesley Publishing Co., London (1962).
43. Forsythe, F.E. and Wasow, W.R.: Finite-Difference Methods for Partial Differential Equations, John Wiley and Sons, Inc., New York, NY (1960).
44. Coats, K.H., Tek, M.R., and Katz, D.L.: "Unsteady-State Liquid Flow Through Porous Media Elliptic Boundaries", Trans., AIME (1959) Vol. 216, 460.
45. Handbook of Mathematical Functions, National Bureau of Standards, Washington, D.C. (1964).
46. Douglas, J., Jr., Peaceman, D.W., and Rachford, H.H., Jr.: "A Method for Calculating Multi-Dimensional Immiscible Displacement", Trans., AIME (1959) Vol. 216, 297.
47. Nicol, L.R.: "Gas Turbulence Factor in a Microvugular Carbonate", paper submitted to Journal of Canadian Petroleum Technology (1966).
48. Lee, A.L., Gonzolez, M.H., and Eakin, B.E.: "The Viscosity of Natural Gases", Trans., AIME (1966) Vol. 237, 997.
49. Craft, B.C., and Hawkins, M.F.: Applied Petroleum Reservoir Engineering, Prentice-Hall, Inc., Englewood Cliffs, NY (1959).
50. Gladfelter, R.E., Tracy, G.W., and Wilsey, L.E.: "Selecting Wells Which Will Respond to Production Stimulation Treatment", Drill. and Prod. Prac., API (1955) 117.

51. Collins, R.W.: Flow of Fluids Through Porous Materials, Reinhold Publishing Corp., New York (1961).
52. Walsh, J.A., Ahlberg, J.H., and Nilson, E.N.: "Best Approximation Properties of the Spline Fit", Journal of Mathematics and Mechanics (1962) Vol. 11, No. 2, 225.
53. Carr, N.L., Kobayashi, R., and Burrows, D.: "Viscosity of Hydrocarbon Gases Under Pressure", Trans., AIME (1954) Vol. 201, 270.
54. Clark, K.K.: "Transient Pressure Testing of Water Injection Wells", J. Pet. Tech. (June 1968), 693.
55. Millheim, K.K. and Cichowicz: "Testing and Analyzing Low-Permeability Fractured Gas Wells", J. Pet. Tech. (Feb., 1968), 193.
56. Raghavan, R., Cady, G.V., and Ramey, H.J., Jr.: "Well Test Analysis for Vertically Fractured Wells", J. Pet. Tech. (Aug., 1972), 1014.
57. Dranchuk, P.M., and Abou-Kassem, J.H.: "Calculation of Z Factor for Natural Gases Using Equations of State", The Journal of Canadian Petroleum Technology, (July-September, 1975), Montreal.
58. Lee, A.L. and Gonzalez, M.H.: "The Viscosity of Natural Gases", J. Pet. Tech. (August 1966), 997-1000.
59. Al-Hussainy, R., Ramey, H.J., Jr., and Crawford, P.B.: "The Flow of real gas in porous media", J. Pet. Tech. (May 1966), 624.
60. Klinkenberg, L.J.: The permeability of porous media to liquid and gases, Drilling and Production, p. 200, American Petroleum Institute, 1941.

VITA

NAME: MAHMOUD AHMED SHAGRONI

BORN: July 20, 1952, Jefren, Libya

PERMANENT ADDRESS: Tripoli, Libya Tel. (37051)

EDUCATION: Public schools in Jefren, Libya

B.SC. in Petroleum Engineering,
Al-Fatah University, 1975.

M.SC. in Petroleum Engineering,
Colorado School of Mines, 1977.

Doctor of Philosophy in Petroleum
Engineering, Colorado School of Mines,
1979.

This dissertation was typed by: Patricia Jewett &
Kathy Houlihan